Connected Automated Traffic Management Over Bottlenecks

by

Yifan Yao

A dissertation submitted in partial fulfillment of
the requirements for the degree of

Doctor of Philosophy

(Department of Civil and Environmental Engineering)
at the

UNIVERSITY OF WISCONSIN–MADISON

2024

Date of final oral examination: 04/15/2024

The dissertation is approved by the following members of the Final Oral Committee:
Bin Ran, Professor, Civil and Environmental Engineering
David A. Noyce, Professor,Civil and Environmental Engineering
Soyoung (Sue) Ahn, Professor, Civil and Environmental Engineering
Xin Wang, Assistant Professor, Industrial and Systems Engineering
Yang Zhou, Assistant Professor, Civil and Environmental Engineering,
Texas A&M University

ACKNOWLEDGMENTS

The completion of my PhD journey would not have been possible without the support and guidance of many individuals and institutions.

First and foremost, I would like to express my deepest gratitude to my adviser, Professor Bin Ran. Your unwavering support, insightful guidance, and invaluable expertise have been instrumental throughout my research journey. Your encouragement and belief in my abilities have been a constant source of motivation, and I am truly fortunate to have had the opportunity to learn from you.

I am also immensely grateful to the University of Wisconsin-Madison for providing me with an exceptional academic environment. The resources, facilities, and scholarly community at UW-Madison have greatly enriched my research experience. I would like to extend my appreciation to the faculty and staff for their support and for fostering an environment conducive to academic excellence.

I would also like to thank Professor Xin Wang and Professor Yang Zhou for their help and contributions to my academic development. Your insights and assistance have been crucial in refining my research and broadening my understanding.

My heartfelt thanks go to my parents, whose unconditional love, patience, and encouragement have been my foundation. Your sacrifices and support have enabled me to pursue my dreams, and for that, I am eternally grateful.

To Shunyi Huang, thank you for your love, understanding, and unwavering support. Your encouragement and belief in me have been a constant source of strength, and I am deeply thankful for your presence in my life.

I would also like to thank my best friends, Xueqi Zhao, Yuting Chen, Jiwan Jiang, Tingjia Cao, Dr. Shenwei Zhang, for being a pillar of support throughout this journey. Your companionship, advice, and encouragement

have been invaluable, and I cherish the many moments we have shared.

A special thanks to my lab colleagues, Dr. Shen Li, Dr. Xiaotian Li, Dr. Tianyi Chen, Dr. Shuoxuan Dong, Dr. Kunsong Shi, Dr. Ran Yi, Dr. Haotian Shi, Dr. Keshu Wu, Han Cao, Jingwen Zhu, Sicheng Fu, Kexin Tian, Jumwei You, Rui Gan, Junyi Ma, Weizhe Tang, whose camaraderie, collaboration, and support have been integral to my research experience. Your feedback, shared challenges, and collective wisdom have significantly contributed to the progress of this work. I am grateful for the stimulating discussions and the supportive environment you all have created.

Thank you to my project manager, Dr. Steven Parker, for your guidance and unwavering support. Your leadership has been instrumental in keeping the project on track and ensuring its successful completion.

Finally, I would like to express my gratitude to my cats, Kiwi and Peachtea, for the comfort and companionship you have provided during the long hours of research and writing. Your presence has been a constant source of joy and relaxation.

I extend my appreciation to everyone who has contributed to my research and personal growth in ways both big and small. Your collective support has been vital in the completion of this journey.

Thank you all.

Yifan Yao

CONTENTS

LIST OF TABLES

LIST OF FIGURES

ABSTRACT

The rapid development of CAV technology has revolutionized urban transportation by introducing innovative approaches to enhance traffic efficiency. Leveraging advanced communication capabilities such as vehicle-to-vehicle (V2V) and vehicle-to-infrastructure (V2I), CAVs can seamlessly exchange information with their surroundings, while automation functions enable precise individual control over these vehicles. Amidst these advancements, signalized intersections and weaving sections remain critical nodes in urban traffic, often leading to congestion and safety concerns.

This Ph.D. research focuses on optimizing CAV movements with a primary objective of enhancing throughput and maximizing capacity under bottleneck. To address this challenge, two novel approaches are proposed: a grid-based mixed-integer programming optimization model for CAV sorting and a macroscopic control strategy. The former facilitates coordination of individual CAV movement, while the latter takes a holistic view, considering controlling the collective behavior of CAVs.

Traditional control strategies that solely focus on infrastructure and geometries are transcended through the grid-based mixed-integer programming optimization model, which exhibits promising results in tackling congestion challenges at bottlenecks. To overcome the scalability limitations of microscopic individual vehicle control, the macroscopic control strategy employs the Cell Transmission Model (CTM) to macroscopic control traffic flow. This approach showcases improved traffic capacity, especially in heavy traffic conditions, and exhibits robustness in dynamic traffic scenarios.

To ensure practicality and real-time responsiveness, a rolling-horizon-based solution method is introduced, accelerating the algorithms employed in both models and enabling coordinated CAV movements, even in the presence of uncertain vehicle arrivals.

Comprehensive numerical experiments validate the effectiveness and reliability of the proposed models, demonstrating improved traffic throughput, and efficient lane utilization.

This research contributes to the advancement of CAV-enabled transportation systems, offering valuable insights into addressing congestion challenges and optimizing traffic flow dynamics. The proposed approaches hold tremendous potential in transforming urban transportation, facilitating the seamless integration of CAVs, and fostering the development of more efficient, sustainable, and safer cities.

1 INTRODUCTION

This chapter starts with discussing the remaining challenges of CAV control at bottlenecks such as intersection and weaving section. In particular, the challenge at bottlenecks lies in the underutilization of lanes and green time, leading to congestion and safety concerns. Coordinating individual vehicles efficiently in real-time presents computational challenges and limits scalability, especially in scenarios with a large fleet of connected automated vehicles (CAVs). Additionally, the proportion of vehicles with specific directions is highly time-varying and uncertain, necessitating fast and adaptive sorting algorithms to optimize traffic flow and increase capacity.

1.1 Motivation

The rapid development of CAV technology has presented a transformative opportunity to revolutionize urban transportation and improve traffic efficiency. Through advanced communication capabilities like V2V and V2I, CAVs can seamlessly exchange information with their surroundings, while automation functions allow for precise individual control over these vehicles. These advancements open the door to sophisticated cooperative control strategies that can significantly enhance the effectiveness of traffic systems. However, despite these promising developments, signalized intersections and weaving section continue to pose significant challenges in urban traffic, leading to congestion and safety concerns.

The main objective of this Ph.D. research is to optimize CAV movements, focusing on enhancing throughput and maximizing intersection and weaving section capacity. To achieve this, we propose three novel approaches: a grid-based mixed-integer programming optimization model for CAV sorting and a macroscopic control strategy. The former allows

real-time coordination of individually controlled CAV traffic movements, while the latter provides a holistic outlook by macroscopic control of CAVs.

Bottleneck of Traffic Flow

Traffic congestion is a ubiquitous challenge in urban transportation systems, often leading to inefficiencies, delays, and increased environmental impact. Among the various elements contributing to congestion, signalized intersections and weaving sections are two critical bottlenecks that significantly impact traffic flow and overall network performance. Signalized intersections, where streams of vehicles from multiple directions converge and compete for right-of-way, often experience queuing, delays, and inefficient utilization of green time. On the other hand, weaving sections, commonly found at freeway interchanges, pose unique challenges due to the complex merging and diverging maneuvers between entering and exiting traffic streams. These sections are prone to congestion, capacity constraints, and safety hazards, especially during peak traffic periods. Addressing these bottleneck areas requires innovative strategies that leverage advanced technologies and intelligent control mechanisms to optimize traffic flow, enhance intersection throughput, and improve overall network efficiency.

As the deployment of Connected Automated Vehicle (CAV) systems expands, the feasibility of traditional microscopic control, involving individual vehicle optimization, diminishes due to computational intensiveness and real-time responsiveness challenges. To overcome these limitations, we explore the potential of macroscopic control as a viable alternative. By adopting the Cell Transmission Model (CTM), we can control CAV traffic and optimize traffic flow on a cell-by-cell basis, discretizing the road segment into cells representing individual lanes. This approach facilitates the development of more efficient and scalable control strategies for CAVs. Through our proposed connected automated flow control

(CAFC) strategy, we effectively optimize lane utilization and green time through coordination sorting, leading to improved capacity, especially in heavy traffic conditions, and demonstrating robustness in dynamic traffic scenarios.

To ensure the practicality and real-time responsiveness of our proposed models, we introduce a rolling-horizon-based solution method that accelerates the algorithms. This enhancement allows for coordinated CAV movements even in the presence of uncertain vehicle arrivals, making our solutions adaptive to real-world traffic scenarios.

To validate the effectiveness and reliability of our proposed models, we conduct a series of comprehensive numerical experiments. The results reaffirm the significant impact of our approaches, showcasing improved intersection and weaving section throughput, efficient lane utilization, and increased diverse traffic conditions. Moreover, the models exhibit minimal sensitivity to parameter variations, further reinforcing their robustness and applicability.

1.2 Objectives and Contributions

This doctoral research seeks to advance the field of CAV-enabled transportation systems by introducing innovative methodologies to enhance traffic bottlenecks efficiency. The proposed grid-based mixed-integer programming optimization and macroscopic control strategies hold tremendous potential in addressing congestion challenges and optimizing traffic flow dynamics. In the subsequent sections of this paper, we provide comprehensive insights into the intricacies of our proposed models, present the results of validation experiments, and conclude with a detailed discussion concerning potential avenues for future research and practical implementation.

2 LITERATURE REVIEW

The inefficiency of intersections and weaving sections has long been a focus of transportation research. While studies have traditionally centered on optimizing signal timing to improve intersection performance under varying traffic conditions (Sawake and Borkar, 2017; Guo et al., 2019), recent efforts have explored pre-signal traffic management as an alternative solution. One notable approach is the pre-signal system (Xuan et al., 2011), which employs a tandem design to group vehicles with the same direction before the intersection signal. While this system enhances intersection capacity, it necessitates additional infrastructure and may exacerbate traffic congestion, especially if human-driven vehicles struggle to adapt to the complex signal system.

Similarly, freeway weaving sections, where traffic streams converge and diverge, present significant challenges for traffic optimization. These sections often experience congestion, reduced capacity, and various issues such as traffic oscillations, increased energy consumption, accidents, and recurrent congestion. Past efforts have focused on implementing active traffic management strategies like ramp metering and variable speed limits (Cassidy and May, 1991; Liu et al., 2012; Bai et al., 2022; Du et al., 2018; Wang et al., 2015; Golob et al., 2004; Cottrell, 1998; Zhang and Levinson, 2010; Wang et al., 2014b; Abdel-Aty and Wang, 2017). However, these approaches have struggled to address the stochastic nature of individual vehicle dynamics, limiting their effectiveness in optimizing traffic flow.

With the development of CAVs, the advantage of traffic sorting by the pre-signal system can be achieved directly without introducing new infrastructures. For pure CAV traffic, such sorting can be achieved by sharing and receiving real-time information through V2V and V2I. V2V communication-based vehicle control is divided into two categories: longitudinal control and lateral control. In a CAV platoon, longitudinal control

is primarily concerned with car-following control (Zhou et al., 2019; Han et al., 2020; Chen et al., 2021a). Longitudinal control via V2V communication is known as the Cooperative Cruise Control system(Gong et al., 2016; Öncü et al., 2014; Shi et al., 2021; Zhou et al., 2020). Lateral control, on the other hand, refers to smooth lane changes. Many studies of lateral control focus on addressing potential conflicts as "proximity cost" in the framework (Wang et al., 2014a; Zhou et al., 2017a; Wang et al., 2021). The existing studies on the CAVs' lateral control are reviewed in Bevly et al., 2016. Meanwhile, CAVs are precisely cooperatively controlled with infrastructure, thanks to V2I communication. Recent research has increased the efficiency of bottlenecks scenarios by using cooperative control CAVs with information from signal timings (Qian et al., 2021; Xu et al., 2017; Li et al., 2021b) and optimized the trajectory in single-lane scenarios (Zhou et al., 2017b; Li et al., 2018; Jiang et al., 2017; Dong et al., 2021).

However, it is important to note that all the aforementioned research primarily focuses on microscopic control, which presents challenges in terms of computation time and scalability. The computational time required for individually controlling a large number of vehicles becomes a critical concern, especially as the scale of CAV systems increases. The computational complexity becomes a bottleneck, hindering real-time responsiveness for practical implementation.

To address the limitations posed by the microscopic control approach, researchers have considered a macroscopic perspective that encompasses the collective behavior of vehicles rather than focusing on each individual vehicle. One of the approaches employed to achieve this macroscopic view is the CTM.

The CTM is a finite differences approximation based on hydrodynamic theory, providing a practical representation of traffic flow and density (Daganzo, 1995, 1994). It employs a piecewise linear function to describe the FD of traffic flow, which convergently approximates a reduced form of

the Lighthill-Whitham-Richards (LWR) hydrodynamic model (Lighthill and Whitham, 1955; Richards, 1956). The CTM is capable of modeling various traffic propagation phenomena, including spillback, kinematic wave, and physical queue.

Over the last decade, the CTM has found applications in a wide range of dynamic traffic issues. For instance, it has been incorporated into optimized signal timing for CAVs (Yao et al., 2022b; Al Islam et al., 2020; Tajalli et al., 2020). Additionally, researchers have utilized multiclass CTMs to model the scenarios with mixed traffic involving human and autonomous vehicles (Levin and Boyles, 2016b; Pi et al., 2019; Ngoduy et al., 2021). Furthermore, the CTM has been employed to develop dynamic lane reversal strategies for autonomous vehicles, aimed at reducing traffic congestion and improving spacial utilization (Levin and Boyles, 2016a; Duell et al., 2016). However, it is important to note that these applications do not directly control vehicles; rather, they focus on modeling traffic scenarios or addressing dynamic traffic challenges with operated infrastructure.

While the existing literature on CAV control and sorting strategies has shown promise in improving capacity, there are notable limitations and gaps in current research efforts. Most studies have predominantly focused on microscopic control approaches, which are tailored to enhance efficiency in small-scale scenarios (Yao et al., 2022a; Wu et al., 2021). These microscopic control strategies address individual vehicle movements and interactions, but they face challenges in terms of scalability when dealing with a large fleet of CAVs.

On the other hand, the utilization of the CTM to increase capacity for CAVs has shown potential but remains limited in scope. The existing literature primarily explores modeling traffic scenarios or addressing dynamic traffic challenges with operated infrastructure. However, this approach has not fully exploited the macroscopic control potential of the CTM to optimize traffic flow and capacity in a broader context.

Given these limitations and gaps, there is a pressing need to develop a macroscopic vehicle control approach that can effectively address the scalability challenges and unlock the full potential of CAV-enabled intersections and weaving section.

3 ROLLING-HORIZON BASED STRATEGY OF FULLY COOPERATIVE TRAFFIC UNDER SIGNALIZED INTERSECTIONS

This chapter we present a novel grid-based mixed-integer programming optimization model for CAV sorting to address the challenge of enhancing intersection efficiency. The proposed model allows for real-time coordination of each CAV traffic movement, including speed changes and lane changes, aiming to achieve higher throughput at signal-based, multi-lane intersections. Additionally, we introduce a rolling-horizon based solution method to expedite the algorithm and validate its effectiveness through a series of numerical experiments, providing valuable insights into the system's performance.

3.1 Introduction

Connected automated vehicles (CAVs), enabled by communication functions such as vehicle to vehicle (V2V) and vehicle to infrastructure (V2I) can share the information with the ambient environment. Meanwhile, enabled by automation functions, CAVs can be precisely controlled individually. With the awareness of the environment and the resulted cooperative control strategies, CAVs can significantly improve traffic system efficiency. As the crucial module of urban transportation, signalized intersections are often the bottlenecks causing congestion and safety concerns. The adoption of connected and automated traffic in the near future brings many new challenges and opportunities to enhance intersection efficiency with wisely managed CAVs.

To enhance the intersection efficiency, the core is to improve the throughput, that is the maximum number of vehicles passing through the intersection per unit time. Unlike traditional signal control strategies, which only focus on the signal timing side, CAVs can coordinate with signals

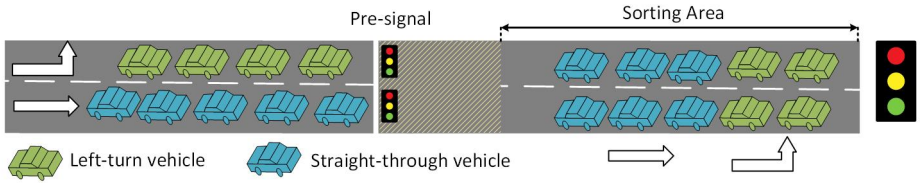

Figure 3.1: Pre-Signal System

at an individual vehicle level and better utilize the limited green time to yield higher throughput. However, current research largely optimizes the intersection efficiency by controlling CAVs' longitudinal motions in single-lane, single-phase scenarios(Jiang et al., 2017; Li et al., 2018; Zhou et al., 2017b). Although the results of these researches are encouraging, the single-lane, single-phase scenarios are greatly simplified and limited. An intersection with heavy traffic, left-turn movement, and through movement are normally in different phases. Without grouping vehicles with the same direction in advance, some through traffic may block the left-turn traffic and vice versa. Some intersections may have dedicated left-turn lanes and through lanes separately to avoid blocking, but this sacrifices the capacity hugely by reducing the number of lanes for each traffic direction. Therefore, to fully utilize the spatial and temporal resource of intersections to improve intersection capacity, Xuan et al. (2011) proposed a pre-signal system to dynamically aggregate those traffic with the same direction (e.g., left turn) together in the area between the designed pre-signal and intersection, and let one phase of the intersection signal be dedicated to one group of vehicles with the same direction, as shown in Fig.3.1.

Although this work has already shown the advantage of sorting vehicles with their respective directions in advance, its implementation is heavily constrained by the obedience of human drivers and the stochasticity of driving behaviors. Fortunately, with the help of V2V and V2I, pure CAVs can achieve such sorting directly without additional pre-signal systems. Based on the information of fixed signal-timing and the desired

direction of CAVs, lane changes and speed change can be optimized over the whole traffic flow in a coordinated way, which can significantly improve the intersection capacity.

However, many challenges exist to achieve the CAV sorting optimally. First, when vehicles approach an intersection, the space and, time allowing the sorting operations are pretty limited, especially in urban areas where intersections are densely located. Sorting vehicles may involve quick acceleration, deceleration, and frequent lane changes. Without proper coordination, such frequent vehicle operations may not improve the traffic condition but cause additional traffic congestion. Second, the proportion of vehicles with respective directions is highly time-varying and uncertain. Hence the sorting algorithm has to be fast and adaptive to the real-time traffic situation. Given the number of all vehicle conditions and their combination with different signal phases, the decision space can be extremely huge. Some simplification modeling techniques are necessary to make the problem tractable. Therefore, to address these challenges, one way is to discretize the vehicle movement into grids, e.g., Wu et al. 2021 discretized the platoon into a grid system in which vehicles with different directions can be represented as a vector state. After such discretization, each vehicle's movement can be simplified into three actions, i.e., unit acceleration, unit declaration, and lane change movement. Such grid system usually forms constrained combinatorial optimization problem, which is typically NP-hard and intractable for moderate or large-scale cases (Garey, 1979).

Noticing the above challenges, we establish a holistic framework to address the coordinated CAV sorting problem for passing through a signal-based, multi-lane intersection. The target is to find the optimal coordinated CAV traffic movement strategy that can significantly increase the traffic throughput, given the real-time uncertain traffic input and predetermined multi-phase signal timing. The strategy can guide the movement of each CAV, including speed change and lane change decisions in real-time. Our

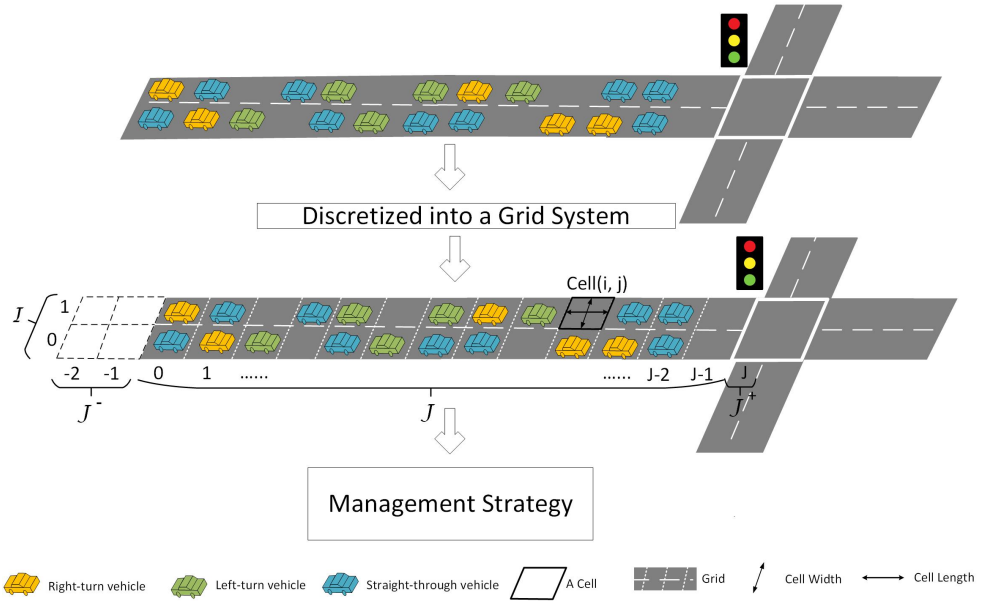

Figure 3.2: Problem Setting

contribution can be summarized as follows. (i) We establish a grid-based mixed-integer programming optimization model to implement CAVs sorting strategy near an intersection; (ii) We developed a rolling-horizon based solution method to accelerate the solution algorithm, which conquers the computational issue.(iii)A series of numerical experiments are conducted to verify and validate our algorithm and provide insights.

3.2 Model

Problem Setting

We consider a signalized intersection and one of its connected upstream road segments with two lanes, as shown in Fig.4.2. Here, the two-lane road segment is representative of general cases. Those with more lanes can

be easily extended from this work. The signal phases of this intersection include left-turn movements and through movements. All vehicles passing through this road segment and the intersection is assumed to be pure CAVs, i.e., 100% CAV market penetration. During the left-turn phase, only left-turn traffic can pass the intersection through both lanes. On the other hand, during the through phase, through traffic and right-turn traffic can both pass the intersection, whereas the through traffic can utilize both lanes but the right-turn traffic can only use the right lane.

To characterize the traffic management process, we consider a time-rolling strategy on a fixed-length planning horizon, denoted by $t \in T := \{0, 1, ..., T\}$. The strategy of CAV movements will be planned across the entire T, but only the action at time $t = 0$ will be implemented. This strategy will be updated at each time step. For tractability, we focus on a discretized grid-based modeling framework as follows.

Road Geometry. This upstream road segment is divided into a grid of homogeneous cells to simplify the problem, following the practice of Wu et al. (2021). After such discretization, each lane is represented as a row of cells, where the width of the cell is equal to the lane width. On the other hand, the cell length is based on the cruising speed of CAVs and the "critical gap." Here the critical gap indicates the minimum acceptable time gap to complete a lane-changing maneuver Toledo et al. (2003). Without loss of generality, we assume one vehicle can occupy one cell at a time. Hence, each cell can be indexed by (i, j), where $i \in I := \{0, 1\}$ is the lane (0: right lane, and 1: left lane) and $j \in J := \{0, ..., J - 1\}$ indicates the distance of the cell to the intersection. In addition, we extend its definition to $J^- := \{-2, -1\}$ and $J^+ := \{J\}$, respectively. Specifically, J^- indicates the entering buffer zone where vehicles will appear at the sorting area at the next time step, and $j = J$ is the exiting buffer zone holding those vehicles that have just passed the intersection. Hence, J^+ and J^- are "virtual" and designed to describe the boundary condition of the traffic. It will be

elaborated further in the following context. The cells in J are real cells aligned with the road segment, representing the effective sorting area, where vehicles are managed cooperatively to achieve the best grouping result given their directions.

Signal State. We discretize the signal state into integers. Let $n \in N := \{0, 1, 2\}$ be the phases, where 0 indicates the "Red", 1 indicates the "Through", and 2 indicates the "Left-turn". Further, suppose $s_{nt} \in \{0, 1\}$ for $n \in N, t \in T$ is the indicator of the signal at time t. For example, $s_{10} = 1$ means the signal is "Through" at time 0. Here we assume the signal timing is endogenously determined. Hence, $\{s_{nt}\}$ is a given parameter.

Traffic State. We consider three types of states of each cell, occupancy, speed, and vehicle's desired direction. Occupancy is denoted by $x_{ijt} \in \{0, 1\}$ for $i \in \mathcal{I}, j \in \mathcal{J}, t \in \mathcal{T}$, where $x_{ijt} = 1$ indicates a vehicle occupies cell (i, j) at time t. For the speed, we let $v \in \mathcal{V} := \{0, 1, 2\}$ be the speed level, where the value of the level indicates the number of cells a vehicle can move across in a unit of time. Here we assume the maximum speed level is 2, which can be extended if necessary. Further, suppose $y_{ijvt} \in \{0, 1\}$ is the speed indicator of the vehicle occupied the cell (i, j) at time t. For example, $y_{1,2,2,3} = 1$ means the cell $(1, 2)$ is occupied by a vehicle with a speed level 2 at time 3. Similarly, let $u \in \mathcal{U} := 0, 1, 2$ be the desired direction of a vehicle, where 0 indicates the straight-through, 1 indicates the left-turn, and 2 indicates the right-turn. Hence, we use $z_{ijut} \in \{0, 1\}$ to be the indicator for the desired direction of the vehicle occupied the cell (i, j) at time t.

Traffic management. We assume each vehicle is fully controlled under a centralized system after it arrives in the sorting area. For each vehicle, its controls include lateral and longitudinal movements, i.e., lane change and speed change. We define $\alpha_{ijt} \in \{0, 1\}$ for $i \in \mathcal{I}, j \in \mathcal{J}, t \in \mathcal{T}$ to be the indicator of lane change action for the vehicle in cell (i, j) at time t. Since we only have two lanes, there is no need to differentiate the lane change direction. Further, the speed change indicator is similarly captured

by $\beta_{ijt} \in \{0, 1\}$. To differentiate the acceleration/deceleration action, we introduce $\gamma_{ijt} \in \{0, 1\}$, where the acceleration and deceleration are denoted by 1 and 0, respectively.

Management Strategy

Given the discrete environment above, we focus on designing the management strategy with an integer programming problem. First, the ultimate goal of the strategy is to let the most number of vehicles pass through the intersection given the planning horizon T. In particular, the total number of vehicles passed can be expressed as $\sum_{i\in I, t\in T} x_{iJt}$. In addition, since we run our management strategy on a rolling horizon, we hope to let the vehicle pass the intersection as early as possible to reduce the burden for later management. Therefore, we introduce a bonus term $w_x(t)$ on the time a vehicle passes through the intersection, which is a decreasing function over time. Moreover, to stabilize the traffic, we hope the entire traffic can go through the intersection with the least state changes. To this end, we introduce corresponding penalty terms and lead to the following objective for our policy, i.e.,

$$\begin{aligned}\max_{x,y,z,\alpha,\beta,\gamma} & \sum_{i\in I, t\in T} w_x(t) x_{iJt} \\ & - \sum_{i\in I j\in J, t\in T} (c_\alpha(j)\alpha_{ijt} + c_\beta \beta_{ijt}) \\ & - \sum_{i\in I j\in J, t\in T, v\in\{0,1\}} c_y(v) y_{ijvt}. \end{aligned} \tag{3.1}$$

The first term is the adjusted number of vehicles passing through the intersection. The second term is the penalty to lane changes and speed changes, where $c_\alpha(j)$ is the penalty for a lane change, increasing over the proximity to the intersection (since we hope the lane changes are conducted relatively far away), and c_β is a constant penalty for speed

change. Then the third term penalizes the speed reduction with $c_y(v)$, which is decreasing over the speed level v.

Now, we provide a series of constraints that help guarantee the management strategy is feasible.

Vehicle Dynamics.

First, we give the dynamics of vehicles in the sorting area for $i \in I$, $j \in J$, $t \in T\backslash\{T\}$. The buffer area and the passing through of the intersection will be discussed separately. Since our system is represented by multiple indicator functions, we define a notation $\bar{x}$ as $1 - x$ for convenience. Then, based on the state of cells and vehicles, we have

$$x_{ij(t+1)} = x_{ij(t+1)}\hat{x}_{ij(t+1)}, \tag{3.2}$$

$$\begin{aligned}\hat{x}_{ij(t+1)} =& y_{ij0t}x_{ijt} + \bar{\alpha}_{i(j-1)t}y_{i(j-1)1t}x_{i(j-1)t} \\ &+ y_{i(j-2)2t}(\bar{x}_{i(j-1)t} + x_{i(j-1)t}y_{i(j-1)2t})x_{i(j-2)t} \\ &+ \alpha_{(i-1)(j-1)t}y_{(i-1)(j-1)1t}x_{(i-1)(j-1)t} \\ &+ \alpha_{(i-1)(j-2)t}y_{(i-1)(j-2)2t}x_{(i-1)(j-2)t}\left(\bar{x}_{(i-1)(j-1)t}\bar{x}_{i(j-1)t}\right),\end{aligned} \tag{3.3}$$

$$\begin{aligned}x_{ijt} =& x_{ijt}\hat{x}_{ijt}, \\ \hat{x}_{ijt} =& y_{ij0t}x_{ij(t+1)} \\ &+ \bar{\alpha}_{ijt}y_{ij1t}x_{i(j+1)(t+1)} \\ &+ y_{ij2t}x_{i(j+2)(t+1)} \\ &+ \alpha_{ijt}y_{ij1t}x_{(i-1)(j+1)(t+1)} \\ &+ \alpha_{ijt}y_{ij2t}x_{(i-1)(j+2)(t+1)}\left(\bar{x}_{(i-1)(j+1)t}\bar{x}_{i(j+1)t}\right).\end{aligned} \tag{3.4}$$

Here, Constraint 3.2 and (3.3) are a group of boolean algebra expressions that characterizes the dynamic of all possible states for a vehicle from time t to arrive at cell $(i.j)$ at time $t + 1$. Here, the auxiliary variable $\hat{x}$ is introduced to form as an activation for this arrival dynamic, which means

if no vehicle occupied cell (i, j) at $t + 1$, we do not need to enforce any traffic condition at time t. These constraints look redundant but are useful in some cases, which will be mentioned later. In particular, there are four possible cases when the cell (i, j) becomes occupied at time $t + 1$ based on the state at time t, that is cell (i, j) is occupied with a vehicle at speed level 0, cell $(i, j - 1)$ is occupied with a vehicle at speed level 1 without lane changing, cell $(i, j - 2)$ is occupied with a vehicle with speed level 2, and cell $(i - 1, j - 1)$ is occupied with a vehicle with speed level 1 and lane changing, and cell $(i - 1, j - 2)$ is occupied with a vehicle with speed level 2 and lane changing. Similarly, Constraint 3.4 characterizes the dynamic of all possible states at the next time step when a vehicle departs from the cell $(i.j)$. In addition, we consider the case when $i = -1$ as that for $i = 1$ to simplify the expression.

Moreover, the direction information follows a similar pattern. We have

$$z_{iju(t+1)} = z_{iju(t+1)}\hat{z}_{iju(t+1)}, \tag{3.5}$$

$$\begin{aligned}\hat{z}_{iju(t+1)} =& y_{ij0t}z_{ijut} \\ &+ \bar{\alpha}_{i(j-1)t}y_{i(j-1)1t}z_{i(j-1)ut} \\ &+ y_{i(j-2)2t}(\bar{z}_{i(j-1)t} + z_{i(j-1)t}y_{i(j-1)2t})z_{i(j-2)ut} \\ &+ \alpha_{(i-1)(j-1)t}y_{(i-1)(j-1)1t}z_{(i-1)(j-1)ut} \\ &+ \alpha_{(i-1)(j-2)t}y_{(i-1)(j-2)2t}z_{(i-1)(j-2)ut}\left(\bar{z}_{(i-1)(j-1)ut}\bar{z}_{i(j-1)ut}\right),\end{aligned} \tag{3.6}$$

$$z_{ijut} = z_{ijut}\hat{z}_{ijut}, \tag{3.7}$$

$$\begin{aligned}\hat{z}_{ijut} =& y_{ij0t}z_{iju(t+1)} \\ &+ \bar{\alpha}_{ijt}y_{ij1t}z_{i(j+1)u(t+1)} \\ &+ y_{ij2t}z_{i(j+2)u(t+1)} \\ &+ \alpha_{ijt}y_{ij1t}z_{(i-1)(j+1)u(t+1)} \\ &+ \alpha_{ijt}y_{ij2t}z_{(i-1)(j+2)u(t+1)}\left(\bar{z}_{(i-1)(j+1)ut}\bar{z}_{i(j+1)ut}\right).\end{aligned} \tag{3.8}$$

This indicates that vehicles will not change their desired directions under management.

As for the speed, the dynamic is relatively complicated as it involves acceleration and deceleration,

$$y_{ijv(t+1)} = y_{ijv(t+1)}\hat{y}_{ijv(t+1)}, \quad \forall v \in V, \tag{3.9}$$

$$\begin{aligned}\hat{y}_{ij1(t+1)} =& \bar{\alpha}_{i(j-1)t} y_{i(j-1)1t} x_{i(j-1)t} \bar{\beta}_{i(j-1)t} \\ &+ (y_{ij0t} x_{ijt} \beta_{ijt} \gamma_{ijt} \\ &+ y_{i(j-2)2t} (\bar{x}_{i(j-1)t} + x_{i(j-1)t} y_{i(j-1)2t}) \\ &\qquad \cdot x_{i(j-2)t} \beta_{i(j-2)t} \bar{\gamma}_{i(j-2)t}) \\ &+ \alpha_{(i-1)(j-1)t} y_{(i-1)(j-1)1t} x_{(i-1)(j-1)t} \bar{\beta}_{(i-1)(j-1)t},\end{aligned} \tag{3.10}$$

$$\begin{aligned}\hat{y}_{ij0(t+1)} =& y_{ij0t} x_{ijt} \bar{\beta}_{ijt} + \bar{\alpha}_{i(j-1)t} y_{i(j-1)1t} x_{i(j-1)t} \beta_{i(j-1)t} \bar{\gamma}_{i(j-1)t} \\ &+ \alpha_{(i-1)(j-1)t} y_{(i-1)(j-1)1t} x_{(i-1)(j-1)t} \beta_{(i-1)(j-1)t} \bar{\gamma}_{(i-1)(j-1)t},\end{aligned} \tag{3.11}$$

$$\begin{aligned}\hat{y}_{ij2(t+1)} =& y_{i(j-2)2t} (\bar{x}_{i(j-1)t} + x_{i(j-1)t} y_{i(j-1)2t}) x_{i(j-2)t} \bar{\beta}_{i(j-2)t} \\ &+ \bar{\alpha}_{i(j-1)t} y_{i(j-1)1t} x_{i(j-1)t} \beta_{i(j-1)t} \gamma_{i(j-1)t} \\ &+ \alpha_{(i-1)(j-1)t} y_{(i-1)(j-1)1t} x_{(i-1)(j-1)t} \beta_{(i-1)(j-1)t} \gamma_{(i-1)(j-1)t} \\ &+ \alpha_{(i-1)(j-2)t} y_{(i-1)(j-2)2t} x_{(i-1)(j-2)t} \\ &\qquad \cdot \bar{\beta}_{(i-1)(j-2)t} \left(\bar{x}_{(i-1)(j-1)t} \bar{x}_{i(j-1)t}\right).\end{aligned} \tag{3.12}$$

$$y_{ijvt} = y_{ijvt}\hat{y}_{ijvt}, \quad \forall v \in V, \tag{3.13}$$

$$\begin{aligned}\hat{y}_{ij1t} =& \bar{\alpha}_{ijt} y_{i(j+1)1(t+1)} x_{i(j+1)(t+1)} \bar{\beta}_{ijt} \\ &+ (y_{i(j+1)0(t+1)} x_{i(j+1)(t+1)} \beta_{ijt} \bar{\gamma}_{ijt} \\ &+ y_{i(j+1)2(t+1)} x_{i(j+1)(t+1)} \beta_{ijt} \gamma_{ijt}) \\ &+ \alpha_{ijt} y_{(i-1)(j+1)1(t+1)} x_{(i-1)(j+1)(t+1)} \bar{\beta}_{ijt},\end{aligned} \tag{3.14}$$

$$\begin{aligned}\hat{y}_{ij0t} =& y_{ij0t}(y_{ij0(t+1)} x_{ij(t+1)} \bar{\beta}_{ijt} \\ &+ \bar{\alpha}_{ijt} y_{ij1(t+1)} x_{ij(t+1)} \beta_{ijt} \gamma_{ijt},\end{aligned} \tag{3.15}$$

$$\begin{aligned}\hat{y}_{ij2t} =& y_{i(j+2)2(t+1)} x_{i(j+2)(t+1)} (\bar{x}_{i(j+1)t} + x_{i(j+1)t} y_{i(j+1)2t}) \bar{\beta}_{ijt} \\ &+ \bar{\alpha}_{ijt} y_{i(j+2)1(t+1)} x_{i(j+2)(t+1)} \\ &\qquad \cdot (\bar{x}_{i(j+1)t} + x_{i(j+1)t} y_{i(j+1)2t}) \beta_{ijt} \bar{\gamma}_{ijt} \\ &+ \alpha_{ijt} y_{(i-1)(j+2)2(t+1)} x_{i(j+2)(t+1)} \bar{\beta}_{ijt}.\end{aligned} \tag{3.16}$$

Here, for each speed level, the first term shows the condition when the speed level remains; the second term shows the speed level is reached from acceleration/deceleration; the third and fourth terms show the lane change operation. Note that here we assume the lane change can happen at speed level 1 and speed level 2. Speed level 2 is the free-flow speed. Recall that we introduced the auxiliary Boolean variables, which is $\hat{y}_{ijvt}$ in Constraint 3.13. The introduction of $\hat{y}_{ijvt}$ is to allow y_{ijvt} being 0 while the right hand side of Constraint 3.14 can be 1. First, when y_{ijvt} is 1, Constraint 3.13 enforces $\hat{y}_{ijvt}$ to be 1 as well, which implies there is no impact on introducing $\hat{y}_{ijvt}$ at all. Constraint 3.14 just describes the dynamic of the vehicle at cell (i, j), that is all possible cells the vehicle may reach in the next time step. When y_{ijvt} is 0, i.e., no vehicle at cell (i, j) at time t, the introduction of $\hat{y}_{ij1t}$ relaxes the right hand side of Constraint 3.14 to be any value, either 0 or 1. This is necessary. For example, if one vehicle is located at its nearby cell $(i-1, j)$, and changes lane at time t, it will result in $y_{i(j+1)1(t+1)} = 1$ and $x_{i(j+1)(t+1)} = 1$. Since there is no vehicle at cell (i, j), there is no lane change $\bar{\alpha}_{ijt} = 1$ nor speed change, i.e., $\bar{\beta}_{ijt} = 1$. Hence

the first term on the right hand side of Constraint 3.14 will take 1 as its value. Hence if $\hat{y}_{ij1t}$ is not introduced, this constraint will ban the lane change of nearby cells. To avoid similar potential issues, we just introduce the auxiliary Boolean variables for each vehicle dynamic constraint.

Next, we provide the criteria for the boundary conditions.

Boundary and Initial conditions.

Besides the management strategy provided above, we provide the boundary condition. First, we consider the constraints related to J^-, i.e., incoming vehicles for this road segment. Because a rolling-horizon method is used, which can update the newly arrived vehicles at each time step, we simply neglect the impact of future incoming vehicles when we solve each planning horizon, i.e., assuming the boundary condition for incoming vehicles is always 0. In addition, we consider the constraints related to J^+, i.e., vehicles that have passed the intersection. Recall that $n = 0, 1, 2$ represents Red, Through, and Left phases, respectively, and $u = 0, 1, 2$ represent Through Left and Right desired direction of vehicles. Hence, let η_{iun} be the capability of a vehicle passing the intersection under various combinations of direction and signals, we have

$$\eta_{iun} = \begin{cases} 1, & \text{if } u = 0, n = 1, \\ 1, & \text{if } u = 1, n = 2, \\ 1, & \text{if } u = 2, n = \{0, 1, 2\}, i = 0, \\ 0, & \text{otherwise.} \end{cases} \tag{3.17}$$

Here, the first case indicates that the through traffic can pass at the through phase, the second case is that the left traffic passes at the left phase, while the third case is that the right traffic can pass at any phase at the right lane.

Then, for $i \in I$, $t \in T\backslash\{T\}$we have

$$x_{iJ(t+1)} = \sum_{n\in N, u\in U} s_{nit}\eta_{iun}\big(x_{i(J-1)t}y_{i(J-1)1t}z_{i(J-1)ut} + \left(\bar{x}_{i(J-1)t} + x_{i(J-1)t}y_{i(J-1)2t}\right)x_{i(J-2)t}y_{i(J-2)2t}z_{i(J-2)ut}\big), \quad (3.18)$$

which involves the cases that the traffic passing through the intersection at speed level 1 and 2.

Considering the traffic rules, where vehicles should not change lanes near the intersection, we add the following constraint.

$$\alpha_{ijt} = 0, j \in \{J - J_0, J - J_0 + 1, ..., J - 1\}, \quad (3.19)$$

where J_0 is the length of the region where the lane change is forbidden.

Then we discuss about the initial condition. Suppose at time $t = 0$, the traffic state is observed as $\{x^0_{ij}, y^0_{ijv}, z^0_{iju}\}$ for $i \in I, j \in J, v \in V, u \in U$. Then we simply have

$$x_{ij0} = \begin{cases} x^0_{ij}, & j \in J, \\ 0, & j \in J^- \cup J^+, \end{cases} \quad (3.20)$$

$$y_{ijv0} = \begin{cases} y^0_{ijv}, & j \in J, \\ 0, & j \in J^- \cup J^+, \end{cases} \quad (3.21)$$

$$z_{iju0} = \begin{cases} z^0_{iju}, & j \in J, \\ 0, & j \in J^- \cup J^+. \end{cases} \quad (3.22)$$

Variable Feasibility.

Note that only if a vehicle occupies the cell (i, j), i.e., $x_{ijt} = 1$, the cell can have other meaningful states and movements, such as speed, direction,

and speed/lane change. Hence,

$$\sum_{v \in V} y_{ijvt} = x_{ijt}, \tag{3.23}$$

$$\sum_{u \in U} z_{iju t} = x_{ijt}, \tag{3.24}$$

$$\alpha_{ijt} \leqslant x_{ijt}, \tag{3.25}$$

$$\beta_{ijt} \leqslant x_{ijt}. \tag{3.26}$$

To maintain the count of vehicles stable, we need to apply the conservation law,

$$\sum_{i \in I, j \in J \cup J^- \cup J^+} x_{ijt} + \sum_{i \in I, \tau \in \{0,1,\ldots,t-1\}} x_{iJ\tau} = M_0, \tag{3.27}$$

where the first term is the total number of vehicles on the road segment, the second term is the total number of vehicles that have passed the intersection, and M_0 is the initial number of vehicles.For notional connivance, we define $C^0(\boldsymbol{x}, \boldsymbol{y}, z, \boldsymbol{\alpha}, \boldsymbol{\beta}, \boldsymbol{\gamma})$ as the constraint set containing all constraints, i.e., Constraints 3.2 - 3.27. Therefore, the management strategy, i.e., the Sorting Problem, can be modeled as the following binary programming,

$$\begin{aligned} \text{(SP)} \qquad & \max_{\boldsymbol{x}, \boldsymbol{y}, z, \boldsymbol{\alpha}, \boldsymbol{\beta}, \boldsymbol{\gamma} \in C^0(\boldsymbol{x}, \boldsymbol{y}, z, \boldsymbol{\alpha}, \boldsymbol{\beta}, \boldsymbol{\gamma})} \sum_{i \in I, t \in T} w_x(t) x_{iJt} \\ & - \sum_{i \in I j \in J, t \in T} (c_\alpha(j) \alpha_{ijt} + c_\beta \beta_{ijt}) \\ & - \sum_{i \in I j \in J, t \in T, v \in \{0,1\}} c_y(v) y_{ijvt}. \end{aligned}$$

Rolling-Horizon Scheme

Note that SP handles the scenario of complete information, i.e., all vehicle information is given at the beginning as initial conditions. The optimal decision will be the control of all vehicles over T. However, new vehicles will always arrive in the system in reality. Hence, we will need to

extend the above strategy to be adaptive concerning any arrival scenarios.

In theory, as the states of arrival vehicles are uncertain, the optimal management policy should be obtained through a stochastic programming structure, which leads to a huge problem scale and intractability. Given the practical need, we consider an adaptive rolling-horizon strategy. Suppose we solve a problem with the entire time horizon $T^L = \{0, 1, ..., T_{max}\}$ with a rolling horizon length $T + 1$. Let $T(\tau) = \{\tau, \tau + 1, ..., \tau + T\}$ be the moving planning horizon starting at τ. For demonstration convenience, we define the time index mapping $\Gamma(t; \tau) = t - \tau$ to convert the actual time index t to the corresponding time index inside the moving horizon $T(\tau)$. Then we have Rolling-Horizon SP Algorithm (5.2). Step 0: At time 0, initialize the planning horizon $T = T(0)$; obtain the state of all vehicles in the sorting area $\{x^0_{ij}, y^0_{ijv}, z^0_{iju}\}$ and signal phase $\{s_{nt}\}_{t\in T(0)}$;

Step 1: At time τ, solve SP within planning horizon $T(\tau)$, and obtain management strategy $\{\alpha_{ij\Gamma(t;\tau)}, \beta_{ij\Gamma(t;\tau)}, \gamma_{ij\Gamma(t;\tau)}\}_{t\in T(\tau)}$;

Step 2: Utilize the one-step movement $\{\alpha_{ij\Gamma(0;\tau)}, \beta_{ij\Gamma(0;\tau)}, \gamma_{ij\Gamma(0;\tau)}\}$ and vehicle dynamics constraint to obtain $\{x_{ij\Gamma(1;\tau)}, y_{ijv\Gamma(1;\tau)}, z_{iju\Gamma(1;\tau)}\}$ as new vehicle states;

Step 3: Update the initial vehicle state $\{x^0_{ij}, y^0_{ijv}, z^0_{iju}\}$ $\leftarrow$the combination of $\{x_{ij\Gamma(1;\tau)}, y_{ijv\Gamma(1;\tau)}, z_{iju\Gamma(1;\tau)}\}$ and new arrivals;

Step 4: Update $\tau \leftarrow \tau + 1$; update the rolling horizon to $T(\tau)$,and the signal phase to $\{s_{n\Gamma(t;\tau)}\}_{t\in T(\tau)}$;

Go back to Step 1 until $\tau+T > T_{max}$. With Algorithm (5.2), our strategy can be applied to an infinitely long time of management scenarios. The overarching framework of management strategy is shown in Fig. 3.3.

Linearization reformulation

Note that the above formulation of SP contains Boolean algebra equations which are not linear. Fortunately, we can simply convert them into corresponding linear forms. In particular, for constraints with multiplications

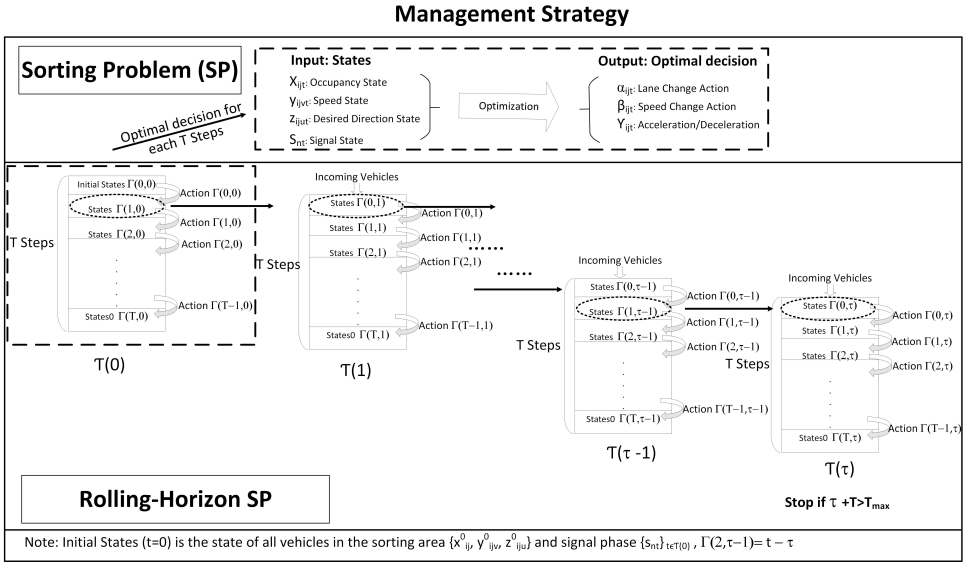

Figure 3.3: Management Strategy

of arbitrary many binary variables, i.e., $y = \Pi_{\xi=1}^{p} x_\xi$ we have its equivalent linear constraints reformulation as follows.

$$
\begin{aligned}
& w \geqslant \sum_{\xi=1}^{p} x_\xi - p + 1, \\
& w \leqslant x_\xi, \ \forall \xi, \\
& w \in \{0, 1\}.
\end{aligned}
$$

Hence, SP is equivalent to a linear integer programming problem, which can be solved by commercial solvers such as Gurobi. For modeling conciseness, we omit the reformulation of each nonlinear constraint with multiplications.

Methodology Extension

Our framework is easy to be extended into various scenarios. In this section, we show a series of extension examples, which include but are not

limited to multi-lane, mixed traffic, and downstream congestion scenarios. Each extension scenario is revised based on the basic case we introduced above. The combination of different extension scenarios can also be easily incorporated but is omitted here.

Multi-Lane Road Segment

We first extend the above basic model into its multi-lane version. In particular, we need to modify the road geometry, slightly adjust the vehicle dynamic for changing lanes, and revise the boundary condition. Objective and Constraints that haven't mention remain the same as the basic case.

To capture the road geometry of multi-lane in general, we extend the index of each cell into (i, j), where $i \in I := \{i_{min}, i_{min} + 1, ..., i_{max} - 1, i_{max}\}$, while $j \in J^-, J, J^+$ remain the same as the two-lane case.

Further, we extend the vehicle dynamic constraints of lane changing in the multi-lane scenario. Note that vehicles on the side lanes such as lane i_{min} and lane i_{max} can only change lanes to one direction, i.e., lane $i_{min} + 1$ and $i_{max} - 1$. Respectively, while vehicles on other mid-lanes $i \in I \backslash \{i_{min}, i_{max}\}$ can change lanes to two directions. For notation convenience, we set $i_{min} - 1$ takes the value of $i_{min} + 1$ in the corresponding subscript. Thus, vehicle dynamic Constraints 3.2 - 3.4 are revised as follows.

$$x_{ij(t+1)} = x_{ij(t+1)}\hat{x}_{ij(t+1)}, \tag{3.28}$$

$$\hat{x}_{ij(t+1)} = \begin{cases} y_{ij0t}x_{ijt} + \bar{\alpha}_{i(j-1)t}y_{i(j-1)1t}x_{i(j-1)t} \\ \quad + y_{i(j-2)2t}(\bar{x}_{i(j-1)t} + x_{i(j-1)t}y_{i(j-1)2t})x_{i(j-2)t} \\ \quad + \alpha_{(i+1)(j-1)t}y_{(i+1)(j-1)1t}x_{(i+1)(j-1)t} \\ \quad + \alpha_{(i-1)(j-1)t}y_{(i-1)(j-1)1t}x_{(i-1)(j-1)t} \\ \quad + \alpha_{(i+1)(j-2)t}y_{(i+1)(j-2)2t}x_{(i+1)(j-2)t}\left(\bar{x}_{(i+1)(j-1)t}\bar{x}_{i(j-1)t}\right) \\ \quad + \alpha_{(i-1)(j-2)t}y_{(i-1)(j-2)2t}x_{(i-1)(j-2)t}\left(\bar{x}_{(i-1)(j-1)t}\bar{x}_{i(j-1)t}\right), \\ \qquad\qquad i \in I\backslash\{i_{min}, i_{max}\}, \\ y_{ij0t}x_{ijt} + \bar{\alpha}_{i(j-1)t}y_{i(j-1)1t}x_{i(j-1)t} \\ \quad + y_{i(j-2)2t}(\bar{x}_{i(j-1)t} + x_{i(j-1)t}y_{i(j-1)2t})x_{i(j-2)t} \\ \quad + \alpha_{(i-1)(j-1)t}y_{(i-1)(j-1)1t}x_{(i-1)(j-1)t} \\ \quad + \alpha_{(i-1)(j-2)t}y_{(i-1)(j-2)2t}x_{(i-1)(j-2)t}\left(\bar{x}_{(i-1)(j-1)t}\bar{x}_{i(j-1)t}\right), \\ \qquad\qquad i = \{i_{min}, i_{max}\}, \end{cases} \tag{3.29}$$

$$x_{ijt} = x_{ijt}\hat{x}_{ijt} \tag{3.30}$$

$$\hat{x}_{ijt} = \begin{cases} y_{ij0t}x_{ij(t+1)} \\ \quad +\bar{\alpha}_{ijt}y_{ij1t}x_{i(j+1)(t+1)} \\ \quad +y_{ij2t}x_{i(j+2)(t+1)} \\ \quad +\alpha_{ijt}y_{ij1t}x_{(i+1)(j+1)(t+1)} \\ \quad +\alpha_{ijt}y_{ij1t}x_{(i-1)(j-1)(t+1)} \\ \quad +\alpha_{ijt}y_{ij2t}x_{(i+1)(j+2)(t+1)}\left(\bar{x}_{(i+1)(j+1)t}\bar{x}_{i(j+1)t}\right) \\ \quad +\alpha_{ijt}y_{ij2t}x_{(i-1)(j+2)(t+1)}\left(\bar{x}_{(i-1)(j+1)t}\bar{x}_{i(j+1)t}\right), \\ \qquad\qquad i \in I\backslash\{i_{min}, i_{max}\}, \\ y_{ij0t}x_{ij(t+1)} \\ \quad +\bar{\alpha}_{ijt}y_{ij1t}x_{i(j+1)(t+1)} \\ \quad +y_{ij2t}x_{i(j+2)(t+1)} \\ \quad +\alpha_{ijt}y_{ij1t}x_{(i-1)(j+1)(t+1)} \\ \quad +\alpha_{ijt}y_{ij2t}x_{(i-1)(j+2)(t+1)}\left(\bar{x}_{(i-1)(j+1)t}\bar{x}_{i(j+1)t}\right), \\ \qquad\qquad i = \{i_{min}, i_{max}\}. \end{cases} \tag{3.31}$$

Constraints for the desired direction $\{z_{ijut}\}$ and speed information $\{y_{ijvt}\}$, i.e., Constraints 3.5 – 3.16, are revised correspondingly with a similar pattern, which are omitted here due to the page limit.

As for the boundary conditions with multi-lanes, we adjust Constraints 3.17 from the basic case as follows to show only the rightest lane allows right turn during the through phase,

$$\eta_{iun} = \begin{cases} 1, & \text{if } u = 0, n = 1, \\ 1, & \text{if } u = 1, n = 2, \\ 1, & \text{if } u = 2, n = \{0, 1, 2\}, i = i_{min}, \\ 0, & \text{otherwise.} \end{cases} \tag{3.32}$$

We summarize the above revised constraints for the multi-lane scenario and denote them by $C^{ML}(x, y, z, \alpha, \beta, \gamma)$. Therefore, the management strategy for the multi-lane scenario can be modeled as the following problem.

$$\begin{aligned}(\text{MLSP}) \qquad & \max_{x,y,z,\alpha,\beta,\gamma \in C^{ML}(x,y,z,\alpha,\beta,\gamma)} \sum_{i\in I, t\in T} w_x(t) x_{iJt} \\ & - \sum_{i\in Ij\in J, t\in T} (c_\alpha(j)\alpha_{ijt} + c_\beta \beta_{ijt}) \\ & - \sum_{i\in Ij\in J, t\in T, \nu\in\{0,1\}} c_y(\nu) y_{ij\nu t}.\end{aligned}$$

Mixed Traffic

Besides the multi-lane scenario, we further extend the basic model into its mixed traffic version, that is the traffic can include both CAVs and human-driven vehicles (HDVs). In particular, we add another set of vehicle dynamic constraints for HDVs. To differentiate CAVs with HDVs, we introduce a superscript for each decision variables as $x^{type}, y^{type}, z^{type}, \alpha^{type}, \beta^{type}, \gamma^{type}, type \in \{CAV, HDV\}$. Further, for notation convenience, we further define x_{ijt} as the value of $x_{ijt}^{CAV} + x_{ijt}^{HDV}$, which helps the boundary conditions and variable feasibility remain a similar form of the basic model. The other decision variables $y_{ijvt,} z_{ijut}, \alpha_{ijt}, \beta_{ijt}, \gamma_{ijt}$ are set correspondingly with a similar pattern.

Since HDVs will not follow a centralized control strategy, and in many states changing lanes close to the intersection is illegal (such as Ohio and Arizona) we assume that HDVs should not change lanes when they approach an intersection.magenta

$$\alpha_{ijt}^{HDV} = 0, j \in \{J - j^*, J - j^* + 1, ...J - 1\}.$$

Here, $j \in \{J-j^*, J-j^*+1, ...J-1\}$ is the corresponding area where HDVs should not change lanes.

Note that due to the existence of both CAVs and HDVs, we need to revise the vehicle dynamics at speed level 2. Thus, Constraints 3.2 -- 3.4 are revised based on the type of vehicles as follows.

$$x^{type}_{ij(t+1)} = x^{type}_{ij(t+1)} \hat{x}^{type}_{ij(t+1)}, \tag{3.33}$$

$$\begin{aligned}\hat{x}^{type}_{ij(t+1)} =& y^{type}_{ij0t} x^{type}_{ijt} \\ &+ \bar{\alpha}^{type}_{i(j-1)t} y^{type}_{i(j-1)1t} x^{type}_{i(j-1)t} \\ &+ y^{type}_{i(j-2)2t} (\bar{x}_{ijt} + x_{ijt} y_{ij2t}) x^{type}_{i(j-2)t} \\ &+ \alpha^{type}_{(i-1)(j-1)t} y^{type}_{(i-1)(j-1)1t} x^{type}_{(i-1)(j-1)t} \\ &+ \alpha^{type}_{(i-1)(j-2)t} y^{type}_{(i-1)(j-2)2t} x^{type}_{(i-1)(j-2)t} \left(\bar{x}^{type}_{(i-1)(j-1)t} \bar{x}^{type}_{i(j-1)t} \right),\end{aligned} \tag{3.34}$$

$$x^{type}_{ijt} = x^{type}_{ijt} \hat{x}^{type}_{ijt}, \tag{3.35}$$

$$\begin{aligned}\hat{x}^{type}_{ijt} =& y^{type}_{ij0t} x^{type}_{ij(t+1)} \\ &+ \bar{\alpha}^{type}_{ijt} y^{type}_{ij1t} x^{type}_{i(j+1)(t+1)} \\ &+ y^{type}_{ij2t} x^{type}_{i(j+2)(t+1)} \\ &+ \alpha^{type}_{ijt} y^{type}_{ij1t} x^{type}_{(i-1)(j+1)(t+1)} \\ &+ \alpha^{type}_{ijt} y^{type}_{ij2t} x^{type}_{(i-1)(j+2)(t+1)} \left(\bar{x}^{type}_{(i-1)(j+1)t} \bar{x}^{type}_{i(j+1)t} \right).\end{aligned} \tag{3.36}$$

Constraints for the desired direction $\{z_{ijut}\}$ and speed information $\{y_{ijvt}\}$, i.e., Constraints 3.5 – 3.16, are revised correspondingly with a similar pattern, which are omitted here due to the page limit.

We summarize the above revised constraints for the mixed-traffic scenario and denote them by $C^{Mix}(x, y, z, \alpha, \beta, \gamma)$. Therefore, the management strategy for the mixed-traffic scenario can be modeled as the follow-

ing problem.

$$\begin{aligned}(\text{MixSP}) \qquad & \max_{x,y,z,\alpha,\beta,\gamma \in C^{Mix}(x,y,z,\alpha,\beta,\gamma)} \sum_{i\in I, t\in T} w_x(t) x_{iJt} \\ & - \sum_{i\in I j\in J, t\in T} (c_\alpha(j)\alpha_{ijt} + c_\beta \beta_{ijt}) \\ & - \sum_{i\in I j\in J, t\in T, v\in\{0,1\}} c_y(v) y_{ijvt}.\end{aligned}$$

Downstream Congestion

Furthermore, we extend the basic model to consider the possible downstream congestion. We only need to focus on the boundary condition, the rest constraints remain the same as the basic case.

We introduce a binary indicator s'_{it} to capture the downstream traffic condition, where it takes 1 if the downstream traffic is not congested, and 0, otherwise. Then, Constraint 3.18 can be revised as follows,

$$\begin{aligned}x_{iJ(t+1)} = \sum_{n\in N, u\in U} & s'_{it} s_{nit} \eta_{iun} (x_{i(J-1)t} y_{i(J-1)1t} z_{i(J-1)ut} \\ & + \left(\bar{x}_{i(J-1)t} + x_{i(J-1)t} y_{i(J-1)2t}\right) x_{i(J-2)t} y_{i(J-2)2t} z_{i(J-2)ut}).\end{aligned}$$

Here, vehicles will be blocked at the intersection if the downstream traffic is congested, i.e., $s'_{it} = 0$, even if the signal is green s_{nit}=1.

We summarize the above revised constraints for the possible downstream congestion scenario and denote them by $C^{DC}(x, y, z, \alpha, \beta, \gamma)$. Therefore, the management strategy for the possible downstream congestion

scenario can be modeled as the following problem.

$$\begin{aligned}(\text{DCSP}) \qquad & \max_{x,y,z,\alpha,\beta,\gamma \in C^{DC}(x,y,z,\alpha,\beta,\gamma)} \sum_{i\in I, t\in T} w_x(t) x_{iJt} \\ & - \sum_{i\in Ij\in J, t\in T} (c_\alpha(j)\alpha_{ijt} + c_\beta \beta_{ijt}) \\ & - \sum_{i\in Ij\in J, t\in T, \nu\in\{0,1\}} c_y(\nu) y_{ij\nu t}.\end{aligned}$$

3.3 Case Study

In this section, we conduct a series of case studies to show the effectiveness of the proposed sorting strategy. To achieve this goal, we first provide a benchmark case and illustrate the detailed operations over the entire sorting area step-by-step. Then, a sensitivity analysis is conducted to reveal interesting managerial insights. Later on, the sorting strategy is compared with several scenarios, such as those without any management strategies. All algorithms are solved by Gurobi on a desktop computer with i7-10700F CPU @2.90 GHz and 16.0GB RAM.

First, the fundamental settings in the benchmark case are as follows. We set a road segment with two lanes with a speed limit of 12 m/s (≈26.8 mph). This sorting area is set to a grid withmagenta 6 m length for each cell and ten columns of cells in total (i.e., 60 m), which guarantees one vehicle can pass one cell per second at the speed limit. Let the time unit be one second and the length for a rolling planning horizon be 15 seconds. The cycle of the signal phases is 60 seconds with 30 seconds green phase and 30 seconds red phase. In addition, the length of the region forbidding lane changes is set to 2 cells (12 m) ahead of the intersection.

To validate the correctness of our proposed sorting strategy, we consider a simple benchmark case, where the through and left-turn phases are both 15 seconds. The new vehicles arriving in the sorting area are

assumed to be random at a certain probability for each lane at each step, called the arrival rate. We set the arrival rate to be 0.7 in the benchmark case. In addition, we investigate two representative cases for vehicles with different directions. Traditionally, a two-lane road segment with Left-turn and Through traffic is usually split into two dedicated lanes, where the left lane only allows Left-turns and the right lane allows Through and Right-turn traffic. Hence, the arrival vehicles must follow the restrictions of lanes, i.e., Left-turn traffic arrives at the left lane, while the other traffic arrives at the right lane. We name this scenario of arrival vehicles as "traditional input". For the traditional input case, we set the turning movement ratio as Through: Right-turn = 5:2. On the other hand, the design of the sorting strategy can allow more flexible traffic arrivals. There is no need to enforce the vehicles on the left (right) lane to be Left-turn (Right-turn or Through) traffic through coordinated lane changes. Hence, we allow the traffic with different directions to arrive at both lanes. We name this scenario "random input." For the random input case, we set the turning movement ratio as Through: Left-turn: Right-turn = 5:7:2 to reach a similar turning movement ratio with traditional input. Based on these settings, a sample result of the proposed sorting algorithm is shown in Fig.5.4 for demonstration convenience. Since there are 30 seconds for the red phase, where vehicles are almost waiting and not moving, we show the traffic state and operations during the green phase. In these figures, the bird view of the sorting area is plotted for each time step, the driving direction of vehicles is from left to right, and the intersection is on the right end of the road.

Specifically, the 11 columns in each bird view plot correspond to the whole sorting area (Columns 0-9) and the exiting buffer zone (Column 10). A vehicle occupying a specific cell is plotted with colors, showing its speed status (where "red" indicate stop, "yellow" indicate speed level 1, and "green" indicate speed level 2). The arrow on each vehicle indicates

its desired direction. The light in the front/back of each vehicle shows its acceleration/declaration action. In addition, the lane change actions are illustrated by arrows across the cells (where solid arrows indicate the lane change action and hollow arrows indicate the vehicle just finished the lane change). Graphics, including crossmark and arrows with directions, in the right gray area, shows the corresponding signal phases at that particular time step.

Fig.**??** shows the green phase example under sorting for a traditional input case. It is observed that from time 59 to time 64, on the Through phase, those Left-turn vehicles gather and wait in the left lane. Meanwhile, Through and Right-turn vehicles gather in the right lane to pass the intersection, intuitive. Interestingly, Left-turn vehicles leave a cell at the left lane just before the intersection to pass more Through and Right-turn vehicles under sorting operations. A more interesting sorting pattern can be seen from time 71 to time 74. Since the signal phase switches from the Through to the Left-turn at time 75, those Left-turn vehicles are wisely sorted and grouped in advance at the front of the sorting area to maximize the utilization in the following phase.

Similar sorting patterns are also observed in the result of the random input case, as shown in Fig.**??**. Intuitively, since the incoming vehicles are not located based on their desired directions, more actions of lane change are necessary.

To choose hyper-parameters in the objective function mentioned in Equation (5.18), we conduct a series of sensitivity analysis by introducing a variable k. The k is set to vary from 10^{-6} to 10 with the common ratio 10. The result is shown in Table (5.2). After sensitivity analysis, we choose hyper-parameters with the largest throughput. Thus, we set $w_x(t) = \frac{10^3(15-t)}{15}$, $c_\alpha(j) = j$, $c_\beta = 10^{-5}$, $c_y(0) = 10^{-3}$, and $c_y(1) = c_y(2) = 0$ as hyper-parameters.The average computational time for solving the Rolling-Horizon SP is controlled to less than one second.

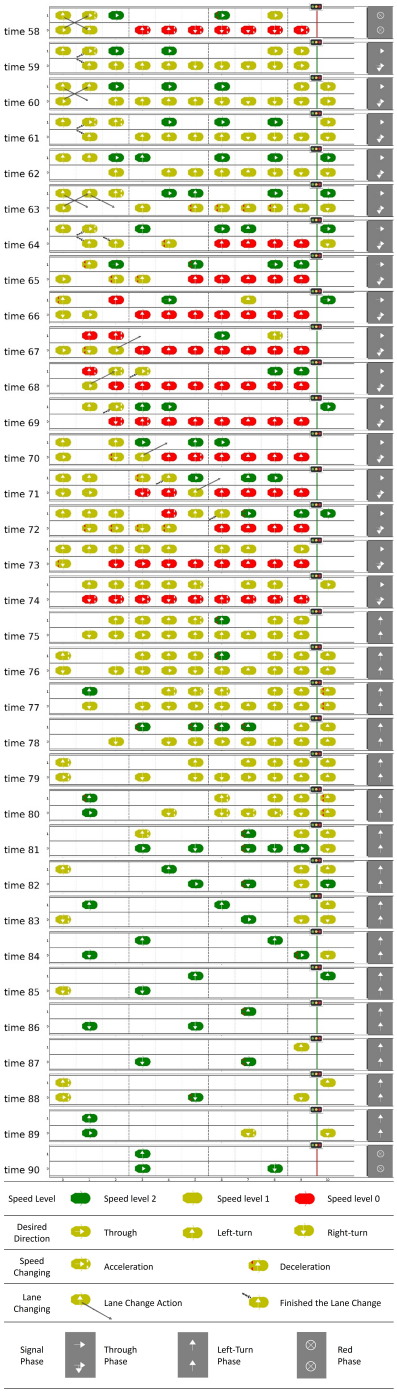

Figure 3.4: Sample Results of Sorting for a Traditional Input Case

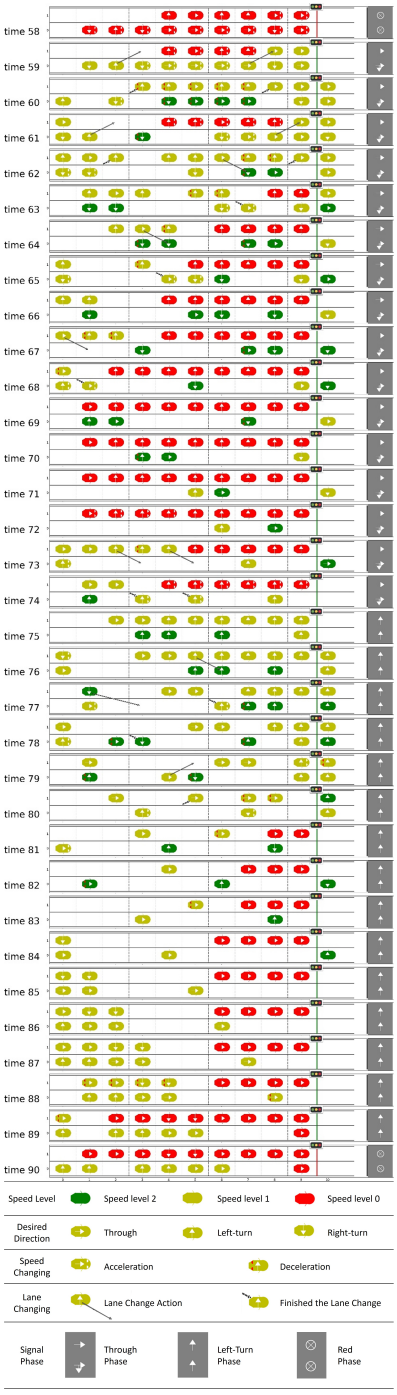

Figure 3.5: Sample Results of Sorting for a Random Input Case

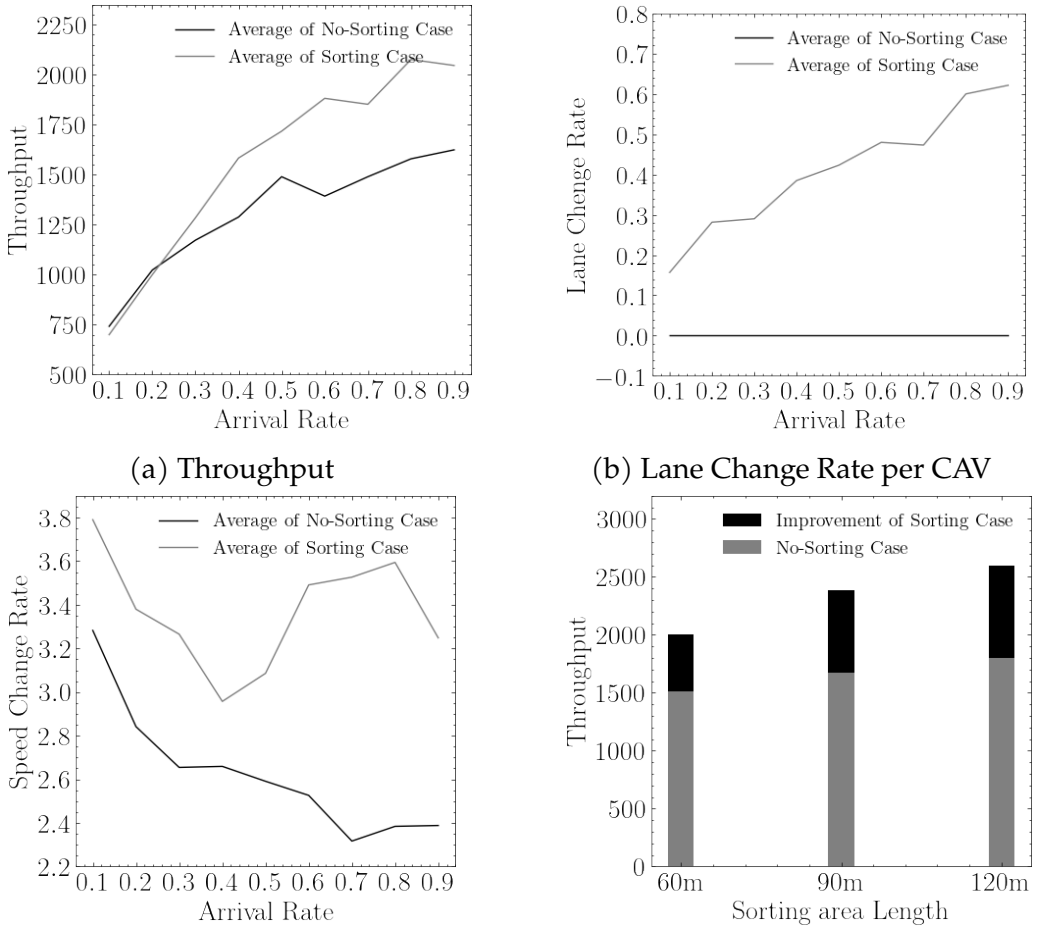

(a) Throughput

(b) Lane Change Rate per CAV

(c) Speed Change Rate per CAV

(d) Impact of Sorting Area Length

Figure 3.6: Performance comparison with and without implementing the sorting strategy under varying arrival rates.

	Throughput			
k	$w_x(t) = \frac{10^5(15-t)}{15}k$	$c_\alpha(j) = jk$	$\mathbf{c_\beta = k}$	$c_y(0) = k$
0	-	1760	1637	1043
10^{-6}	1600	1555	1886	1842
10^{-5}	1654	1782	**2046**	1923
10^{-4}	1645	1700	2034	1880
10^{-3}	1720	1811	1985	**2046**
10^{-2}	**2046**	1609	1967	1695
10^{-1}	1991	1877	1877	1717
1	1934	**2046**	1540	1542
10	1968	1963	1335	1434

Benchmark: $w_x(t) = 10^3(1 - \frac{1}{15}t)$, $c_\alpha(j) = j$, $c_\beta = 10^{-5}$, $c_y(0) = 10^{-3}$, and $c_y(1) = c_y(2) = 0$.

Table 3.1: Sensitivity Analysis

Moreover, to evaluate the effectiveness of the proposed sorting strategy, we compare its performance with the corresponding counterpart without using the sorting strategy. To remove the lane change impact, we focus on traditional input when no sorting strategy is implemented, denoted by the No-Sorting case. First, to investigate the impact of different arrival rates, the other parameters remain the same as the benchmark case. The arrival rate is set to vary from 0.1 to 0.9 with 0.1 intervals. For demonstration convenience, we define the number of vehicles passing through the intersection per hour as throughput and the average number of lane changes and speed changes per vehicle as lane change rate" and "speed change rate", respectively. Due to the uncertainty of incoming traffic states, we run the Monte Carlo simulation ten times for each case, with 300 seconds, i.e., 300 time-step for every single run.

The results are shown in Fig.**??**. For each case, the mean values of Monte Carlo simulation results are plotted as curves to show the trend. Comparing the performance between the sorting and the no-sorting cases, we find that the sorting strategy always increases the throughput. Espe-

cially when the arrival rate is above 0.5, i.e., the traffic is relatively busy, the throughput improvement under the sorting strategy is significant. The result shows that it achieves the maximum throughput (i.e., 2046) when the arrival rate is 0.9, and the improvement from the benchmark throughput (i.e., 1624) is about 26%magenta On the other hand, we also investigate the impact of the sorting area length. The variation of the sorting area length is set to 60m (10 cells), 90m (15 cells), and 120m (20 cells). We choose 0.9 as the arrival rate and the other parameters remain the same as the benchmark case, The result is shown as the last figure in Fig.**??**. It shows that with the increasing sorting area length, the throughput improvement of the proposed sorting strategy increases. In particular, the throughput improvement for a 120m sorting area can reach over 44%.

Next, we further investigate the impact of signal phases and the ratio of vehicle directions. We fixed the 30s red phase and the arrival rate to be 0.7, under a random input setting. Three representative cases of signal phases are selected, including the Left-turn dominating phase "T5L25" (i.e., 5s Through phase, 25s Left-turn phase,), the balanced phase "T15L15" (i.e., 15s Through phase, 15s Left-turn phase), and the Through dominating phase "T25L5" (i.e., 25s Through phase, 5s Left-turn phase). As for the vehicle direction, we also select five representative direction portfolios, including the count-balanced direction case "111" (i.e., Through:Left-turn:Right-turn = 1:1:1), signal-balanced case "121" (Through:Left-turn:Right-turn = 1:2:1), right-turn dominating case "118" (Through:Left-turn:Right-turn = 1:1:8), Left-turn dominating case "181" (Through:Left-turn:Right-turn = 1:8:1), and Through dominating case "811" (Through:Left-turn:Right-turn movement = 8:1:1).

Based on these settings, Table 4.3 shows the result under different combinations of signal phases and direction ratios. First, for the throughput, it is observed that Through movement dominating case "811" and Right-turn movement dominating case "118" show the same trend, increasing

Table 3.2: Performance among Different Turning Movement Ratio with Different Signal Phases.

Ratio of Vehicle Directions (Through:Left-turn:Right-turn)	Signal Phase (Through:Left-turn)	Throughput			Lane Change Rate			Speed Change Rate		
		Max	Mean	Min	Max	Mean	Min	Max	Mean	Min
1:1:1	T5L25	1416	1291	1200	0.5	0.4	0.4	3.2	3.1	2.7
	T15L15	1908	1761	1596	0.5	0.5	0.4	3.6	3.4	3.1
	T25L5	1680	1404	1068	0.5	0.5	0.3	4.1	3.8	3.2
1:1:8	T5L25	2652	2558	2496	0.6	0.5	0.5	2.4	2.4	2.3
	T15L15	2784	2625	2532	0.6	0.5	0.5	2.6	2.4	2.2
	T25L5	2940	2620	2184	0.6	0.5	0.5	2.8	2.4	2.2
1:2:1	T5L25	1608	1459	1356	0.3	0.3	0.2	3.4	3.1	2.9
	T15L15	1884	1706	1620	0.5	0.4	0.2	3.4	3.0	2.7
	T25L5	1128	1022	960	0.4	0.4	0.4	3.1	2.9	2.5
1:8:1	**T5L25**	1956	1876	1788	0.4	0.4	0.4	3.2	2.9	2.7
	T15L15	1596	1526	1428	0.4	0.3	0.3	3.8	3.5	3.3
	T25L5	852	792	744	0.3	0.2	0.1	4.2	3.9	3.7
8:1:1	T5L25	900	830	756	0.5	0.5	0.4	3.4	3.3	4.0
	T15L15	1644	1574	1488	0.5	0.5	0.4	3.8	3.5	3.4
	T25L5	2016	1912	1764	0.6	0.4	0.3	4.4	4.1	3.9

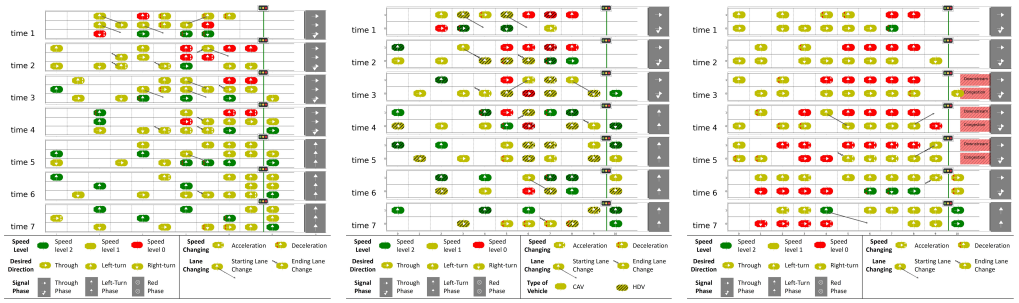

(a) Multi-lane Scenario (b) Mixed-Traffic Scenario (c) Downstream Congestion Scenario

Figure 3.7: Extended Scenarios

with the increasing time of the Through phase. Since the Right-turn traffic can pass the intersection at any phase, the throughput of Case "118" is much larger than others, given its dominating Right-turn traffic. Moreover, the Left-turn dominating case "181" has the opposite trend. These two balanced cases, "111" and "121", have the best performance of throughput at the balanced phase. Hence the throughput highly depends on the alignment of signal timing and the traffic direction.

As for the lane change rate and the speed change rate are almost the highest overall signal phases, these two balance turning movement cases, "111" and "121". This is mainly due to random input, where a balanced

ratio of directions generates more complicated direction states. Comparing the three turning movements dominating case, the Left-turn dominating case ("181") under the Through-turn dominating phase needs more speed change.

Extended Scenarios

Furthermore, we conduct a case study for extended scenarios proposed in Section 3.2 to show the generality of our framework.

For the multi-lane scenario, we use a three-lane road segment as an example. The other parameters remain the same as the benchmark case. We vary for the "traditional input" to fit the multi-lane, Left-turn vehicles can arrive on the left and middle lane, Right-turn vehicles can only arrive on the right lane, and Through vehicles can arrive at any lane.

The example output for the multi-lane scenario is shown in Fig. 3.7a. Interestingly, the sorting pattern can be seen from time 1 to time 7. Since the signal phase switches from the Through to the Left-turn at time 5, those Left-turn vehicles are wisely sorted and grouped in advance at the front of the sorting area to maximize the utilization in the following phase.

Next, for the mixed-traffic scenario, the other parameters remain the same as the benchmark case. We consider a 4-columns length (24 m) area close to the intersection where HDVs should not change lanes. In addition, we set the mixed traffic ratio CAV: HDV as 1:1. An example result is shown in Fig. (3.7b). Although HDVs are uncontrollable, mixed traffic platoons led by CAVs can follow the sorting strategy and indirectly manage HDVs.

For the downstream congestion scenario, with the same parameters set as the benchmark case with the traditional input, we consider a downstream congestion period with three seconds, which is shown in Fig. (3.7c). The downstream congestion happens from time 3 to time 5,magenta where through and left traffic are blocked at the intersection temporarily, even if the signal is green.

3.4 Conclusion and Future Work

In summary, this research established a modeling framework for pure CAV traffic passing through intersections and proposed a rolling time-horizon based CAV sorting strategy to improve the intersection capacity. Given the signal timing for multiple phases, all CAVs with different desired directions can optimally coordinate without additional infrastructure support. To find the best coordination strategy, a mixed-integer programming model with Boolean logic constraints can characterize critical features of the CAV behaviors. Then, an accelerated rolling time-horizon algorithm can be solved by commercial solvers to yield real-time decisions, which can be utilized in practice. A series of numerical experiments have shown that the improvement of the proposed sorting strategy is significant compared with traditional intersections without coordination, especially when the traffic is relatively busy.

There are two major limitations to this study. The first is the description of detailed vehicle dynamics due to the grid representation, such as the heterogeneity of the vehicle length.The second is the scalability of the model. We leave them for future research. For example, we can embed the continuous vehicle dynamic models on top of the grid system and develop an advanced heuristic algorithm to accelerate the algorithm in large-scale instances. Furthermore, the work can also be extended to incorporate more complex traffic scenes such as those with multi-direction and multi-intersection.

4 CELL TRANSMISSION MODEL BASED MACROSCOPIC CAV CONTROL FOR SIGNALIZED INTERSECTIONS

This chapter proposes a novel macroscopic control approach. Unlike traditional microscopic control, this approach considers the collective behavior of vehicles and employs the Cell Transmission Model (CTM) to model traffic dynamics efficiently. The contribution of the model includes the development of a CTM-based CAV control model that integrates lateral and longitudinal control using cells, a rolling-horizon-based solution method for real-time coordination of CAVs, and the demonstration of significant capacity enhancement at signalized intersections through numerical experiments, along with robustness and reliability across diverse traffic conditions.

4.1 Introduction

Connected automated vehicles (CAVs) possess vehicle-to-vehicle (V2V) and vehicle-to-infrastructure (V2I) communication capabilities, enabling them to exchange information with their surroundings. Alongside the automation features of CAVs, these advancements allow for precise individual vehicular-level control. By that, traffic systems have been brought with the potential to significantly enhance their effectiveness of traffic systems via vehicular cooperative control strategies. Despite the rapid progress witnessed in CAV-enabled transportation systems in recent years(Sharma and Zheng, 2021), signalized intersections, which are vital components of urban traffic, continue to experience congestion. This congestion stems from the underutilization of lanes and green time. Therefore, there is still substantial room for improvement in the efficiency of CAV-enabled intersections through better coordination of CAVs.

The prevailing research on employing CAV technology at intersections

can be largely classified into two main categories. The first category concentrates on optimizing individual vehicle trajectories to improve traffic flow. Researchers are evaluating diverse control algorithms to efficiently direct CAVs through intersections, with a specific emphasis on reducing stops, minimizing delays, and enhancing overall traffic performance (Li et al., 2021a; Chen et al., 2021b; Dong et al., 2022; Mirheli et al., 2018). Concurrently, the second category aims to increase intersection capacity by addressing challenges related to limited green light duration and optimal lane utilization. Various methods to boost capacity through coordinated efforts of CAVs are under active investigation, including adjusting individual vehicle control based on signal phases to maximize lane utilization and green light time (Wu and Qu, 2022; Yao et al., 2022a).

While for pure CAV scenarios, these approaches have shown promise in improving intersection performance, but challenges are also posed for large-scale implementation. As the scale of CAV systems increases, the computational time required for individual control becomes a significant hindrance, limiting real-time responsiveness essential for practical applications. Consequently, an alternative approach is urgently needed to address these challenges and achieve efficient and scalable control of CAVs. This substitute approach must encapsulate both effectiveness and scalability, allowing for optimal control over CAVs in various traffic scenarios.

In addressing the challenges associated with traffic management for CAVs, a macroscopic approach is adopted. Specifically, cell Transmission Model (CTM) (Daganzo, 1995, 1994) is utilized, segmenting roadways near intersections into cells for modeling traffic flow and density. This perspective enables a comprehensive understanding of traffic dynamics and the development of scalable and efficient control strategies for CAVs. The connected automated flow control (CAFC) method centers on the CTM framework as shown in Figure 5.1. Road segments near intersections are divided into pre-sorting, sorting, and post-sorting areas. In the pre-sorting

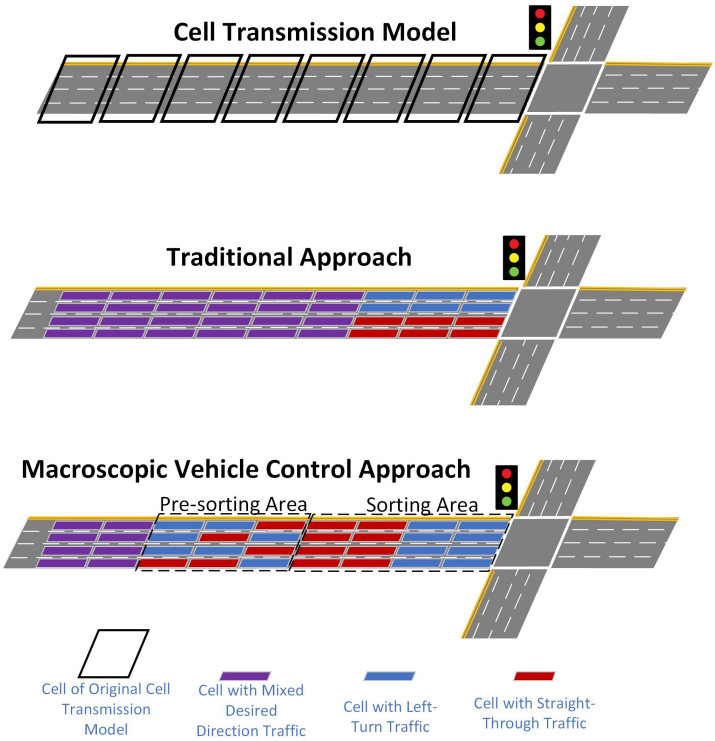

Figure 4.1: Connected automated flow control

area, traffic flows of different movements are separated and directed towards the sorting area. Here, traffic alignment in each cell corresponds with a specific direction, as determined by signal timing, to optimize green time and lane usage. The post-sorting area, conceptualized as a virtual segment, manages vehicles that have passed the intersection. The aim is to improve multilane, signalized intersection efficiency by aligning CAV movements with signal phases, using a macroscopic control approach. This strategy optimizes throughput by regulating cell inflow and outflow, ensuring traffic flow aligns with signal timings and complies with traffic laws. The approach, formulated as a quadratic programming problem, is efficiently solvable by modern solvers, representing a breakthrough in

scalable traffic management for CAV environments.

The subsequent sections of this paper are structured as follows. Section 2 offers an extensive literature review on the subject. In Section 3, we present a comprehensive description of the scenario-based intersection model, addressing the cooperative control problem. The outcomes of the numerical experiments are presented in Section 4. Finally, Section 5 concludes our work, highlighting its contributions, and explores potential avenues for future research.

4.2 Literature Review

Systems, methods, and algorithms to comprehensively improve intersection efficiency have been a subject of research for several decades. One area of research focuses on improving signal timing under various traffic conditions, as documented in previous studies (Sawake and Borkar, 2017; Guo et al., 2019). More recently, researchers have begun exploring pre-signal traffic management as a potential solution. A well-known approach in this domain is the pre-signal system (Xuan et al., 2011), which proposes a tandem design to aggregate traffic in the same direction, allowing them to pass through the intersection efficiently through pre-sorting between the pre-signal and the intersection signal. While this system has shown benefits in improving intersection capacity, it also introduces the need for new infrastructure, potentially leading to new traffic bottlenecks and even worsening traffic conditions, particularly if human-driven vehicles do not adapt well to the complex signal system.

With the development of vehicle automation and communication, CAVs are brought with the ability to achieve precise control manifested by longitudinal (Zhou et al., 2019; Han et al., 2020; Chen et al., 2021a) and lateral control (Wang et al., 2014a; Zhou et al., 2017a; Wang et al., 2021) to achieve car following and lane keeping or lane changing driving

tasks in a precise and efficient manner. The longitudinal control, widely known as Cooperative Cruise Control system, are shown to improve traffic efficiency, throughput and stability(Gong et al., 2016; Öncü et al., 2014; Shi et al., 2021; Zhou et al., 2020). Lateral control, on the other hand, ensures the smoothness of vehicle trajectory and improves the lane change safety(Wang et al., 2014a; Zhou et al., 2017a; Wang et al., 2021; Bevly et al., 2016). Not limited to the research above, which focused on the freeway scenarios, V2I communication enables CAVs to be precisely cooperatively controlled with infrastructure, which shows great potential to increase the efficiency of signalized intersections by vehicle and signal timing coordination (Qian et al., 2021; Xu et al., 2017; Li et al., 2021b), though the majority of research mainly focus on optimizing the vehicles' trajectory in single-lane, single-phase scenarios (Zhou et al., 2017b; Li et al., 2018; Jiang et al., 2017; Dong et al., 2021).

Due to the advantages offered by pre-signal traffic management and the continuous development of CAV technology, recent studies have explored the incorporation of the sorting idea from the pre-signal system into microscopic CAV control. Notably, Wu et al. (2021) addressed the sorting of a constant number of CAVs before passing through a signalized intersection. Furthermore, Yao et al. (2022a) established a microscopic control approach for uncertain CAV traffic with a sorting strategy based on cooperative signal timing.

However, it is important to note that all the aforementioned research primarily focuses on microscopic control, which presents challenges in terms of computation time and scalability. The computational time required for individually controlling a large number of vehicles becomes a critical concern, especially as the scale of CAV systems increases. The computational complexity becomes a bottleneck, hindering real-time responsiveness for practical implementation.

To address the limitations posed by the microscopic control approach,

researchers have considered a macroscopic perspective that encompasses the collective behavior of vehicles rather than focusing on each individual vehicle. One of the approaches employed to achieve this macroscopic view is the CTM, which is a finite differences approximation based on hydrodynamic theory, providing a practical representation of traffic flow and density (Daganzo, 1995, 1994). It employs a piecewise linear function to describe the FD of traffic flow, which convergently approximates a reduced form of the Lighthill-Whitham-Richards (LWR) hydrodynamic model (Lighthill and Whitham, 1955; Richards, 1956).

The value of CTM extends to versatile applications in dynamic traffic scenarios with CAVs. Notably, researchers have integrated CTM to optimize signal timing for CAVs (Yao et al., 2022b; Al Islam et al., 2020; Tajalli et al., 2020). Multiclass CTM builds on this, effectively analyzing mixed traffic scenarios with human-driven and autonomous vehicles (Levin and Boyles, 2016b; Pi et al., 2019; Ngoduy et al., 2021). These studies address complexities introduced by autonomous vehicles, such as reduced following headways, increased capacity, and enhanced backward wave speed. For example, Levin and Boyles (2016b) developed a model accommodating variations in capacity and backward wave speed based on vehicle proportions. Pi et al. (2019) extended this to a spatio-temporal model considering travel modes and vehicle classes, while Ngoduy et al. (2021) proposed a dynamic system optimum formulation for a multi-class dynamic traffic assignment problem. Simultaneously, researchers leverage CTM for dynamic lane reversal strategies tailored to autonomous vehicles, aiming to alleviate traffic congestion and enhance intersection utilization (Duell et al., 2016; Levin and Rey, 2017). Levin and Rey (2017) introduced a CTM formulation for dynamic lane reversal, offering insights for both single-link scenarios and network-wide implementation with stochastic demand. Building on this, Duell et al. (2016) explored the impact of autonomous vehicles on traffic management, emphasizing dynamic lane

reversal to optimize lane configurations in real time. Together, these studies provide crucial perspectives on applying CTM to address challenges in traffic flow dynamics, particularly in the context of autonomous vehicle integration. However, these works do not fully explore the potentials of CAVs in terms of control, especially in a constrained environment (e.g., signalized intersection).

Given these limitations and gaps, there is a pressing need to effectively address the scalability challenges and unlock the full potential of CAV-enabled intersections. Hence, we propose a CAFC method based on the customized CTM, to sort the CAVs with pre-signal philosophy and from a macroscopic perspective. The detailed method is given in the following section.

4.3 Methodology

Problem Setting

We consider a typical four-leg signalized intersection, focusing on the approach of a single leg. This particular approach to the intersection is assumed to be exclusively Connected and Autonomous Vehicles (CAVs). For the sake of demonstration, we assume that the CAV-only traffic consists solely of left-turn and through movements. Although more intricate scenarios, such as those involving right-turn or U-turn vehicles, can be readily extrapolated from this framework, we've chosen to omit them here for simplicity. Given this setup, the signal phases for this intersection only need to contain left-turn and through movements. In order to maximize the intersection's capacity by leveraging the controllability of CAVs, we don't set specific movement constraints for each lane. In other words, both left-turn and through movements are allowed to use any lane as they traverse the intersection, provided the signal allows it. While this approach can make full use of the lane capacity during the respective

Table 4.1: Notation of parameters and variables

Notation	Description
I	Set of cells in the road segment
I^-	Set of cells in pre-sorting area
I^+	Set of cells in post-sorting area
$I_i^\alpha; I_i^{\tilde{\alpha}}; I_i^{\bar{\alpha}}$	Upstream neighbor set; Upstream set with lane-changing; Upstream set without lane-changing
$I_i^\beta; I_i^{\tilde{\beta}}; I_i^{\bar{\beta}}$	Downstream neighbor set; Downstream set with lane-changing; Downstream set without lane-changing
$T; \tau$	Set of discrete time points; Starting time index for the rolling-horizon strategy
$P; p_t$	Set of signal phases; Signal phase at time t
D	Set of desired directions for vehicles
n_{idt}	Number of vehicles in cell i with desired direction d at time t
y_{ijdt}	Traffic flow from cell i to cell j with desired direction d at time t
r_{ijdt}	Receiving flow from cell i to cell j with desired direction d at time t
s_{ijdt}	Sending flow from cell i to cell j with desired direction d at time t
k_{idt}	Traffic density in cell i with desired direction d at time t
q_{ijdt}	Traffic flow rate from cell i to cell j with direction d at time t
z_{idt}	Binary auxiliary variable indicating the number of desired direction of traffic in the cell
m_{ijdt}	Binary auxiliary variable preventing conflict during lane changing
$b_{out}(t)$	Time-dependent bonus term for vehicles passing through intersection
b_{in}	Bonus coefficient for vehicles driving into the sorting area
γ	Penalty coefficient for lane changes
v_f	Desired free-flow speed
v	Speed of CAVs
w	Shockwave speed
q_{max}	Maximum flow rate
k_j	Jam density
g_0	Minimum spacing between CAVs

signal phases, it necessitates sophisticated operations for each CAV to prevent blockages. For clarity and consistency in our presentation, the notations used throughout this paper are consolidated in Table 5.1.

Specifically, we consider a fixed-length planning horizon, denoted by $t \in \mathcal{T} := \{0, 1, \ldots, T\}$. At each time $t \in \mathcal{T}$, we provide the CAV moving strategy for both longitudinal and lateral control. Following our early work (Yao et al., 2022a), we extend the per-vehicle control strategy into a more practical and scalable version, which is a discretized grid-based modeling framework as follows.

Road Geometry

To address the challenges of large-scale CAV control strategies, we adopt a macroscopic method instead of focusing on individual CAV actions. We draw inspiration from the well-known Cell Transmission Model (CTM), an established method in traffic flow analysis (Daganzo, 1994, 1995). The CTM allows us to represent the control of CAVs in groups, each distinguished by its intended direction, e.g., left-turn or straight-through movement. These groups can then cross the intersection collectively.

In particular, as illustrated in Figure 4.2a, we partition the targeted upstream road segment's lanes into a grid of uniform cells. This differs from conventional CTMs, where a cell typically encompasses multiple lanes; in our model, each cell corresponds to a single lane. As a result, a lane is depicted as a sequence of cells, with each cell's width matching the lane's width. The length of a cell is determined by the distance a vehicle travels at its free-flow speed in a one time unit. This structure allows for a unique indexing of each cell in the grid with $i \in \mathcal{I} := \{0, 1, \ldots, I\}$. Central to our method is the development of a control strategy for each cell, representing a group of CAVs sharing the same movement (left-turn/straight-through). We call the CAV group control strategy "Sorting", and the cells within $\mathcal{I}$ are referred to as the "Sorting Area".

However, the incoming CAV traffic usually consists of mixed movements. The first step, therefore, is to segregate this mixed-movement CAV traffic into separate cells, such that each cell contains only one movement. For this purpose, we introduce the concept of the "Pre-Sorting Area," located just before the sorting area. This is represented as a column of additional cells at the entrance of the sorting area and is denoted by $\mathcal{I}^-$. In this manner, CAVs situated within a cell in $\mathcal{I}^-$ that have mixed movements can be organized, with their specific movements separated in the subsequent time step, enabling them to reach the first column of cells in the sorting area. Additionally, for the sake of modeling convenience, we also monitor

the CAVs that have passed through the intersection, using extra cells for this purpose. This is called the "Post-Sorting Area," and is denoted by $\mathcal{I}^+$. Conceptually, this is viewed as a virtual zone without capacity constraints, accommodating all traffic that has traversed the intersection.

With the aid of the CTM, the longitudinal and lateral behaviors of CAVs can be described by transitions between adjacent cells. To facilitate this, we categorize the cells involved in such transitions as neighboring sets. For each cell i, its upstream neighbors are represented by the set $\mathcal{I}_i^\alpha$, while its downstream neighbors are denoted by $\mathcal{I}_i^\beta$. For any given cell i, traffic from any cell in $\mathcal{I}_i^\alpha$ can transition to cell i in the next time step. Likewise, traffic within cell i can advance to any cell in the downstream neighbor set $\mathcal{I}_i^\beta$ in the subsequent time step. To distinguish between traffic that changes lanes and traffic that does not, we partition the downstream neighbor set $\mathcal{I}_i^\beta$ into two subsets: $\mathcal{I}_i^{\tilde{\beta}}$ and $\mathcal{I}_i^{\bar{\beta}}$. The subset $\mathcal{I}_i^{\tilde{\beta}}$ comprises cells accessible by traffic that undergoes a lane change from cell i. In contrast, $\mathcal{I}_i^{\bar{\beta}}$ consists of cells reachable without any lane changes from cell i. Similarly, the upstream neighbor sets $\mathcal{I}_i^{\tilde{\alpha}}$ and $\mathcal{I}_i^{\bar{\alpha}}$ are both subsets of $\mathcal{I}_i^\alpha$. The configuration of these neighbor sets is illustrated in Figure 4.2.

Signal State

To reflect the changes in signal phases, we represent them with the parameter $p_t \in \mathcal{P} := \{-1, 0, 1\}$. Here, 0 indicates the "Red" phase, -1 denotes the "Through" phase, and 1 is the "Left-turn" phase. Note that our modeling framework sets a fixed signal timing. Therefore, p_t serves as an input parameter to the system.

Traffic State

To describe the traffic state in cells, we let n_{idt} be the number of vehicles at cell $i \in \mathcal{I}$ at time $t \in \mathcal{T}$. Here, $d \in \mathcal{D} := \{-1, 1\}$ represents the desired directions of vehicles within a cell: -1 corresponds to the straight-through direction and 1 denotes the left-turn direction. For example, $n_{2,1,3} = 1$ suggests that there is one left-turn vehicle in cell 2 at time 3. Further exten-

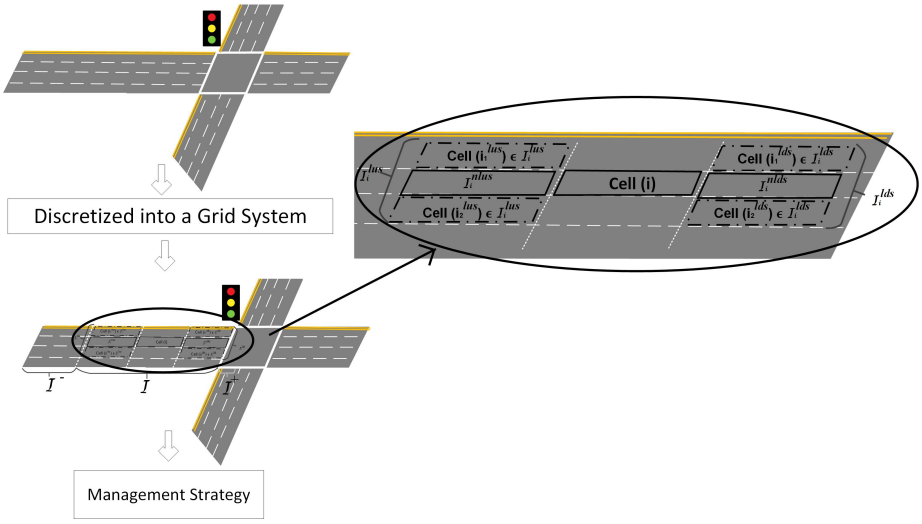

(a) Decomposition of the road segment prior to the intersection

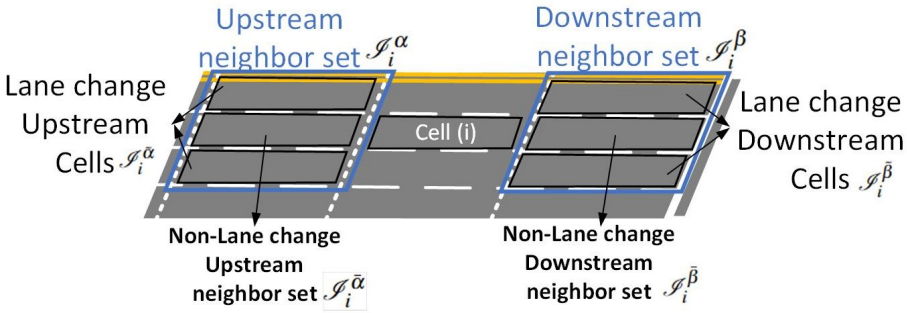

(b) Neighbor set setting

Figure 4.2: Problem setting

sions for complicated scenarios such as those with right-turn movements can be easily extended by adding more values to $\mathcal{D}$.

Traffic Management

We assume that all CAV traffic, upon reaching the pre-sorting area, will be fully controlled by a centralized system. Our control strategy involves adjusting the inflow and outflow from each cell to its adjacent cells. This adjustment includes both the quantity and direction of the CAV flow. Specifically, the number of CAVs exiting one cell and their respective destination cells. For each cell $i \in \mathcal{I}^- \bigcup \mathcal{I}$ at time $t \in \mathcal{T}$, we define its flow decision as $y_{ijdt} \in [0, Y)$, where Y is the maximum flow. Here, $j \in \mathcal{I}_i^\beta$ represents the downstream neighbor cell of i, and $d \in \mathcal{D}$ denotes the direction.

Strategy Design

With all the states and decisions introduced above, we are able to describe the cell-based CAV flow control strategy through a quadratic programming framework. First, our primary goal is to maximize the number of vehicles passing through the intersection during the planning horizon T. In addition, we hope more CAVs can enter the pre-sorting area so that our strategy can coordinate vehicles on a larger scale. Note that we should limit the number of lane changes in practice without necessity hence this would cause more energy and raise the risk of vehicle collisions. By jointly considering these factors, we can have the following connected automated flow control (CAFC) strategy,

$$\begin{aligned} \max_{y} b_{out}(t) & \sum_{j \in I^+, d \in D, t \in T} \sum_{i \in I_j^\alpha} y_{ijdt} \\ & - \gamma \sum_{i' \in I, t \in T, d \in D} \sum_{j' \in I_{i'}^{\tilde{\beta}}} y_{i'j'dt} + b_{in} \sum_{i'' \in I^-, t \in T, d \in D} \sum_{j'' \in I_{i''}^\beta} y_{i''j''dt}. \end{aligned} \tag{4.1}$$

Here, the first term expresses the cumulative traffic flow that has passed through the intersection. In order to push vehicles passing through the intersection quickly, we introduce a time-dependent bonus term $b_{out}(t)$, which decreases over time t. The second term represents the penalty for lane changes, where γ is a positive penalty. The last term accounts for the bonus to traffic entering the sorting area, where b_{in} is also a positive constant.

Then, to ensure that the CAFC strategy is feasible, we need to provide a series of constraints.

Fundamental Diagram of CAV

The behaviors of CAVs described by transitions between adjacent cells are characterized by the CTM. Critical parameters in the CTM can be derived from the fundamental diagram (FD). Among multiple variations of the FD, we choose the triangular FD due to its simplicity and representative quality (Daganzo, 1994).

It's important to note that the FD describes the macroscopic traffic flow behavior for vehicles. The focus of our work is on CAVs, which differ slightly from traditional Human-Driven Vehicles (HDVs). To select the appropriate parameters for CAV traffic, we conducted a comparative analysis of traffic dynamics between CAVs and HDVs, as illustrated in Figure 5.2.

Figure **??** depicts the relationship between spacing and speed for both CAVs and HDVs. A spacing-speed profile for traffic flow represents the car-following behavior. The triangular FD corresponds to a piece-wise linear car-following law. Initially, the following vehicle will remain stationary when its headway to the leading vehicle is less than the minimum spacing, denoted by g_0. Subsequently, it accelerates at a constant rate to maintain a consistent spacing with the leading vehicle, denoted by h. Finally, it reaches the free flow speed, denoted by v_f. It's noteworthy that due to the rapid "reaction time" of CAVs, they can maintain a shorter desired headway,

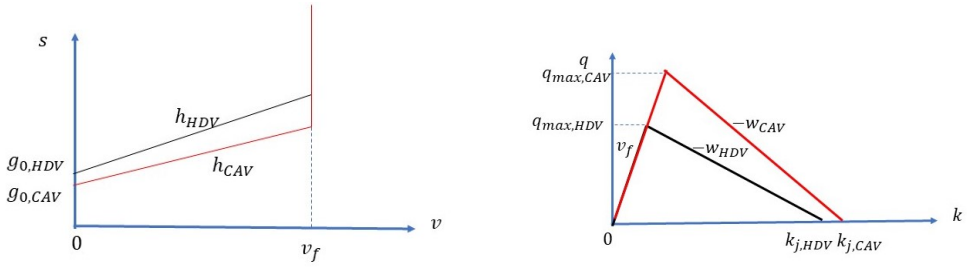

(a) Spacing-Speed Profile

(b) Triangular Fundamental Diagram

Figure 4.3: CAV and HDV behavior comparison

resulting in reduced spacing compared to HDVs traveling at identical speeds. Therefore, in contrast to HDV traffic, we opt for a relatively short headway h_{CAV} and a smaller minimal spacing $g_{0,CAV}$ for CAV traffic.

Given the speed-spacing car-following law, the corresponding triangular FD is illustrated in Figure 5.2b. Specifically, let q_{max} denote the maximum flow rate, k_j represents the jam density, and w is the shockwave speed. The parameters in the FD can be derived from those in the speed-spacing profile as follows:

$$k_j = \frac{1}{g_0},$$

$$q_{max} = \frac{v_f}{g_0 + v_f * h},$$

$$-w = \frac{q_{max}}{k_j - \frac{1}{g_0 + v_f * h}}.$$

The reduced minimum spacing and desired headway of CAVs result in a slightly higher flow-density curve in the FD. This suggests that CAVs can achieve a higher maximum flow under the same road conditions and are less prone to congestion.

Vehicle Dynamics based on CTM

To apply CTM, we first normalize the traffic state and flow decision

with respect to the discretization resolution. Let $\triangle\, l$ represent the length of each cell and $\triangle\, t$ represent the length of the time interval. We have

$$y_{ijdt} = q_{ijdt} \triangle\, t, \tag{4.2}$$

$$n_{idt} = k_{idt} \triangle\, l. \tag{4.3}$$

Here, q_{ijdt} indicates the traffic flow rate with desired direction d from cell i to one of the downstream cells j during one time interval t, while k_{idt} indicates the traffic density with desired direction d in cell i during a time interval t.

Further, given the triangular FD, we introduce the upper and lower bounds of traffic flow rate and traffic density as follows:

$$0 \leqslant \sum_{d \in D} q_{ijdt} \leqslant q_{max}, \tag{4.4}$$

$$0 \leqslant \sum_{d \in D} k_{idt} \leqslant k_j. \tag{4.5}$$

Here, q_{max} and k_j are the corresponding max flow and jam density, respectively, for CAVs. Note that the flow moving out from cell i is limited by the number of vehicles in the cell. Hence,

$$n_{idt} \geqslant \sum_{j \in N(i)} y_{ijdt}. \tag{4.6}$$

Then, we describe the vehicle dynamics in the sorting area for $i \in I$ and $t \in T$. The pre-sorting areas I^- and post-sorting area I^+ will be discussed separately. Based on the state of cells and vehicles, we have:

$$n_{idt} = n_{id(t-1)} + \sum_{j' \in I_i^{\alpha}} y_{j'id(t-1)} - \sum_{j'' \in I_i^{\beta}} y_{ij''d(t-1)}. \tag{4.7}$$

Here, Equation (5.7) characterizes the dynamic state of cell i from time

$t-1$ to time t. Specifically, the number of vehicles in cell i at time t depends on the number of vehicles in cell i at time $t-1$, considering the traffic flow exiting cell i (the cumulative outflow to its downstream neighbor set) and entering cell i (the cumulative inflow from its upstream neighbor set) during the previous time step $t-1$.

Furthermore, we calculate receiving flow r_{ijdt} and sending flow s_{ijdt} according to the CTM. If cell i and cell j are neighbors, the traffic flow from cell i to cell j with direction d at time t depends as follows:

$$r_{ijdt} = min\{w/v_f(k_j \triangle l - \sum_{d\in D} n_{idt}), q_{max} \triangle t\}, \tag{4.8}$$

$$s_{ijdt} = min\{\sum_{d\in D} n_{idt}, q_{max} \triangle t\}, \tag{4.9}$$

$$y_{ijdt} = min\{r_{ijdt}, s_{ijdt}\}. \tag{4.10}$$

Here, the variable w represents the CAV's shockwave speed, and v_f denotes the CAV's free flow speed. Equation (5.8) shows the maximum traffic flow that cell j can receive from cell i, while Equation (5.9) characterizes the maximum traffic flow that cell i can send to cell j. The exact traffic flow y_{ijdt} between cell i and cell j is determined by taking the minimum value of r_{ijdt} and s_{ijdt}.

Next, we provide the criteria for the boundary and initial conditions.

Boundary and Initial Conditions

Firstly, we consider the constraints related to the pre-sorting area I^-. To help group CAVs according to the signal phase, we set that the desired direction d of traffic in any cell of the sorting area be with unique direction. Note that in the pre-sorting area, the CAVs are allowed to have mixed directions. Thus, we introduce $z_{idt} \in \{0, 1\}$ as a binary indicator variable, representing if cell i at time t contains CAVs with direction d . Then, we have

$$n_{idt} \leqslant z_{idt} n_{idt}, \tag{4.11}$$

which activates the indicator with the traffic state. Then we use

$$\sum_{d \in D} z_{idt} \leqslant 1, \forall i \in I, \forall t \in T, \tag{4.12}$$

to guarantee at the sorting area, CAV's direction is exclusive.

Then we model the impact of traffic signals. Recall that $p_t \in P := \{-1, 0, 1\}$ represents the signal phases which include Through, Red, and Left phases, respectively, while $d \in \{-1, 1\}$ indicates the desired direction of vehicles, either Through or Left, respectively. Therefore, to facilitate the passage of traffic through the intersection during the corresponding signal phase, we use the following conditions:

$$y_{ijdt} = \begin{cases} 0 & \text{if } d \neq p_t, \\ 0 & \text{if } p_t = 0, \\ 1 & \text{otherwise.} \end{cases} \tag{4.13}$$

Considering the traffic rules, where vehicles should not change lanes near the intersection, we add the following constraint,

$$y_{ijdt} = 0, \forall i \in I_j^{\tilde{\beta}}, j \in I^+, d \in D, t \in T. \tag{4.14}$$

We also discuss the initial condition. At time $t = 0$, suppose the system observes the traffic state as n_{id}^0 for $i \in I$ and $d \in D$. We have

$$n_{id0} = n_{id}^0, \forall i, d. \tag{4.15}$$

Variable Feasibility

Note that we have mixed directions in the pre-sorting area, the dynamic of mixed traffic is more complicated. When mixed CAVs enter the sorting area from the pre-sorting area, we separate the flow into two cells, hence the are with to ensure traffic feasibility within each cell, particularly for

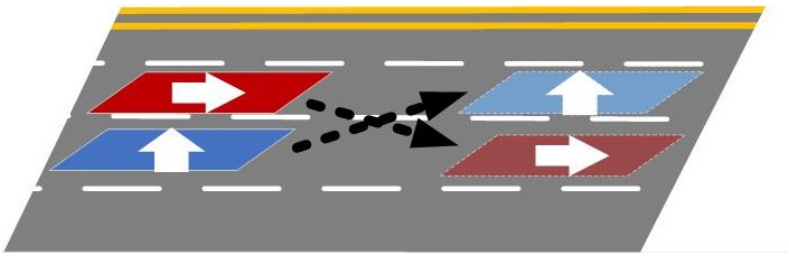

Figure 4.4: Example of "crossing" lane change

cells containing mixed desired direction traffic, only vehicles with the same speed are permitted within the cell. Thus, we have the following conditions:

$$\sum_{j \in I_i^\beta} y_{ij1t} n_{i(-1)t} = \sum_{j \in I_i^\beta} y_{ij(-1)t} n_{i1t}. \tag{4.16}$$

To avoid conflict during lane changing, i.e. cannot do "crossing" lane change, as shown in Figure 5.3, we define conflict set $((i_1^c, i_2^c), (i_1'^c, i_2'^c)) \in F$ with cells where the traffic flow could conflict when doing lane changing. Hence, we have

$$y_{ijdt} = m_{ijdt} y_{ijdt}, \tag{4.17}$$

$$\sum_{d \in D} m_{i_1^c, i_2^c, d, t} + m_{i_1'^c, i_2'^c, d, t} \leqslant 1. \tag{4.18}$$

Here, $m_{ijdt} \in \{0, 1\}$ is a binary variable.

For notional connivance, we define $C(\mathbf{y}, \mathbf{n})$ as the constraint set containing all constraints, i.e., Constraints 5.2 - 5.17. Therefore, the connected automated flow control problem (CAFCP) can be modeled as the follow-

ing,

$$\text{(CAFCP)} \qquad \max_{y,n\in C(y,n)} b_{out}(t) \sum_{j\in I^+,d\in D,t\in T} \sum_{i\in I_j^\alpha} y_{ijdt}$$
$$-\gamma \sum_{i'\in I,t\in T,d\in D} \sum_{j'\in I_{i'}^{\bar\beta}} y_{i'j'dt} + b_{in} \sum_{i''\in I^-,t\in T,d\in D} \sum_{j''\in I_{i''}^{\beta}} y_{i''j''dt}.$$

Rolling-Horizon Scheme

Note that CAFC handles the scenario of complete information, i.e., all traffic information is given at the beginning as initial conditions. The optimal decision will be the control of all traffic flow over T. However, traffic will always arrive in the system in reality. Hence, we will need to extend the above strategy to be adaptive concerning any arrival scenarios.

To address traffic uncertainty and achieve real-time control, a time-rolling strategy is adopted. The CAV movement strategy is planned across the entire $\mathcal{T}$, but only the action at time $t = 0$ is implemented. This strategy is updated at each successive time step.

In theory, as the states of arrival traffic are uncertain, the optimal management policy should be obtained through a stochastic programming structure, which leads to a problem scale and intractability. Given the practical need, we consider an adaptive rolling-horizon strategy. Suppose we solve a problem with the entire time horizon $T^L = \{0, 1, ..., T_{max}\}$ with a rolling horizon length of $T + 1$. We define $T(\tau) = \{\tau, \tau + 1, ..., \tau + T\}$ as the moving planning horizon starting at τ. We define a time index mapping $\Gamma(t; \tau) = t - \tau$ to convert the actual time index t to the corresponding time index inside the moving horizon $T(\tau)$. Then we have Rolling-Horizon CAFC Algorithm (5.2).

Step 0: At time 0, initialize the planning horizon $T = T(0)$, obtain the state of all vehicles in the sorting area n_{idt}^0 and the signal phase $s_{ntt\in T(0)}$.

Step 1: At time τ, solve the quadratic programming problem within the planning horizon $T(\tau)$ and obtain the management strategy $y_{jid\Gamma(t;\tau)}$.

Step 2: Use the one-step movement $y_{jid\Gamma(0;\tau)}$ and the vehicle dynamics constraint to obtain $n_{id\Gamma(1;\tau)}$ as new vehicle states.

Step 3: Update the initial vehicle state $n^0_{idt} \leftarrow$ the combination of $n_{id\Gamma(1;\tau)}$ and new arrivals.

Step 4: Update $\tau \leftarrow \tau + 1$, update the rolling horizon to $T(\tau)$, and update the signal phase to $p_{\Gamma(t;\tau)_{t\in T(\tau)}}$.

Repeat Steps 1-4 until $\tau + T > T_{max}$.

With Algorithm (5.2), our strategy can be applied to an infinitely long time of management scenarios.

4.4 Case Study

In this section, we present a series of case studies aimed at demonstrating the effectiveness of the proposed CAFC approach. To this end, we begin by defining a benchmark case and providing a detailed step-by-step illustration of the operations involved in the sorting area. We then proceed to compare the performance of the CAFC against scenarios without coordination. All algorithms were executed on a desktop computer equipped with an i7-10700 CPU operating at 2.90 GHz and 32.0GB RAM and were solved using Gurobi optimization software.

First, we consider the fundamental settings of the benchmark case. A road segment with four lanes is set, with a speed limit of 40 mph ($\approx$64.4 km/h). The area is divided into a grid with 0.055 mile ($\approx$88.5 m) length for each cell, and a total of four columns of cells, spanning a distance of 265.5 m. This setup ensures that vehicles can pass through one cell per unit time at the speed limit. The time unit is set to five seconds, and the length of the rolling planning horizon is 40 seconds (i.e., 8 time steps). The signal phases operate on a cycle of 120 seconds, with a green phase of 60 seconds and a red phase of 60 seconds.

The traffic flow in this benchmark case is uniformly distributed between

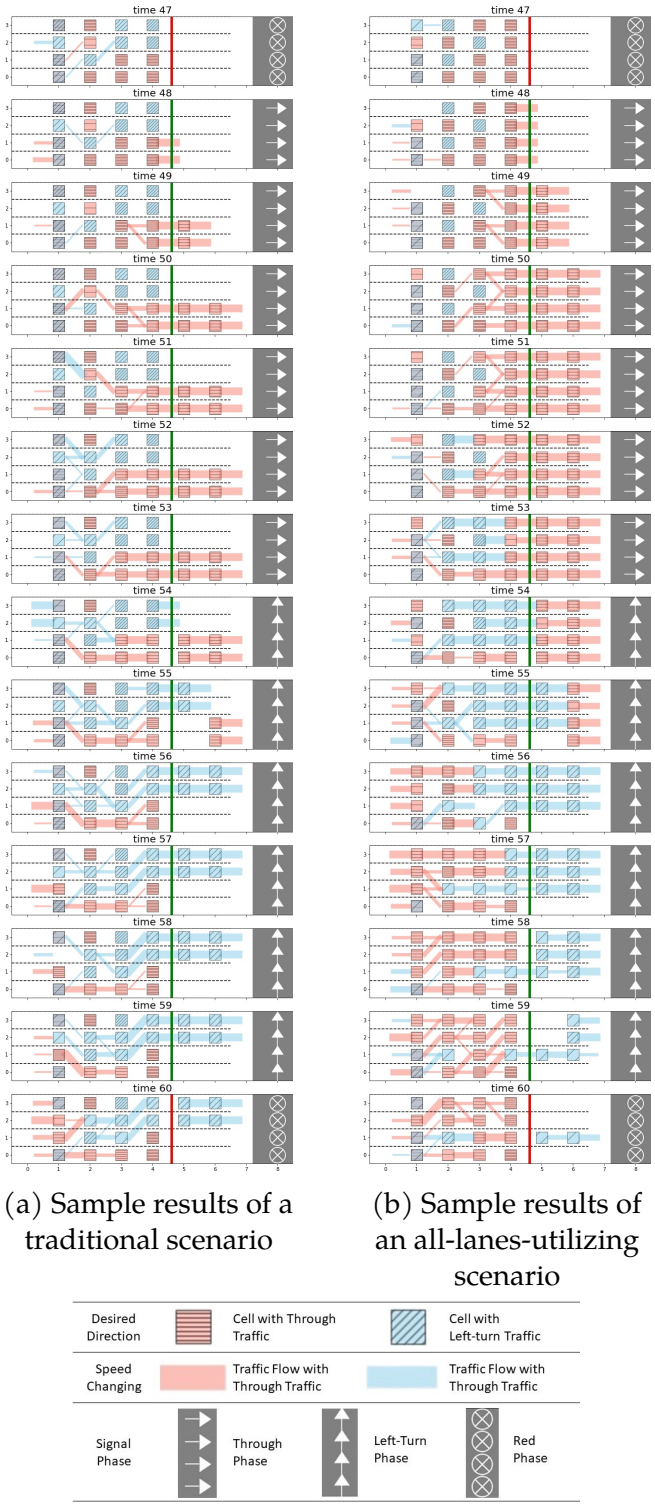

(a) Sample results of a traditional scenario

(b) Sample results of an all-lanes-utilizing scenario

Figure 4.5: Sample results comparison with and without implementing the CAFC for a left turn from two dedicated left lanes

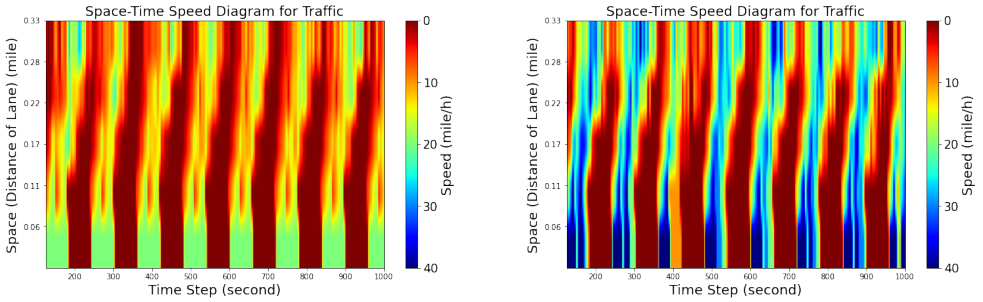

(a) Space-time-speed diagram for a traditional traffic scenario

(b) Space-time-speed diagram for an all-lanes-utilizing scenario

Figure 4.6: Sample space-time-speed diagram comparison with and without implementing the CAFC for a left turn from two dedicated left lanes

0.6 and 1 vehicle/second, with 50% of traffic flow being through traffic and 50% being left-turn traffic. To validate the correctness of our proposed CAFC, we consider a matched signal phase case where the through and left-turn phases are equal length, i.e., both set to 30 seconds. The minimum spacing between vehicles is set to 5 meters, and based on the FD, the jam density is calculated to be 324.3 veh/mile. In addition, we investigate two representative cases for vehicles with different directions. Traditionally, a road segment with left-turn and through traffic often has a protective left turn from the dedicated left lanes, i.e., several of the left lanes only allow the left turn movements and the right lanes allow through and right-turn movements. For our example, we use two left lanes that only allow left-turn traffic passing through the intersection and two right lanes that only allow through traffic passing through the intersection. We refer to this scenario as the "Traditional Case." On the other hand, for traffic with both desired directions, all lanes can be used to pass through the intersection. We refer to this scenario as the " All Lanes Utilizing Scenario." It is important to note that vehicles arriving in the sorting area can use any lane without considering their desired direction. Based on these settings, a sample result of the proposed CAFC algorithm is shown in Figure 5.4

for demonstration purposes. In this sample result, the arrival rate is 0.7 vehicles per second per lane. Since there are 60 seconds for the red phase, where vehicles are almost waiting and not moving, we show the traffic state and operations during the green phase. In these figures, the bird's eye view of the sorting area is plotted for each time step, the driving direction of vehicles is from left to right, and the intersection is located at the right end of the road.

To clarify, each bird view plot presented in the paper represents the traffic conditions in the sorting area for a specific time step. The 6 columns in each plot correspond to the whole sorting area (Columns 2-4), the pre-sorting area (Columns 0), and the post-sorting area (Columns 5-6). The grids on the plot indicate cells, and the color of the cell shows the desired direction status of the traffic in the cell. Specifically, "red" indicates through traffic, and "blue" indicates left-turn traffic. The density of the stripes on the grid indicates the number of vehicles present in the cell. Additionally, the lines between cells indicate the traffic flow between corresponding cells, with the width of the line representing the amount of the traffic flow. Finally, the graphics presented in the right gray area of each plot show the corresponding signal phases at that particular time step, with crossmarks and arrows.

Figure5.4a illustrates the effectiveness of the proposed CAFC algorithm in an All Lanes Utilizing Scenario. It is observed that from time 47 to time 52, on the Through phase, Left-turn traffic gathers and waits in the second left lane. Meanwhile, Through traffic gathers in the other lanes to pass the intersection, intuitively. Remarkably, Left-turn vehicles exit a cell in the left lane just before the intersection to pass more Through vehicles under CAFC operations. A more interesting sorting pattern can be seen from time 53 to time 54. Since the signal phase switches from the Through to the Left-turn at time 54, those Left-turn vehicles are wisely sorted and grouped in advance at the front of the sorting area to maximize the utilization in

the following phase. On the other hand, Figure4.5a shows the example result of the traditional scenario in the same set of vehicle input.

To facilitate demonstration, we define the number of vehicles passing through the intersection per hour as throughput. The throughput of the Traditional Scenario without CAFC operation is 3600 vehicles per hour, whereas the All Lanes Utilizing Scenario with CAFC operation achieves a throughput of 6182 vehicles per hour, indicating an improvement rate of about 72%.

To further analyze the comparison between scenarios with and without the implementation of CAFC, the Space-Time Speed Diagram, as depicted in Figure 4.6, serves as a crucial visualization tool to assess the impact of CAFC implementation on the average speed across all lanes. The diagram illustrates the temporal and spatial evolution of traffic speed along both the pre-sorting and sorting areas over seven 120-second cycles, each comprising 60 seconds of green signal time followed by 60 seconds of red signal time.

In comparison to the traditional scenario, i.e., without CAFC implementation, where left-turn vehicles use two dedicated left lanes (as illustrated in Figure 4.6a), the average speeds during green signal intervals exhibit a significant improvement when CAFC is applied, as shown in Figure **??**. Figure **??** demonstrates that with the assistance of CAFC, traffic can reach free-flow speeds (40 mph), signifying that vehicles from all lanes can attain free-flow speeds simultaneously. In contrast, without CAFC, the average speed is limited to approximately 20 mph during green phases, as only half of the lanes allow vehicle passage at each green phase. Further, as can be found that, the general speed of the system with CAFC achieves a larger speed, demonstrating the effectiveness of the CAFC approach in enhancing overall traffic performance at the intersection.

To select appropriate hyper-parameters for the objective function stated in Equation (5.18), we conducted a sensitivity analysis by introducing

Table 4.2: Sensitivity analysis

	Throughput		
k	$b_{out}(t) = \frac{(8-t)}{8}k$	$\gamma = k$	$\mathbf{b}_{in} = k$
0	-	**4309.9**	3721.7
1	3731.8	4522.8	4340.3
10	**4502.5**	4005.6	4147.6
50	4350.4	3062.5	**4340.3**
100	4046.2	3143.7	4015.8

Benchmark: $b_{out}(t) = 10(1 - \frac{1}{8}t)$, $\gamma = 1$, $b_{in} = 1$,

a variable k that varied from 0 to 100. The results of this analysis are presented in Table (5.2). Based on the sensitivity analysis, we selected the hyper-parameters that produced the highest throughput. Thus, we set $b_{out}(t) = \frac{10(8-t)}{8}$, $\gamma(j) = 0$, and $b_{in} = 50$ as the hyper-parameters. We ensured that the computational time for solving the Rolling-Horizon CAFC was less than the unit time, i.e., 5 seconds.

Furthermore, to assess the efficiency of the proposed CAFC, we compare its performance with the Tradition Scenario without implementing the CAFC. To investigate the impact of varying arrival rates, we keep the other parameters constant and vary the arrival rate from 0.2 vehicles per second per lane to 1 vehicle per second per lane with 0.1 intervals. Recall that we define the number of vehicles passing through the intersection per hour as throughput. Owing to the uncertainty of incoming traffic states, we perform the Monte Carlo simulation ten times for each case, with 360 seconds, i.e., 72-time steps for each run.

The findings from our simulations are illustrated in Figure **??**. In each case, the light grey curves represent the mean values of the Monte Carlo simulation results, highlighting the overall trends. The blue shadow surrounding the curves denotes the range of throughput observed in each scenario, spanning from the maximum to the minimum throughput values.

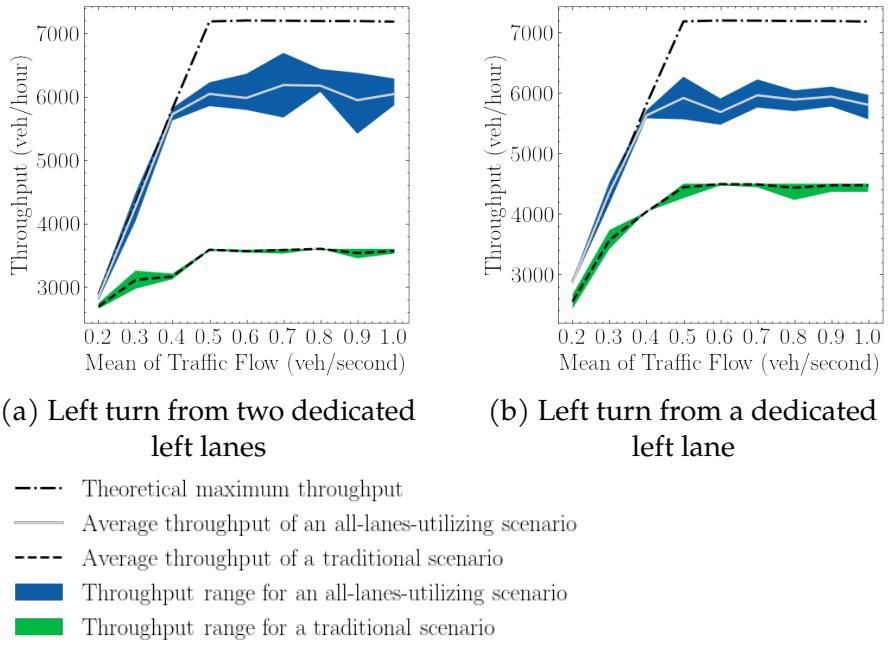

(a) Left turn from two dedicated left lanes

(b) Left turn from a dedicated left lane

Figure 4.7: Performance comparison with and without implementing the CAFC

A comprehensive comparison between the Traditional Scenario and the All Lanes Utilizing Scenario reveals that the CAFC consistently improves throughput across all scenarios.

For instance, when the arrival rate is 0.7 vehicles per second per lane, the throughput improvement is approximately 72%. Under the All Lanes Utilizing Scenario, the average maximum throughput reaches 6182 vehicles per hour, which significantly surpasses the traditional scenario's throughput of 3600 vehicles per hour. These results affirm that the proposed All Lanes Utilizing Scenario, with the employment of the CAFC approach, demonstrates superior performance compared to the traditional approach, effectively enhancing intersection throughput and optimizing traffic flow.

Note that the dotted line in the graph represents the theoretical maximum throughput achievable when traffic flow efficiently utilizes all avail-

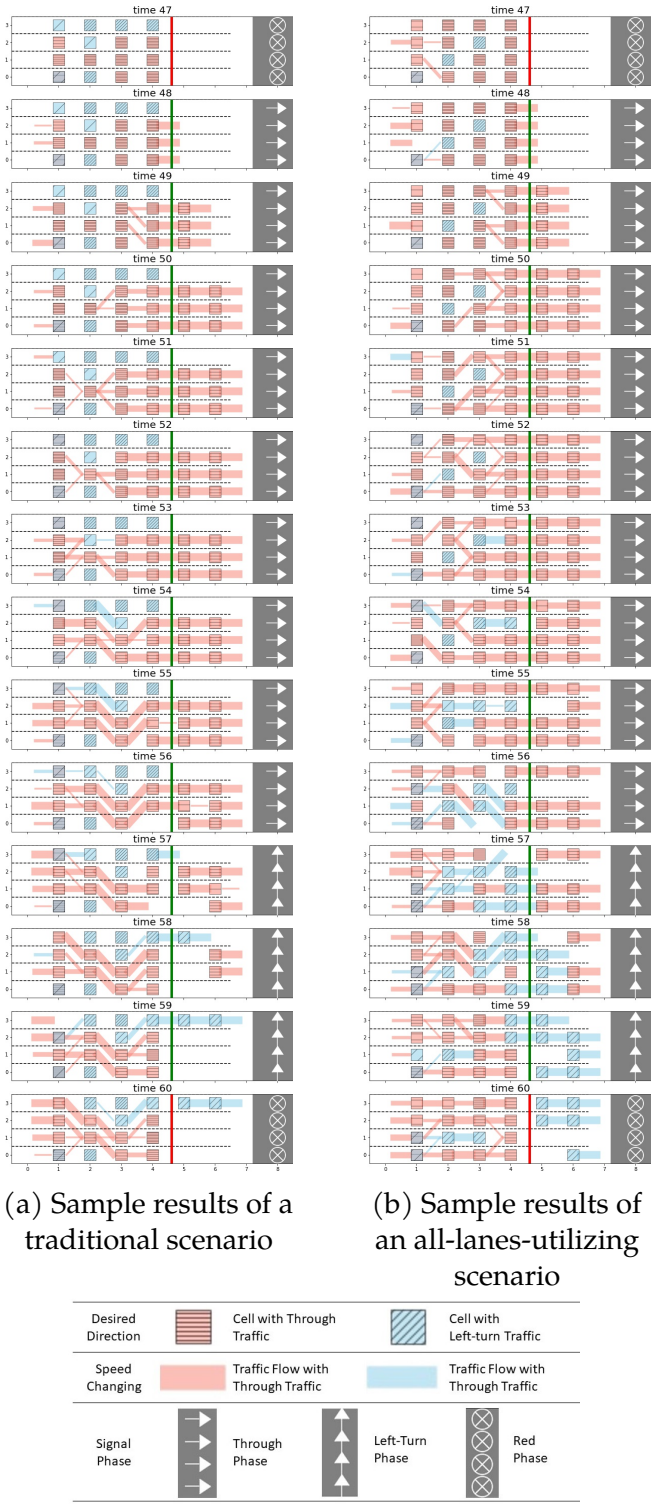

(a) Sample results of a traditional scenario

(b) Sample results of an all-lanes-utilizing scenario

Figure 4.8: Sample results comparison with and without implementing the CAFC for a left turn from a dedicated left lane

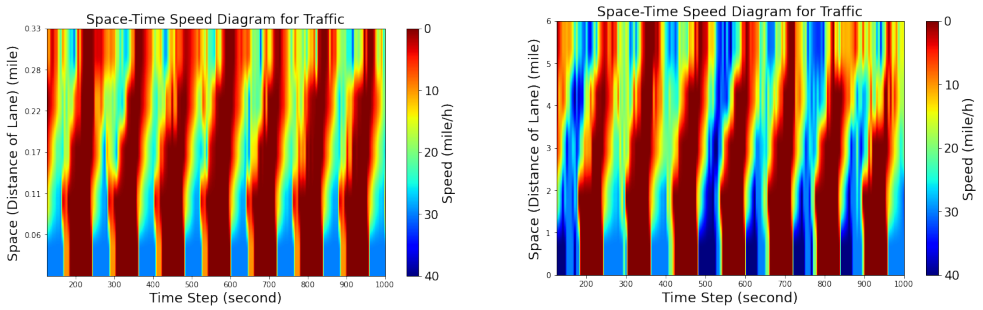

(a) Space-time-speed diagram of a traditional scenario

(b) Space-time speed diagram of an all-lanes-utilizing scenario

Figure 4.9: Sample space-time-speed diagram comparison with and without implementing the CAFC for a left turn from a dedicated left lane

able lanes with the largest possible amount of traffic flow at each green second. Figure **??** demonstrates that at relatively low arrival rates (< 0.4), the throughput using the CAFC approach closely approaches the theoretical maximum throughput. Even during relatively busy traffic conditions, when compared to the traditional scenario, the CAFC approach remains competitive.

Furthermore, it is imperative to consider a real-life scenario characterized by a protected left turn from a dedicated left lane configuration. In this specific scenario, a single lane is exclusively designated for left-turn traffic, while the remaining three lanes are for through traffic. Notably, the direction ratio for left-turn traffic to through traffic is altered to 1:3, which matches the ratio of the lane allocation, in conjunction with matched signal phases comprising 45 seconds for the left-turn phase and 15 seconds for the through phase. All other parameters are retained at the benchmark values.

To visually illustrate the effectiveness of the proposed CAFC approach in this left turn from a dedicated left lane scenario, Figure **??** and Figure 4.9 provides a graphical representation. In contrast, Figure 4.8a depicts the outcome of the traditional scenario under identical vehicle input con-

Table 4.3: Performance among different turning movement ratios with various signal phases

Scenario	Ratio of Vehicle Directions (Through:Left-turn)	Signal Phase (Through:Left-turn)	Throughput Min	Mean	Max
All Lanes Utilizing	1:5	T10L50	4500	5142	5505
	2:4	T20L40	5400	5621	6030
	3:3	T30L30	6075	6172	6435
	3:1	T45L15	5700	5892	6045
Traditional Scenario	3:3	T30L30	3600	3600	3600
	3:1	T45L15	4230	4433	4500

ditions. We can also get the same conclusion for the effectiveness of the CAFC, and the improvement is also significant even though the left-turn ratio is different.

Moreover, our investigation extends to examining the influence of fluctuating arrival rates. While keeping all other parameters constant, we systematically vary the arrival rate from 0.2 vehicles per second to 1 vehicle per second, in intervals of 0.1. Figure **??** presents the outcomes of this analysis, demonstrating that the CAFC consistently enhances throughput across all scenarios. For instance, when the arrival rate is 0.7 vehicles per second per lane, the observed throughput improvement is approximately 32.5%. Under the All Lanes Utilizing Scenario, the average maximum throughput reaches 5962.5 vehicles per hour, significantly exceeding the traditional scenario's throughput of 4500 vehicles per hour. Remarkably, these results closely align with those of the benchmark case, in which the left turn from two dedicated left lanes underscores the robustness of the CAFC algorithm across varying traffic conditions.

Next, we further investigate the impact of several key factors on the performance of the proposed CAFC algorithm. To ensure the reliability and consistency of our analyses, we maintained all parameters other than the ones under investigation at values identical to those in the benchmark case. Then compare the performance between the "All Lane Utilizing" scenario, i.e., under the operation of CAFC, while the traditional scenario remained uncoordinated.

To assess the impact of varying direction ratios while maintaining matched signal phases on algorithm performance, we conducted an extensive series of simulations. This inquiry involved four distinct direction ratio scenarios: one direction traffic extreme dominating case, we use left-turn traffic dominating case as an example, '15' (representing a Through:Left-turn ratio of 1:5); one direction traffic relative dominating case, we use left-turn traffic relative dominating case as an example,'24' (indicating a 2:4 ratio); the count-balanced direction case,'33' (equivalent to a 3:3 ratio); and left turn from a dedicated left lane case, '31' (corresponding to a 3:1 ratio). To facilitate a direct comparison with the two traditional scenarios one featuring a '33' scenario with Left turns from two dedicated left lanes, and the other characterized by Left turns from a dedicated left lane we incorporated an additional '31' scenario (3:1 ratio).

In addition to assessing direction ratios, we also explored matched signal phase configurations. These configurations included 'T10L50' (10 seconds Through phase, 50 seconds Left-turn phase), ' T20L40' (20 seconds Through phase, 40 seconds Left-turn phase), 'T30L30' (30 seconds Through phase, 30 seconds Left-turn phase), and 'T45L25' (45 seconds Through phase, 15 seconds Left-turn phase). Through Monte Carlo simulations conducted for each scenario 5 times, we assessed the performance of the CAFC, focusing primarily on throughput as a key performance metric.

The findings, as presented in Table 4.3. First and foremost, the results consistently showcase that, regardless of the specific direction ratio, the adoption of the CAFC algorithm consistently yields higher throughput in the All Lanes Utilizing scenario. This pervasive enhancement in intersection throughput underscores the robustness and consistency of CAFC in its capacity to enhance intersection capacity.

Moreover, the investigation underscores the commendable performance of CAFC across a diverse range of vehicle direction ratios when

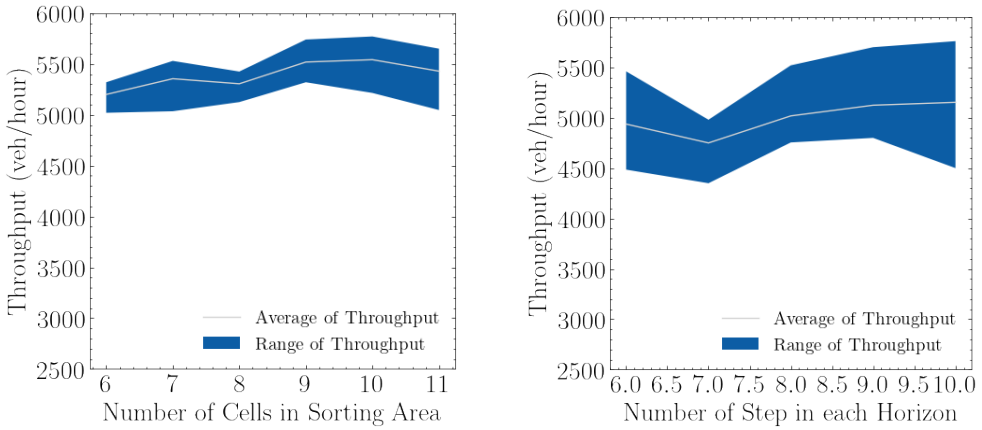

(a) Performance is impacted by the length of the sorting area

(b) Performance is impacted by the number of steps in each horizon

Figure 4.10: Performance influenced by different factors

aligned with suitably matched signal phases. This inherent adaptability and versatility exhibited by CAFC in accommodating various direction ratios further underscore its potential as a viable and effective solution for optimizing traffic at signalized intersections.

Furthermore, we conducted an analysis to examine the impact of the length of the sorting area and the number of steps for each rolling horizon, on the throughput. Surprisingly, our findings indicate that these factors do not significantly affect the throughput. The results, as illustrated in Figure 4.10a and Figure **??**, reveal that the largest variation in throughput is caused by the length of the sorting area, i.e., the number of cells, ranging from 6 cells to 11 cells, is approximately 5.5%. Similarly, the largest variation caused by the number of steps in the rolling horizon, ranging from 6 time steps (30 seconds) to 10 time steps (50 seconds), is approximately 3.7%. These findings suggest that the proposed CAFC remains effective and robust across different configurations of the sorting area and rolling horizon. Therefore, the sorting approach exhibits promising performance regardless of the specific length of the sorting area or the number of steps

in the rolling horizon.

4.5 Conclusion and Future Work

In this study, we proposed a novel CAFC approach specifically designed for CAVs at signalized intersections. The primary objective of this approach is to enhance traffic efficiency and increase intersection capacity by better coordinating CAVs and intersections. By considering the collective behavior of CAVs, we developed a CTM-based control model, which manages the inflow and outflow for each cell of CAV traffic via a holistic optimization. The problem is neatly formulated as a quadratic programming problem that can solved efficiently by a prevailing solver in real time. This macroscopic control approach was particularly valuable in addressing the limitations associated with microscopic control, such as scalability and computation time challenges, especially in scenarios where the number of coordinated CAVs is large. To ensure real-time coordination of CAVs and to handle uncertain vehicle arrivals, we developed a rolling-horizon-based solution method. Our approach demonstrated remarkable robustness, as evidenced by its minimal sensitivity to parameter variations, making it effective and reliable across various traffic conditions.

The results from our numerical experiments have further confirmed the effectiveness of our proposed approach, showing substantial improvements in intersection throughput, particularly in heavy traffic conditions, the throughput improvement can achieve approximately 72%. Our model successfully achieved better utilization of lanes and green time, leading to significantly enhanced traffic flow efficiency.

In conclusion, the CAFC approach integrated with the CTM framework offers a promising solution to increase intersection throughput and improve traffic efficiency for CAVs. By considering the collective behavior of vehicles and optimizing traffic flow, our research contributes to the

development of more efficient and scalable control strategies. This study lays the groundwork for further exploration and implementation of macroscopic control for CAVs in urban traffic management systems, providing valuable insights for transportation authorities and researchers in the field.

5 CONNECTED AUTOMATED TRAFFIC MANAGEMENT FOR FREEWAY WEAVE SECTION

This chapter we present a novel traffic flow management strategy for optimizing the performance of highway interchanges, particularly focusing on the weaving sections. Leveraging the concept of connected automated vehicles (CAVs) and advanced control algorithms, the strategy aims to enhance intersection throughput, minimize congestion, and improve overall traffic efficiency. Through a series of case studies, sensitivity analyses, and Monte Carlo simulations, the effectiveness of the proposed strategy is thoroughly evaluated under various traffic conditions and arrival rates. Results demonstrate consistent improvements in throughput and traffic flow dynamics, highlighting the superior performance of the proposed strategy compared to traditional approaches.

5.1 Introduction

For several decades, transportation research has primarily focused on advancing systems, methodologies, and algorithms aimed at enhancing the efficiency of weave sections on freeways. These segments, where traffic streams converge and diverge, pose significant challenges for optimizing traffic flow due to the potential for congestion and reduced capacity Cassidy and May (1991); Liu et al. (2012). The merging and diverging of ramp vehicles often disrupt traffic flow, resulting in various issues including traffic oscillations Bai et al. (2022), heightened energy consumption, and pollution Du et al. (2018), accidents Wang et al. (2015); Golob et al. (2004), and recurrent congestion Cottrell (1998). Previous approaches have predominantly centered on implementing active traffic management strategies such as ramp metering Zhang and Levinson (2010); Wang et al. (2014b) and variable speed limits Abdel-Aty and Wang (2017). Neverthe-

less, the efficacy of these systems remains limited due to their failure to address the stochastic nature of individual vehicle dynamics.

The emergence of connected and automated vehicles (CAVs) has introduced novel avenues for augmenting the efficiency of weave sections on freeways. Equipped with sophisticated communication and control capabilities, CAVs offer the potential for precise vehicle coordination and real-time traffic management Gokasar et al. (2023); Yao et al. (2023); Chen et al. (2023). Through advancements in vehicle automation and communication technologies, CAVs can seamlessly integrate into traffic streams, modulate speeds, and optimize lane usage to enhance overall freeway throughput Yao et al. (2023). This transformative potential has ignited substantial interest in leveraging CAV technology to address the challenges associated with weave sections and bolster freeway capacity. The evolution of vehicle automation and communication empowers CAVs to achieve precise control both longitudinally Zhou et al. (2019); Han et al. (2020); Chen et al. (2021a) and laterally Wang et al. (2014a); Zhou et al. (2017a); Wang et al. (2021), enabling them to execute driving tasks such as car following, lane keeping, and lane changing with precision and efficiency. Longitudinal control systems, such as Cooperative Cruise Control, have demonstrated effectiveness in enhancing traffic efficiency, throughput, and stability Gong et al. (2016); Öncü et al. (2014); Shi et al. (2021); Zhou et al. (2020). Conversely, lateral control mechanisms ensure the smoothness of vehicle trajectories and enhance lane change safety Wang et al. (2014a); Zhou et al. (2017a); Wang et al. (2021); Bevly et al. (2016). Moreover, the integration of vehicle-to-infrastructure (V2I) communication enables CAVs to be precisely controlled in cooperation with infrastructure, exhibiting significant potential for enhancing highway efficiency through coordinated vehicle and on-ramp signal interactions. While existing research predominantly focuses on optimizing vehicle trajectories in single-lane ramp scenarios Zhou et al. (2017b); Li et al. (2018); Jiang et al. (2017);

Dong et al. (2021), the application of V2I communication holds promise for extending these benefits to more complex traffic scenarios.

Numerous researchers have investigated the potential of Connected and Autonomous Vehicle (CAV) technology in augmenting weave section capacity within freeway networks. In the literature, several CAV-enabled cooperation strategies have been proposed to facilitate the merging and diverging traffic at freeway on-ramps and off-ramps. For merge traffic at on-ramps, researchers have concentrated on devising cooperative strategies to optimize merging efficiency. For instance, Zhu et al. (2022a) propose a flow-level CAV coordination strategy for multilane freeways, integrating lane-change rules, proactive creation of merging gaps, and platooning of ramp vehicles to enhance traffic flow stability and efficiency. Meanwhile, Subraveti et al. (2021) present a novel approach focusing on the strategic assignment of CAVs across lanes to induce necessary lane changes well upstream of potential bottlenecks, thereby improving traffic throughput. Similarly, for diverging traffic at off-ramps, researchers have developed cooperative strategies aimed at enhancing traffic operation and safety. Zheng et al. (2019) introduce a cooperative lane changing strategy near highway off-ramps, utilizing CAV technology to improve traffic flow, safety, and reduce oscillations compared to traditional strategies. Additionally, Hao et al. (2020) address the complexities of highway weaving sections by proposing an analytical method based on driver psychological characteristics to accurately identify mandatory lane-changing processes, enhancing lane-changing recognition for CAVs in heterogeneous traffic flow scenarios. These strategies, as summarized in Rios-Torres and Malikopoulos (2016) and Zhu et al. (2022b), have shown significant promise in advancing the efficiency of weave sections within freeway networks.

Despite these advancements, the majority of strategies primarily focus on the microscopic decisions of individual vehicles, such as trajectory design of CAVs, while affording limited attention to macroscopic con-

siderations like traffic flow efficiency. Furthermore, existing studies are predominantly tailored for single-lane freeways, overlooking the prevalent multilane freeways where free lane-changes between mainstream lanes are substantial. Thus, there exists a notable gap in the literature concerning comprehensive discussions on achieving merging cooperation in multilane freeway settings. Addressing this gap is crucial for enhancing flow control within weave sections and maximizing the potential benefits of CAV technology in augmenting traffic flow efficiency and safety on freeways.

Recognizing these limitations and gaps in current research, it is imperative to adequately address the complexities of multilane main lanes with multilane on-ramps and off-ramps within weave sections to fully harness the capabilities of CAV-enabled intersections. Therefore, we advocate for the development of a flow control method tailored to address these specific challenges, based on a customized Cell Transmission Model (CTM), which enables the macroscopic management of CAVs. The subsequent section provides a detailed exposition of this method, elucidating its intricacies and implementation strategies.

The subsequent sections of this paper are structured as follows: In Section 2, we present a comprehensive description of the scenario-based weaving section model, addressing the cooperative control problem. The outcomes of the numerical experiments are detailed in Section 3. Finally, Section 4 concludes our work, highlighting its contributions, and explores potential avenues for future research.

5.2 Methodology

Problem Setting

We consider a typical weave segment where vehicles entering and exiting the highway must navigate within the same lane for a short distance, focus-

Table 5.1: Notation of parameters and variables

Notation	Description
I	Set of cells in the road segment
$I^-; I^{u-}; I^{v-}$	Set of cells in pre-coordination area; Set of cells in pre-coordination area on main road;
$I^+; I^{u+}; I^{v+}$	Set of cells in post-coordination area; Set of cells in post-coordination area on main road; Set of cells in post-coordination area on off-ramp
$I_i^{\alpha}; I_i^{\tilde{\alpha}}; I_i^{\bar{\alpha}}$	Upstream neighbor set; Upstream set with lane-changing; Upstream set without lane-changing
$I_i^{\beta}; I_i^{\tilde{\beta}}; I_i^{\bar{\beta}}$	Downstream neighbor set; Downstream set with lane-changing; Downstream set without lane-changing
$T; \tau$	Set of discrete time points; Starting time index for the rolling-horizon strategy
$P; p_t$	Set of signal phases; Signal phase at time t
D	Set of desired directions for vehicles
n_{idt}	Number of vehicles in cell i with desired direction d at time t
y_{ijdt}	Traffic flow from cell i to cell j with desired direction d at time t
r_{ijdt}	Receiving flow from cell i to cell j with desired direction d at time t
s_{ijdt}	Sending flow from cell i to cell j with desired direction d at time t
k_{idt}	Traffic density in cell i with desired direction d at time t
q_{ijdt}	Traffic flow rate from cell i to cell j with direction d at time t
z_{idt}	Binary auxiliary variable indicating the number of desired direction of traffic in the cell
m_{ijdt}	Binary auxiliary variable preventing conflict during lane changing
$b_{out}(t)$	Time-dependent bonus term for vehicles passing through intersection
b_{in}	Bonus coefficient for vehicles driving into the sorting area
γ	Penalty coefficient for lane changes
v_f	Desired free-flow speed
v	Speed of CAVs
w	Shockwave speed
q_{max}	Maximum flow rate
k_j	Jam density
g_0	Minimum spacing between CAVs

ing on the merge and diverge of vehicles. This particular weave segment is assumed to be exclusively Connected and Autonomous Vehicles (CAVs). For the sake of demonstration, we assume that the CAV-only traffic consists with two lanes on ramp, two lane off-ramp and a weave lane. Although more intricate scenarios, such as those only content single lane on-ramp and single lane off-ramp, can be readily extrapolated from this framework. While this approach can make full use of the lane capacity for both mainlines, weave lane and off-ramp, it necessitates sophisticated operations

for each CAV to prevent blockages. For clarity and consistency in our presentation, the notations used throughout this paper are consolidated in Table 5.1.

Specifically, we consider a fixed-length planning horizon, denoted by $t \in \mathcal{T} := \{0, 1, \ldots, T\}$. At each time $t \in \mathcal{T}$, we provide the CAV moving strategy for both longitudinal and lateral control. Following our early work Yao et al., we extend a signalized intersection scenario to a highway weave scenario, which is a discretized grid-based modeling framework as follows.

Road Geometry

Similarity with the previous work, we adopt a macroscopic method instead of focusing on individual CAV actions. We draw inspiration from the well-known Cell Transmission Model (CTM), an established method in traffic flow analysis Daganzo (1994, 1995). The CTM allows us to represent the control of CAVs in groups, each distinguished by its intended direction, e.g., keep on mainline or off-ramp movement.

In particular, as illustrated in Figure 5.1, we partition the targeted weave segment's lanes into a grid of uniform cells. This differs from conventional CTMs, where a cell typically encompasses multiple lanes; in our model, each cell corresponds to a single lane. As a result, a lane is depicted as a sequence of cells, with each cell's width matching the lane's width. The length of a cell is determined by the distance a vehicle travels at its free-flow speed in a one-time unit. This structure allows for a unique indexing of each cell in the grid with $i \in \mathcal{I} := \{0, 1, \ldots, I\}$. Central to our method is the development of a control strategy for each cell, representing a group of CAVs sharing the same movement. We call the CAV group control strategy "Coordination," and the cells within $\mathcal{I}$ are referred to as the "Coordination Area."

However, the incoming CAV traffic usually consists of mixed movements. The first step, therefore, is to segregate this mixed-movement CAV

traffic into separate cells, such that each cell contains only one movement. For this purpose, we introduce the concept of the "Pre-coordination Area," located just before merging movement from on-ramp vehicles and it is before the coordination area. This is represented as columns of additional cells at the entrance of the coordination area and is denoted by $\mathcal{I}^{-}$. In this manner, CAVs situated within a cell in $\mathcal{I}^{-}$ that have mixed movements both from the on-ramp and upstream mainline can be organized, with their specific movements separated in the subsequent time step, enabling them to reach the first column of cells in the coordination area. Moreover, for distinguishing vehicles on the main road and ramp, we denote cells of the pre-coordination area on the main road as I^{u-}; denote cells of the pre-coordination area on the ramp as I^{v-}. Additionally, for the sake of modeling convenience, we also monitor the CAVs that have passed through the weave segment, using extra cells for this purpose. This is called the "Post-coordination Area," and is denoted by $\mathcal{I}^{+}$. Conceptually, this is viewed as a virtual zone without capacity constraints, accommodating all traffic that has traversed the intersection. Similarly, we denote cells of the pre-coordination area on the main road as I^{u+}; denote cells of the pre-coordination area on the ramp as I^{v+}.

With the aid of the CTM, the longitudinal and lateral behaviors of CAVs can be described by transitions between adjacent cells. To facilitate this, we categorize the cells involved in such transitions as neighboring sets. For each cell i, its upstream neighbors are represented by the set $\mathcal{I}_i^{\alpha}$, while its downstream neighbors are denoted by $\mathcal{I}_i^{\beta}$. For any given cell i, traffic from any cell in $\mathcal{I}_i^{\alpha}$ can transition to cell i in the next time step. Likewise, traffic within cell i can advance to any cell in the downstream neighbor set $\mathcal{I}_i^{\beta}$ in the subsequent time step.

To describe the traffic state in cells, we let n_{idt} be the number of vehicles at cell $i \in \mathcal{I}$ at time $t \in \mathcal{T}$. Here, $d \in \mathcal{D} := \{-1, 1\}$ represents the desired directions of vehicles within a cell: -1 corresponds to the cell of vehicles

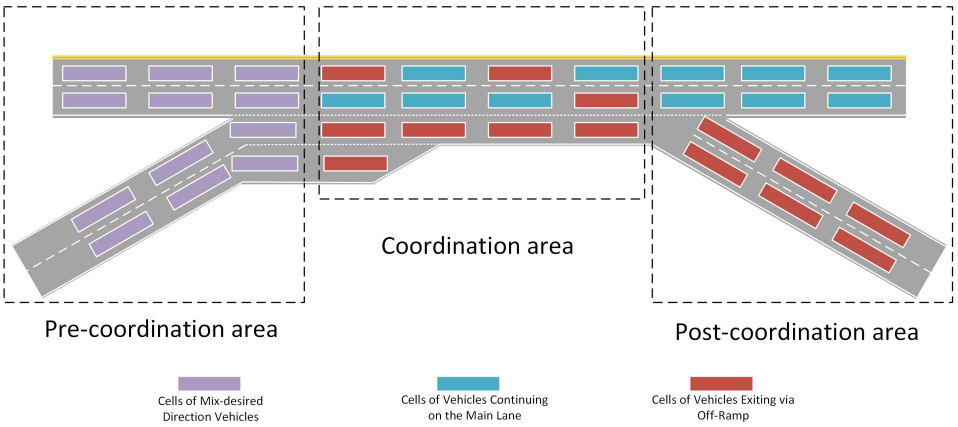

Figure 5.1: Pre-coordination area; coordination area; Post-coordination area

keep on the main road and 1 denotes the cell of vehicle will go down to the off-ramp. For example, $n_{2,1,3} = 1$ suggests that there is one vehicle in cell 2 at time 3 will pass the off-ramp.

Traffic Management

We assume that all CAV traffic, upon reaching the pre-coordination area, will be fully controlled by a centralized system. Our control strategy involves adjusting the inflow and outflow from each cell to its adjacent cells. This adjustment includes both the quantity and direction of the CAV flow. Specifically, the number of CAVs exiting one cell and their respective destination cells. For each cell $i \in \mathcal{I}^- \bigcup \mathcal{I}$ at time $t \in \mathcal{T}$, we define its flow decision as $y_{ijdt} \in [0, Y)$, where Y is the maximum flow. Here, $j \in \mathcal{I}_i^\beta$ represents the downstream neighbor cell of i, and $d \in \mathcal{D}$ denotes the direction.

Strategy Design

With all states and decisions introduced above, we are able to describe the cell-based CAV flow control strategy through a quadratic programming framework. First, our primary goal is to improve the efficiency of the

weave segment, i.e., maximize the number of vehicles passing through the weave segment during the planning horizon T. In addition, we hope more CAVs can enter the pre-coordination area so that our strategy can apply on a larger scale. Note that we should limit the number of lane changes in practice without necessity hence this would cause more energy and raise the risk of vehicle collisions. By jointly considering these factors, we can have the following connected automated flow control (CAFC) strategy,

$$\begin{aligned}\max_{y} b_{out}(t) & \sum_{j\in I^{+},t\in T}\sum_{i\in I_j^{\alpha}} y_{ijdt} \\ & -\gamma \sum_{i'\in I,t\in T,d\in D}\sum_{j'\in I_{i'}^{\tilde{\beta}}} y_{i'j'dt} \\ & -\dot{\gamma} \sum_{i''\in I^{v},t\in T,d\in D}\sum_{j''\in I_{i'}^{\tilde{\beta}}} y_{i''j''dt} \\ & + b_{in} \sum_{i'''\in I^{-},t\in T,d\in D}\sum_{j'''\in I_{i''}^{\beta}} y_{i'''j'''dt}.\end{aligned} \tag{5.1}$$

Here, the first term expresses the cumulative traffic flow that has passed through the weave segment. In order to push vehicles passing through the intersection quickly, we introduce a time-dependent bonus term $b_{out}(t)$, which decreases over time t. The second term represents the penalty for lane changes, where γ is a positive penalty. The last term accounts for the bonus to traffic entering the coordination area, where b_{in} is also a positive constant.

Then, to ensure that the strategy is feasible, we need to provide a series of constraints.

Customized Fundamental Diagram of CAV

The behaviors of CAVs described by transitions between adjacent cells are characterized by the CTM. Critical parameters in the CTM can be derived from the fundamental diagram (FD). Among multiple variations of the FD, we choose the triangular FD due to its simplicity and representative

quality Daganzo (1994).

It's important to note that the FD describes the macroscopic traffic flow behavior for vehicles. The focus of our work is on CAVs, which differ slightly from traditional Human-Driven Vehicles (HDVs). To select the appropriate parameters for CAV traffic, we conducted a comparative analysis of traffic dynamics between CAVs and HDVs, as illustrated in Figure 5.2.

Figure **??** depicts the relationship between spacing and speed for both CAVs and HDVs. A spacing-speed profile for traffic flow represents the car-following behavior. The triangular FD corresponds to a piece-wise linear car-following law. Initially, the following vehicle will remain stationary when its headway to the leading vehicle is less than the minimum spacing, denoted by g_0. Subsequently, it accelerates at a constant rate to maintain a consistent spacing with the leading vehicle, denoted by h. Finally, it reaches the free flow speed, denoted by v_f. It's noteworthy that due to the rapid "reaction time" of CAVs, they can maintain a shorter desired headway, resulting in reduced spacing compared to HDVs traveling at identical speeds. Therefore, in contrast to HDV traffic, we opt for a relatively short headway h_{CAV} and a smaller minimal spacing $g_{0,CAV}$ for CAV traffic.

Given the speed-spacing car-following law, the corresponding triangular FD is illustrated in Figure 5.2b. Specifically, let q_{max} denote the maximum flow rate, k_j represent the jam density, and w be the shockwave speed. The parameters in the FD can be derived from those in the speed-spacing profile as follows:

$$k_j = \frac{1}{g_0},$$

$$q_{max} = \frac{v_f}{g_0 + v_f * h},$$

$$-w = \frac{q_{max}}{k_j - \frac{1}{g_0 + v_f * h}}.$$

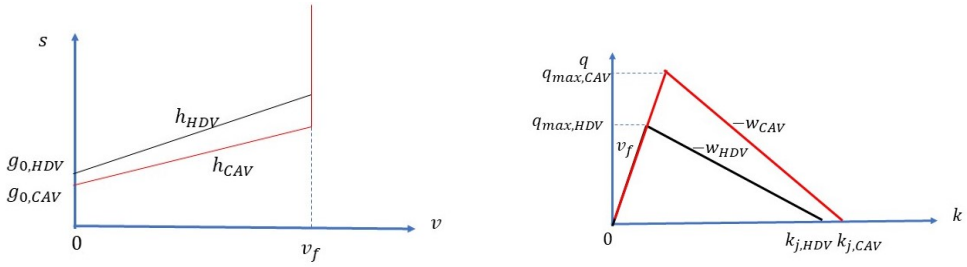

(a) Spacing-Speed Profile

(b) Triangular Fundamental Diagram

Figure 5.2: CAV and HDV behavior comparison

The reduced minimum spacing and desired headway of CAVs result in a slightly higher flow-density curve in the FD. This suggests that CAVs can achieve a higher maximum flow under the same road conditions and are less prone to congestion.

Vehicle Dynamics based on CTM

To apply CTM, we first normalize the traffic state and flow decision with respect to the discretization resolution. Let $\triangle$ l represent the length of each cell and $\triangle$ t represent the length of the time interval. We have

$$y_{ijdt} = q_{ijdt} \triangle t, \tag{5.2}$$

$$n_{idt} = k_{idt} \triangle l. \tag{5.3}$$

Here, q_{ijdt} indicates the traffic flow rate with desired direction d from cell i to one of the downstream cells j during one time interval t, while k_{idt} indicates the traffic density with desired direction d in cell i during a time interval t.

Further, given the triangular FD, we introduce the upper and lower bounds of traffic flow rate and traffic density as follows:

$$0 \leqslant \sum_{d \in D} q_{ijdt} \leqslant q_{max}, \tag{5.4}$$

$$0 \leqslant \sum_{d \in D} k_{idt} \leqslant k_j. \tag{5.5}$$

Here, q_{max} and k_j are the corresponding max flow and jam density, respectively, for CAVs. Note that the flow moving out from cell i is limited by the number of vehicles in the cell. Hence,

$$n_{idt} \geqslant \sum_{j \in I_i^{\beta}} y_{ijdt}. \tag{5.6}$$

Then, we describe the vehicle dynamics in the coordination area for $i \in I$ and $t \in T$. The pre-coordination areas I^- and post-coordination area I^+ will be discussed separately. Based on the state of cells and vehicles, we have:

$$n_{idt} = n_{id(t-1)} + \sum_{j' \in I_i^{\alpha}} y_{j'id(t-1)} - \sum_{j'' \in I_i^{\beta}} y_{ij''d(t-1)}. \tag{5.7}$$

Here, Equation (5.7) characterizes the dynamic state of cell i from time $t-1$ to time t. Specifically, the number of vehicles in cell i at time t depends on the number of vehicles in cell i at time $t-1$, considering the traffic flow exiting cell i (the cumulative outflow to its downstream neighbor set) and entering cell i (the cumulative inflow from its upstream neighbor set) during the previous time step $t-1$.

Furthermore, we calculate receiving flow r_{ijdt} and sending flow s_{ijdt} according to the CTM. If cell i and cell j are neighbors, the traffic flow from cell i to cell j with direction d at time t depends as follows:

$$r_{ijdt} = min\{w/v_f(k_j \triangle l - \sum_{d \in D} n_{idt}), q_{max} \triangle t\}, \tag{5.8}$$

$$s_{ijdt} = min\{\sum_{d \in D} n_{idt}, q_{max} \triangle t\}, \tag{5.9}$$

$$y_{ijdt} = min\{r_{ijdt}, s_{ijdt}\}. \tag{5.10}$$

Here, the variable w represents the CAV's shockwave speed, and v_f denotes the CAV's free flow speed. Equation (5.8) shows the maximum traffic flow that cell j can receive from cell i, while Equation (5.9) characterizes the maximum traffic flow that cell i can send to cell j. The exact traffic flow y_{ijdt} between cell i and cell j is determined by taking the minimum value of r_{ijdt} and s_{ijdt}.

Next, we provide the criteria for the boundary and initial conditions.

Boundary and Initial Conditions

Firstly, we consider the constraints related to the pre-coordination area I^-. To help group CAVs according to the different desired direction of vehicles, we set that the desired direction d of traffic in any cell of the coordination area be with unique direction. Note that in the coordination area, the CAVs in the cells are only allowed to have single direction traffic. Thus, we introduce $z_{idt} \in \{0, 1\}$ as a binary indicator variable, representing if cell i at time t contains CAVs with direction d . Then, we have

$$n_{idt} \leqslant z_{idt} n_{idt}, \tag{5.11}$$

which activates the indicator with the traffic state. Then we use

$$\sum_{d \in D} z_{idt} \leqslant 1, \forall i \in I, \forall t \in T, \tag{5.12}$$

to guarantee at the coordination area, CAV's direction is exclusive.

Then we model the vehicle destination, i.e., keep on the main road or down to the off-ramp. Recall that $d \in D := \{-1, 1\}$ represents the desired direction which include Through (keep on the main road), leave (off-ramp). Recall, we denoted cells of pre-coordination area on the main road as I^{u-}; denoted cells of pre-coordination area on the ramp as I^{v-}. Therefore, to facilitate the passage of traffic through the weave segment, we use the following conditions:

$$y_{ijdt} = \begin{cases} 1 & \text{if } d = 1 \text{ and } i \in I^{u-}, \\ 1 & \text{if } d = -1 \text{ and } i \in I^{v-}, \\ 0 & \text{otherwise.} \end{cases} \tag{5.13}$$

We also discuss the initial condition. At time $t = 0$, suppose the system observes the traffic state as n^0_{id} for $i \in I$ and $d \in D$. We have

$$n_{id0} = n^0_{id}, \forall i, d. \tag{5.14}$$

Variable Feasibility

Note that we have mixed directions in the pre-coordination area, the dynamic of mixed traffic is more complicated. When mixed CAVs enter the coordination area from the pre-coordination area, we separate the flow into two cells, hence the are with to ensure traffic feasibility within each cell, particularly for cells containing mixed desired direction traffic, only vehicles with the same speed are permitted within the cell. Thus, we have the following condition:

$$\sum_{j \in I^\beta_i} y_{ij1t} n_{i(-1)t} = \sum_{j \in I^\beta_i} y_{ij(-1)t} n_{i1t}. \tag{5.15}$$

To avoid conflict during lane changing, i.e. cannot do "crossing" lane change, as shown in Figure 5.3, we define conflict set $((i^c_1, i^c_2), (i'^c_1, i'^c_2)) \in F$ with cells where the traffic flow could conflict when doing lane changing. Hence, we have

$$y_{ijdt} = m_{ijdt} y_{ijdt}, \tag{5.16}$$

$$\sum_{d \in D} m_{i^c_1, i^c_2, d, t} + m_{i'^c_1, i'^c_2, d, t} \leqslant 1. \tag{5.17}$$

Here, $m_{ijdt} \in \{0, 1\}$ is a binary variable.

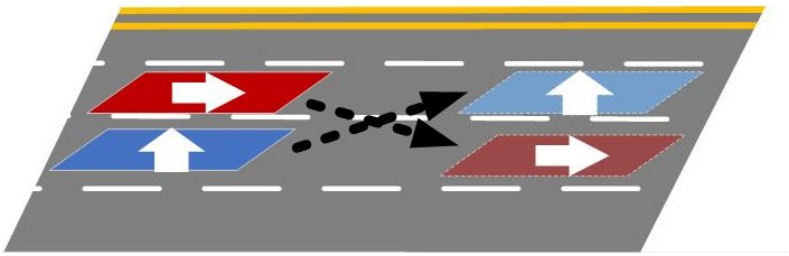

Figure 5.3: Example of "Crossing" Lane Change

For notional connivance, we define $C(\mathbf{y}, \mathbf{n})$ as the constraint set containing all constraints, i.e., Constraints 5.2 - 5.17. Therefore, the connected automated flow control problem (CAFCP) can be modeled as the following,

$$\text{(CAFCP)} \quad \max_{\mathbf{y},\mathbf{n}\in C(\mathbf{y},\mathbf{n})} b_{out}(t) \sum_{j\in I^+,d\in D,t\in T} \sum_{i\in I_j^\alpha} y_{ijdt} \tag{5.18}$$
$$- \gamma \sum_{i'\in I,t\in T,d\in D} \sum_{j'\in I_{i'}^{\tilde{\beta}}} y_{i'j'dt} + b_{in} \sum_{i''\in I^-,t\in T,d\in D} \sum_{j''\in I_{i''}^{\beta}} y_{i''j''dt}.$$

Rolling-Horizon Scheme

Note that CAFC handles the scenario of complete information, i.e., all traffic information is given at the beginning as initial conditions. The optimal decision will be the control of all traffic flow over T. However, traffic will always arrive in the system in reality. Hence, we will need to extend the above strategy to be adaptive concerning any arrival scenarios.

To address traffic uncertainty and achieve real-time control, a time-rolling strategy is adopted. The CAV movement strategy is planned across the entire $\mathcal{T}$, but only the action at time $t = 0$ is implemented. This strategy is updated at each successive time step.

In theory, as the states of arrival traffic are uncertain, the optimal management policy should be obtained through a stochastic programming structure, which leads to a problem scale and intractability. Given the

practical need, we consider an adaptive rolling-horizon strategy. Suppose we solve a problem with the entire time horizon $T^L = \{0, 1, ..., T_{max}\}$ with a rolling horizon length of $T + 1$. We define $T(\tau) = \{\tau, \tau + 1, ..., \tau + T\}$ as the moving planning horizon starting at τ. We define a time index mapping $\Gamma(t; \tau) = t - \tau$ to convert the actual time index t to the corresponding time index inside the moving horizon $T(\tau)$. Then we have Rolling-Horizon Algorithm (5.2).

Step 0: At time 0, initialize the planning horizon $T = T(0)$, obtain the state of all vehicles in the coordination area n^0_{idt} and the signal phase $s_{ntt\in T(0)}$.

Step 1: At time τ, solve the quadratic programming problem within the planning horizon $T(\tau)$ and obtain the management strategy $y_{jid\Gamma(t;\tau)}$.

Step 2: Use the one-step movement $y_{jid\Gamma(0;\tau)}$ and the vehicle dynamics constraint to obtain $n_{id\Gamma(1;\tau)}$ as new vehicle states.

Step 3: Update the initial vehicle state $n^0_{idt} \leftarrow$ the combination of $n_{id\Gamma(1;\tau)}$ and new arrivals.

Step 4: Update $\tau \leftarrow \tau + 1$, update the rolling horizon to $T(\tau)$, and update the signal phase to $p_{\Gamma(t;\tau)t\in T(\tau)}$.

Repeat Steps 1-4 until $\tau + T > T_{max}$.

With Algorithm (5.2), our strategy can be applied to an infinitely long time of management scenarios.

5.3 Case Study

In this section, we conduct a series of case studies to show the effectiveness of the proposed flow management strategy. To achieve this goal, we first provide a benchmark case and illustrate the detailed operations over the entire coordination area step-by-step. Then, the flow management strategy is compared with scenarios without any coordination. All algorithms are

solved by Gurobi on a desktop computer with i7-10700 CPU @2.90 GHz and 32.0GB RAM.

First, the fundamental settings in the benchmark case are as follows. We set a weave section in highway road segment with two-lane main lane, two-lane on-ramp and two lane off-ramp with a speed limit of 70 mph ($\approx$112.65 km/h). This coordination area is set to a grid with 0.097 mile ($\approx$155 m) length for each cell and three columns of cells in total (i.e., 465 m), which guarantees vehicles can pass one cell per unit time at the speed limit. Let the time unit be five seconds and the length for a rolling planning horizon be 40 seconds (i.e., 8 unit times). Traffic flow of this benchmark is under the uniform distribution from 0.6 vehicle/second to 1 vehicle/second with 50% exiting vehicle and 50% continuing vehicle.

The traffic flow in this benchmark case is uniformly distributed between 0.6 and 1 vehicle/second, with 50% of traffic flow being continuing traffic, i.e., wherever they come continuing on the mainline and 50% being exiting traffic, i.e., exiting on the off-ramp. To validate the correctness of our proposed strategy, we consider a case where besides the same desired direction ratio between vehicle input on mainline and ramp, demand from upstream on mainline and ramp is also the same. The minimum spacing between vehicles is set to 5 meters, and based on the FD, the jam density is calculated to be 324.3 veh/mile.

In this research, we investigate two representative cases by applying our proposed management strategy, with full coordination and partial coordination. The difference between these two cases is that with full coordination, all vehicles in the weaving section are controlled, while in the partial coordination case, only freeway interchange traffic under coordination, i.e., freeway to freeway traffic without coordination, freeway to ramp traffic with coordination, ramp to freeway vehicle under coordination until vehicle drive into the freeway.

Based on these settings, a sample result of the proposed algorithm is

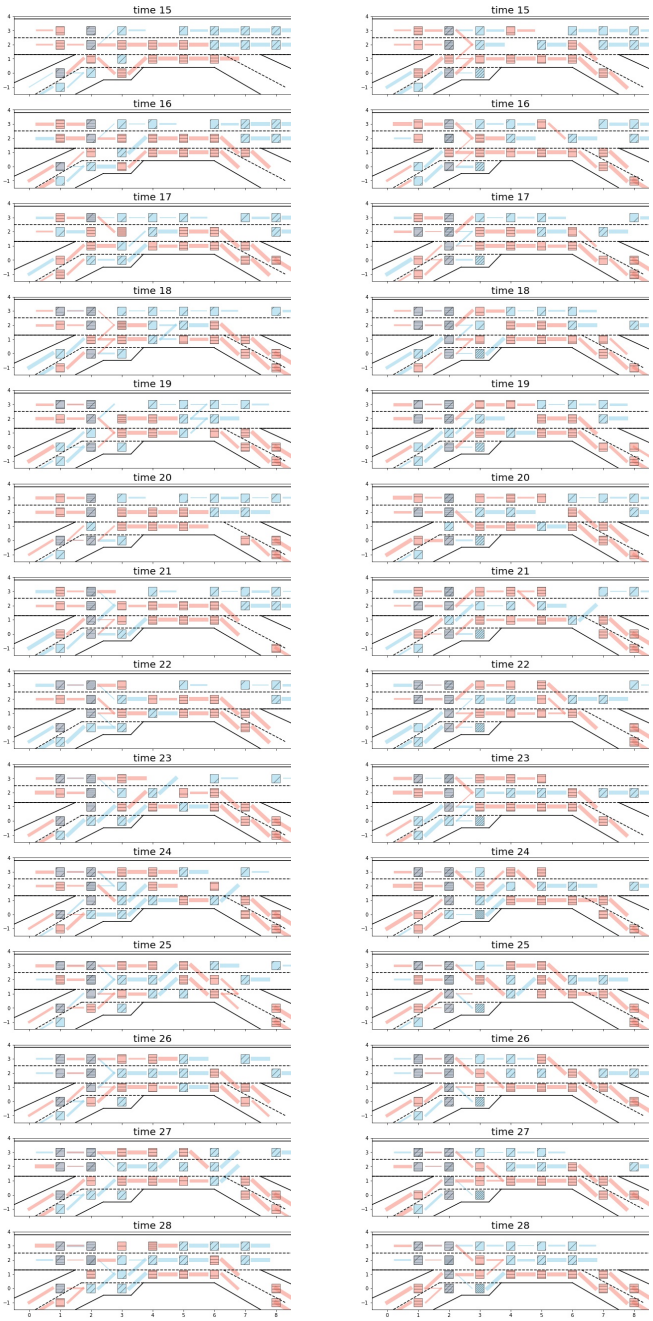

(a) Sample results of with coordination

(b) Sample results of with partial coordination

Figure 5.4: Sample results comparison with coordination and partial coordination

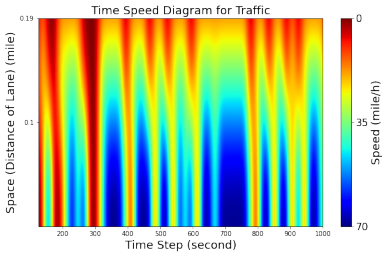

(a) On-ramp

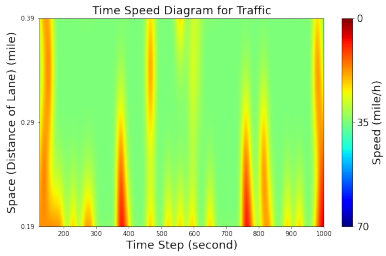

(b) Auxiliary lane

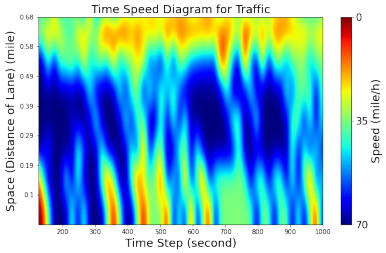

(c) Mainline

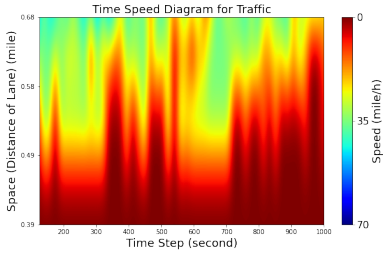

(d) Off-ramp

Figure 5.5: Time-space diagram with coordination

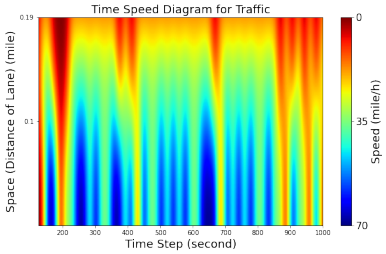

(a) On-ramp

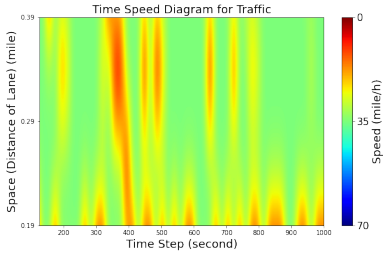

(b) Auxiliary lane

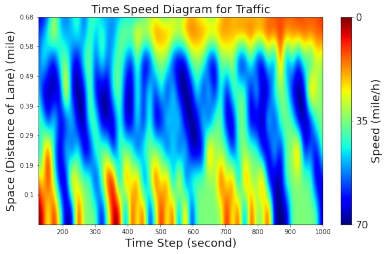

(c) Mainline

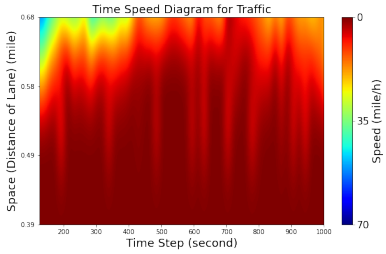

(d) Off-ramp

Figure 5.6: Time-space diagram with partial coordination

shown in Figure 5.4 for demonstration purposes. In this sample result, the arrival rate is 0.8 vehicles per second per lane. In these figures, the bird's eye view of the sorting area is plotted for each time step (5 seconds), and the driving direction of vehicles is from left to right.

To clarify, each bird view plot presented in the paper represents the traffic conditions in the coordination area for a specific time step. The 8 columns in each plot correspond to the whole weaving section (Columns 3-5), the pre-coordination area (Columns 0-1), and the post-sorting area (Columns 6-8). The grids on the plot indicate cells, and the color of the cell shows the desired direction status of the traffic in the cell. Specifically, "blue" indicates continuing traffic (continuing driving on the freeway), and "red" indicates exiting traffic. The density of the stripes on the grid indicates the number of vehicles present in the cell. Additionally, the lines between cells indicate the traffic flow between corresponding cells, with the width of the line representing the amount of the traffic flow.

Figure 5.4a illustrates the effectiveness of the proposed algorithm. For merging with entering traffic, it is observed because of the existence of a pre-coordination area to separate mixed-direction traffic, this algorithm perfectly avoids traffic conflict caused by merging. For diverging with exiting traffic, continuing traffic, and exiting traffic alternate occupied the right lane of the mainline to maximum utilization of temporal and spatial resources. To further analyze the scenarios with coordination, the Space-Time Speed Diagram, as depicted in Figure 5.5, serves as a crucial visualization tool to assess the impact of algorithm implementation on the average speed across all lanes. The diagram illustrates the temporal and spatial evolution of traffic speed along the on-ramp, auxiliary lane, mainline, and off-ramp. Figure 5.5c and Figure 5.5a demonstrate that traffic can reach free-flow speeds (70 mph), signifying that vehicles on mainlines and on-ramps can attain free-flow speeds simultaneously. On the other hand, Figure 5.4b and Figure 5.6 show the example result of the

Table 5.2: Sensitivity Analysis

	Throughput			
k	$b_{out}(t) = \frac{(8-t)}{8}k$	$\gamma = k$	$\dot{\gamma} = k$	$\mathbf{b_{in}} = k$
0	-	5846	**6091**	811
0.5	4927	5930	6017	5726
1	5577	5712	5906	5657
5	5937	**5940**	5655	5673
10	**5964**	5510	5798	5765
50	5844	3264	4260	**5844**
100	5923	2738	3276	5744

Benchmark: $b_{out}(t) = 10(1 - \frac{1}{8}t)$, $\gamma = 1$,$\dot{\gamma} = 0.5$, $c_i = 10$

partial coordination scenario in the same set of vehicle input, even though only part of the vehicles are under coordination the sample result also shows a similar behavior with the coordination scenario.

To facilitate demonstration, we define the number of vehicles passing through the intersection per hour as throughput. The throughput of the partial coordination scenario is 6436.8 vehicles per hour, whereas with coordination scenario achieves a throughput of 7581.6 vehicles per hour, indicating an improvement rate of about 17.7%.

To choose hyper-parameters in the objective function mentioned in Equation (5.18), we conduct a series of sensitivity analyses by introducing a variable k. The k is set to vary from 0 to 100. After running each case for 5 time, the result is shown in Table (5.2). After sensitivity analysis, we choose hyper-parameters with the largest throughput. Thus, we set $b_{out}(t) = 10(1 - \frac{1}{8}t)$, $\gamma = 5$, $\dot{\gamma} = 0$, $c_i = 50$ as hyper-parameters. The average computational time for solving the Rolling-Horizon SP is controlled to less than unit time, i.e., 5 seconds.

Furthermore, to assess the efficiency of the proposed strategy, we compare its performance with coordination and partial coordination. To investigate the impact of varying arrival rates, we keep the other parameters constant and vary the arrival rate from 0.4 vehicles per second per lane to

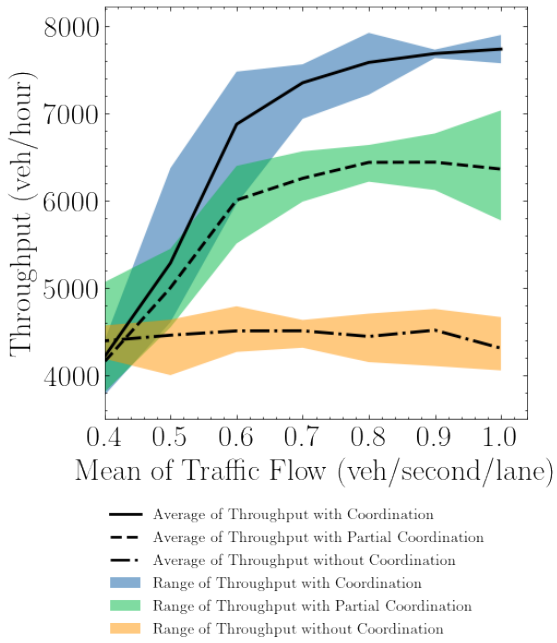

magenta

Figure 5.7: Performance comparison with and without coordination and control

1 vehicle per second per lane with 0.1 intervals. Recall that we define the number of vehicles passing through the intersection per hour as throughput. Owing to the uncertainty of incoming traffic states, we perform the Monte Carlo simulation ten times for each case, with 300 seconds, i.e., 60-time steps for each run.

The findings from our simulations are illustrated in Figure 5.7. In each case, the curves with full line represent the mean values of the Monte Carlo simulation results with coordination, highlighting the overall trends. The blue shadow surrounding the curves denotes the range of throughput observed in each scenario, spanning from the maximum to the minimum throughput values. The curves with dashed lines represent the mean values of the Monte Carlo simulation results with partial coordination, highlighting the overall trends. The green shadow surrounding the curves

denotes the range of throughput observed in each scenario, spanning from the maximum to the minimum throughput values. The curves with long and short dash lines represent the mean values of simulation results from the Vissim for AV setting (under the same geometry and keeping the headway and spacing the same with coordination scenario) called without coordination, highlighting the overall trends. The yellow shadow surrounding the curves denotes the range of throughput observed in each scenario, spanning from the maximum to the minimum throughput values.

Here's the polished version of the provided text:

A comprehensive comparison between coordination and partial coordination consistently enhances throughput across all scenarios. For instance, at an arrival rate of 1 vehicle per second per lane, throughput improves by approximately 21.6%. With coordination, the average maximum throughput reaches 7734 vehicles per hour, significantly surpassing the throughput of 6360 vehicles per hour in the scenario without coordination. These results confirm that the proposed coordination strategy demonstrates superior performance compared to the traditional approach, effectively optimizing traffic flow and enhancing intersection throughput.

Furthermore, a comprehensive comparison between coordination and no coordination reveals throughput improvements across relatively busy scenarios (>0.4 vehicles per second per lane). For instance, at an arrival rate of 1 vehicle per second per lane, throughput improves by approximately 79.6%. With coordination, the average maximum throughput reaches 7734 vehicles per hour, significantly surpassing the throughput of 4308.5 vehicles per hour in the scenario without coordination. These findings underscore the effectiveness of the proposed coordination strategy in optimizing traffic flow and improving intersection throughput.

Figure 9 illustrates the impact of the desired direction ratio for input vehicles on both the ramp and mainline during moderate and busy traffic

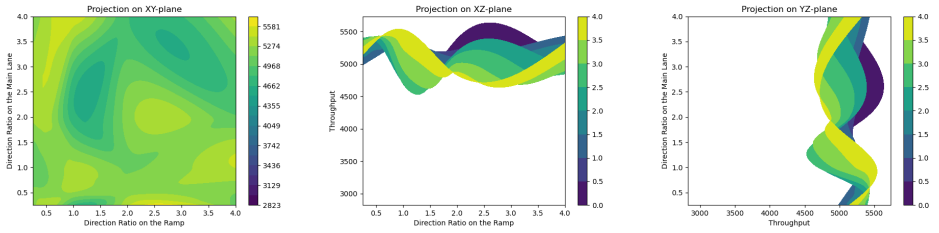

(a) XY-plane with coordination (b) XZ-plane with coordination (c) YZ-plane with coordination

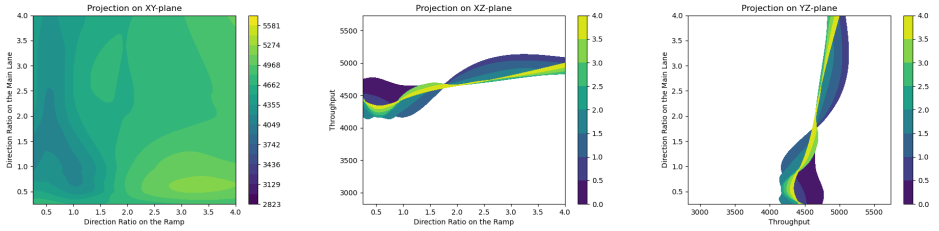

(d) XY-plane with partial coordination (e) XZ-plane with partial coordination (f) YZ-plane with partial coordination

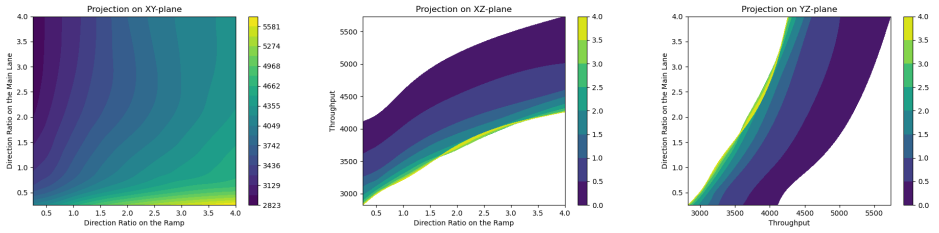

(g) XY-plane without coordination (h) XZ-plane without coordination (i) YZ-plane without coordination

Figure 5.8: Impact of desired direction ratio for input vehicles on the ramp and mainline for moderate traffic hours (0.5 vehicle/s/lane)

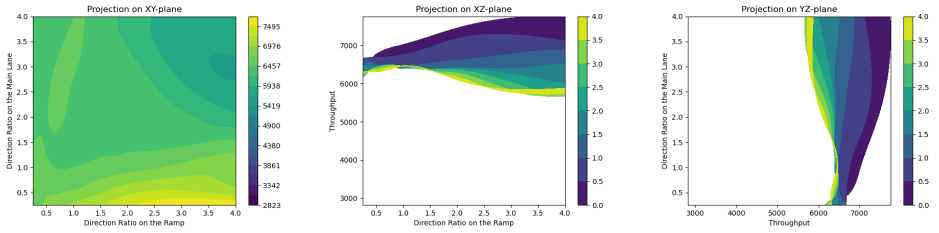

(a) XY-plane with coordination (b) XZ-plane with coordination (c) YZ-plane with coordination

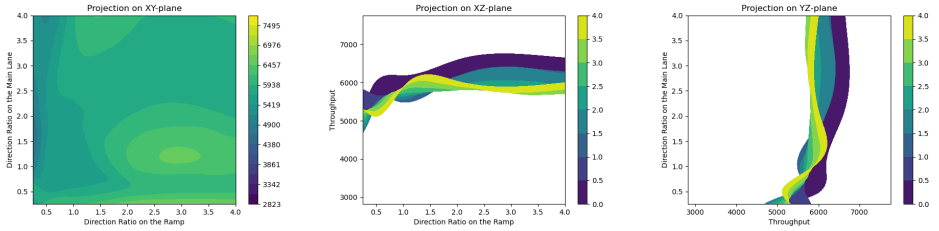

(d) XY-plane with partial coordination (e) XZ-plane with partial coordination (f) YZ-plane with partial coordination

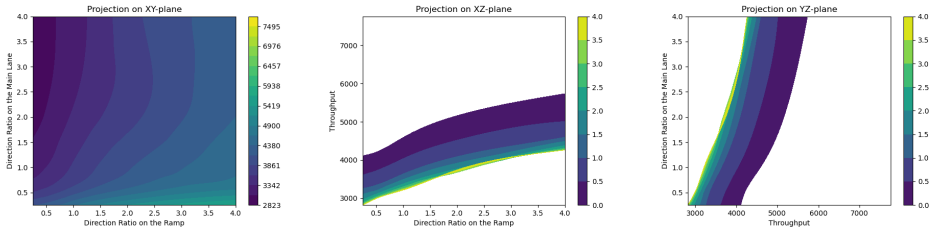

(g) XY-plane without coordination (h) XZ-plane without coordination (i) YZ-plane without coordination

Figure 5.9: Impact of desired direction ratio for input vehicles on the ramp and mainline for busy hour (0.8 vehicle/s/lane)

hours. In the moderate traffic scenario, where the demand is 0.5 vehicles per second per lane for both the on-ramp and mainline, the graphs are divided into three groups: a-c represent the coordination scenario, d-e depict partial coordination, and g-i show the scenario without coordination. Each group presents three plane projections (XY, XZ, and YZ) of the 3D graph. Analyzing the graphs reveals that in scenarios with pre-coordination, where traffic for different desired directions is separated, the change in the desired direction ratio has minimal impact, showcasing the robustness of the algorithm. Furthermore, in Figure 10, which focuses on the busy hour scenario with increased demand (0.8 vehicles per second per lane), it is evident that regardless of the changing ratio of desired direction, coordination, and even partial coordination significantly improves weaving section capacity.

5.4 Conclusion

In this study, we have presented a comprehensive analysis and evaluation of a novel coordination strategy for traffic flow management in a weaving section of a highway interchange. Leveraging advanced control techniques and the concept of connected automated vehicles (CAVs), our proposed strategy aims to optimize traffic flow, enhance intersection throughput, and minimize congestion.

Through a series of case studies and sensitivity analyses, we have demonstrated the effectiveness and robustness of the proposed strategy. By considering both full coordination and partial coordination scenarios, we have shown consistent improvements in throughput across various traffic conditions and arrival rates. In particular, our strategy outperforms traditional approaches by achieving significant enhancements in intersection throughput, even in scenarios with relatively high traffic volumes.

Overall, the results of our study underscore the potential benefits of

integrating advanced control techniques and CAV technologies into traffic management systems. By deploying adaptive and proactive strategies, transportation agencies can significantly improve the efficiency, safety, and sustainability of road networks, ultimately enhancing the overall quality of urban mobility and driving experiences for commuters.

6 CONCLUSION

In summary, this research has significantly contributed to advancing traffic management strategies at intersections and weaving sections through the integration of connected automated vehicle (CAV) technologies. For intersections, we established a modeling framework facilitating optimal CAV coordination without the need for additional infrastructure. Using a mixed-integer programming model with Boolean logic constraints, we proposed a rolling time-horizon-based CAV sorting strategy, enhancing intersection capacity and yielding real-time decisions through an accelerated algorithm. Numerical experiments showcased notable improvements in sorting strategy performance, particularly under heavy traffic conditions. However, identified limitations include the need for a more detailed description of vehicle dynamics and scalability issues with the model. Future research may involve embedding continuous vehicle dynamic models onto the grid system and extending the approach to complex traffic scenarios involving multi-direction and multi-intersection setups.

To address the scalability limitations of microscopic control, we introduced a macroscopic control strategy designed specifically for CAVs at signalized intersections. Leveraging the Cell Transmission Model (CTM), our approach considered collective CAV behavior to optimize traffic flow, demonstrating robustness and minimal sensitivity to parameter variations across various traffic conditions. Numerical experiments revealed substantial improvements in intersection throughput, particularly in heavy traffic conditions, with throughput enhancements reaching approximately 72%. This study lays the groundwork for further exploration and implementation of macroscopic control strategies for CAVs in urban traffic management systems, offering valuable insights for transportation authorities and researchers.

Additionally, we proposed a novel coordination strategy for traffic

flow management in weaving sections of highway interchanges, aiming to optimize traffic flow, enhance throughput, and minimize congestion. Through comprehensive case studies and sensitivity analyses, our strategy consistently improved throughput across various traffic conditions and arrival rates, outperforming traditional approaches even under relatively high traffic volumes. These findings underscore the potential benefits of integrating advanced control techniques and CAV technologies into traffic management systems, promising improvements in efficiency, safety, and sustainability in urban mobility.

REFERENCES

Abdel-Aty, Mohamed, and Ling Wang. 2017. Implementation of variable speed limits to improve safety of congested expressway weaving segments in microsimulation. *Transportation research procedia* 27:577–584.

Al Islam, SMA Bin, Ali Hajbabaie, and HM Abdul Aziz. 2020. A real-time network-level traffic signal control methodology with partial connected vehicle information. *Transportation Research Part C: Emerging Technologies* 121:102830.

Bai, Yu, Yu Zhang, Xin Li, and Jia Hu. 2022. Cooperative weaving for connected and automated vehicles to reduce traffic oscillation. *Transportmetrica A: transport science* 18(1):125–143.

Bevly, David, Xiaolong Cao, Mikhail Gordon, Guchan Ozbilgin, David Kari, Brently Nelson, Jonathan Woodruff, Matthew Barth, Chase Murray, Arda Kurt, et al. 2016. Lane change and merge maneuvers for connected and automated vehicles: A survey. *IEEE Transactions on Intelligent Vehicles* 1(1):105–120.

Cassidy, Michael J, and Adolf D May. 1991. Proposed analytical technique for estimating capacity and level of service of major freeway weaving sections. *Transportation Research Record* 1320(99–109):75.

Chen, Chaoyi, Jiawei Wang, Qing Xu, Jianqiang Wang, and Keqiang Li. 2021a. Mixed platoon control of automated and human-driven vehicles at a signalized intersection: dynamical analysis and optimal control. *Transportation research part C: emerging technologies* 127:103138.

———. 2021b. Mixed platoon control of automated and human-driven vehicles at a signalized intersection: Dynamical analysis and optimal control. *Transportation Research Part C: Emerging Technologies* 127:103138.

Chen, Xiangdong, Xi Lin, Qiang Meng, and Meng Li. 2023. Coordinated traffic control of urban networks with dynamic entrance holding for mixed cav traffic. *Transportation research part E: logistics and transportation review* 178:103264.

Cottrell, Wayne D. 1998. Estimating the probability of freeway congestion recurrence. *Transportation research record* 1634(1):19–27.

Daganzo, Carlos F. 1994. The cell transmission model: A dynamic representation of highway traffic consistent with the hydrodynamic theory. *Transportation Research Part B: Methodological* 28(4):269–287.

Daganzo, Carlos F. 1995. The cell transmission model, part ii: Network traffic. *Transportation Research Part B: Methodological* 29(2):79–93.

Dong, Shiying, Hong Chen, Bingzhao Gao, Lulu Guo, and Qifang Liu. 2022. Hierarchical energy-efficient control for cavs at multiple signalized intersections considering queue effects. *IEEE Transactions on Intelligent Transportation Systems* 23(8):11643–11653.

Dong, Shuoxuan, Yang Zhou, Tianyi Chen, Shen Li, Qiantong Gao, and Bin Ran. 2021. An integrated empirical mode decomposition and butterworth filter based vehicle trajectory reconstruction method. *Physica A: Statistical Mechanics and its Applications* 583:126295.

Du, Jianbang, Qing Li, and Fengxiang Qiao1 Lei Yu. 2018. Vehicle emission estimation on mainline freeway under isolated and integrated ramp metering strategies. *Environmental Engineering and Management Journal* 17(5).

Duell, Melissa, Michael W Levin, Stephen D Boyles, and S Travis Waller. 2016. Impact of autonomous vehicles on traffic management: Case of dynamic lane reversal. *Transportation Research Record* 2567(1):87–94.

Garey, Michael R. 1979. computers and intractqbility. *A Guide to the Theory of NP-Completeness*.

Gokasar, Ilgin, Alperen Timurogullari, Muhammet Deveci, and Harish Garg. 2023. Swscav: Real-time traffic management using connected autonomous vehicles. *ISA transactions* 132:24–38.

Golob, Thomas F, Wilfred W Recker, and Veronica M Alvarez. 2004. Safety aspects of freeway weaving sections. *Transportation Research Part A: Policy and Practice* 38(1):35–51.

Gong, Siyuan, Jinglai Shen, and Lili Du. 2016. Constrained optimization and distributed computation based car following control of a connected and autonomous vehicle platoon. *Transportation Research Part B: Methodological* 94:314–334.

Guo, Qiangqiang, Li Li, and Xuegang Jeff Ban. 2019. Urban traffic signal control with connected and automated vehicles: A survey. *Transportation research part C: emerging technologies* 101:313–334.

Han, Xiao, Rui Ma, and H Michael Zhang. 2020. Energy-aware trajectory optimization of cav platoons through a signalized intersection. *Transportation Research Part C: Emerging Technologies* 118:102652.

Hao, Wei, Zhaolei Zhang, Zhibo Gao, Kefu Yi, Li Liu, and Jie Wang. 2020. Research on mandatory lane-changing behavior in highway weaving sections. *Journal of advanced transportation* 2020:1–9.

Jiang, Huifu, Jia Hu, Shi An, Meng Wang, and Byungkyu Brian Park. 2017. Eco approaching at an isolated signalized intersection under partially connected and automated vehicles environment. *Transportation Research Part C: Emerging Technologies* 79:290–307.

Levin, Michael W., and Stephen D. Boyles. 2016a. A cell transmission model for dynamic lane reversal with autonomous vehicles. *Transportation Research Part C: Emerging Technologies* 68:126–143.

Levin, Michael W, and Stephen D Boyles. 2016b. A multiclass cell transmission model for shared human and autonomous vehicle roads. *Transportation Research Part C: Emerging Technologies* 62:103–116.

Levin, Michael W, and David Rey. 2017. Conflict-point formulation of intersection control for autonomous vehicles. *Transportation Research Part C: Emerging Technologies* 85:528–547.

Li, Shen, Keqi Shu, Chaoyi Chen, and Dongpu Cao. 2021a. Planning and decision-making for connected autonomous vehicles at road intersections: A review. *Chinese Journal of Mechanical Engineering* 34(1):1–18.

Li, Shen, Keqi Shu, Yang Zhou, Dongpu Cao, and Bin Ran. 2021b. Cooperative critical turning point-based decision-making and planning for cavh intersection management system. *IEEE Transactions on Intelligent Transportation Systems* 1–11. Advanced online publication. `https://doi.org/10.1109/TITS.2021.3099484`.

Li, Xiaopeng, Amir Ghiasi, Zhigang Xu, and Xiaobo Qu. 2018. A piecewise trajectory optimization model for connected automated vehicles: Exact optimization algorithm and queue propagation analysis. *Transportation Research Part B: Methodological* 118:429–456.

Lighthill, Michael James, and Gerald Beresford Whitham. 1955. On kinematic waves ii. a theory of traffic flow on long crowded roads. *Proceedings of the Royal Society of London. Series A. Mathematical and Physical Sciences* 229(1178):317–345.

Liu, Xiaoyue Cathy, Yinhai Wang, Bastian J Schroeder, and Nagui M Rouphail. 2012. Quantifying cross-weave impact on capacity reduction

for freeway facilities with managed lanes. *Transportation research record* 2278(1):171–179.

Mirheli, Amir, Leila Hajibabai, and Ali Hajbabaie. 2018. Development of a signal-head-free intersection control logic in a fully connected and autonomous vehicle environment. *Transportation Research Part C: Emerging Technologies* 92:412–425.

Ngoduy, Dong, NH Hoang, HL Vu, and D Watling. 2021. Multiclass dynamic system optimum solution for mixed traffic of human-driven and automated vehicles considering physical queues. *Transportation research part B: methodological* 145:56–79.

Öncü, Sinan, Jeroen Ploeg, Nathan Van de Wouw, and Henk Nijmeijer. 2014. Cooperative adaptive cruise control: Network-aware analysis of string stability. *IEEE Transactions on Intelligent Transportation Systems* 15(4): 1527–1537.

Pi, Xidong, Wei Ma, and Zhen Sean Qian. 2019. A general formulation for multi-modal dynamic traffic assignment considering multi-class vehicles, public transit and parking. *Transportation Research Part C: Emerging Technologies* 104:369–389.

Qian, Guomin, Man Guo, Lihui Zhang, Yibing Wang, Simon Hu, and Dianhai Wang. 2021. Traffic scheduling and control in fully connected and automated networks. *Transportation Research Part C: Emerging Technologies* 126:103011.

Richards, Paul I. 1956. Shock waves on the highway. *Operations research* 4(1):42–51.

Rios-Torres, Jackeline, and Andreas A Malikopoulos. 2016. A survey on the coordination of connected and automated vehicles at intersec-

tions and merging at highway on-ramps. *IEEE Transactions on Intelligent Transportation Systems* 18(5):1066–1077.

Sawake, Vipul Vilas, and Prashant Borkar. 2017. Review of traffic signal timing optimization based on fuzzy logic controller. In *2017 international conference on innovations in information, embedded and communication systems (iciiecs)*, 4–4. IEEE.

Sharma, Anshuman, and Zuduo Zheng. 2021. Connected and automated vehicles: opportunities and challenges for transportation systems, smart cities, and societies. *Automating Cities: Design, Construction, Operation and Future Impact* 273–296.

Shi, Haotian, Yang Zhou, Keshu Wu, Xin Wang, Yangxin Lin, and Bin Ran. 2021. Connected automated vehicle cooperative control with a deep reinforcement learning approach in a mixed traffic environment. *Transportation Research Part C: Emerging Technologies* 133:103421.

Subraveti, Hari Hara Sharan Nagalur, Anupam Srivastava, Soyoung Ahn, Victor L Knoop, and Bart van Arem. 2021. On lane assignment of connected automated vehicles: strategies to improve traffic flow at diverge and weave bottlenecks. *Transportation research part C: emerging technologies* 127:103126.

Tajalli, Mehrdad, Mehrzad Mehrabipour, and Ali Hajbabaie. 2020. Network-level coordinated speed optimization and traffic light control for connected and automated vehicles. *IEEE Transactions on Intelligent Transportation Systems* 22(11):6748–6759.

Toledo, Tomer, Haris N Koutsopoulos, and Moshe E Ben-Akiva. 2003. Modeling integrated lane-changing behavior. *Transportation Research Record* 1857(1):30–38.

Wang, Ling, Mohamed Abdel-Aty, Qi Shi, and Juneyoung Park. 2015. Real-time crash prediction for expressway weaving segments. *Transportation Research Part C: Emerging Technologies* 61:1–10.

Wang, Meng, Winnie Daamen, Serge P Hoogendoorn, and Bart van Arem. 2014a. Rolling horizon control framework for driver assistance systems. part i: Mathematical formulation and non-cooperative systems. *Transportation research part C: emerging technologies* 40:271–289.

Wang, Xu, Md Hadiuzzaman, Jie Fang, Tony Z Qiu, and Xinping Yan. 2014b. Optimal ramp metering control for weaving segments considering dynamic weaving capacity estimation. *Journal of Transportation Engineering* 140(11):04014057.

Wang, Yipei, Shuaikun Hou, and Xin Wang. 2021. Reinforcement learning-based bird-view automated vehicle control to avoid crossing traffic. *Computer-Aided Civil and Infrastructure Engineering* 36(7):890–901.

Wu, Jiaming, Soyoung Ahn, Yang Zhou, Pan Liu, and Xiaobo Qu. 2021. The cooperative sorting strategy for connected and automated vehicle platoons. *Transportation Research Part C: Emerging Technologies* 123:102986.

Wu, Jiaming, and Xiaobo Qu. 2022. Intersection control with connected and automated vehicles: a review. *Journal of intelligent and connected vehicles* 5(3):260–269.

Xu, Biao, Xuegang Jeff Ban, Yougang Bian, Jianqiang Wang, and Keqiang Li. 2017. V2i based cooperation between traffic signal and approaching automated vehicles. In *2017 ieee intelligent vehicles symposium (iv)*, 1658–1664. IEEE.

Xuan, Yiguang, Carlos F Daganzo, and Michael J Cassidy. 2011. Increasing the capacity of signalized intersections with separate left turn phases. *Transportation research part B: Methodological* 45(5):769–781.

Yao, Yifan, Fan Pu, Yang Zhou, Xin Wang, Xiaotian Li, and Bin Ran. Cell transmission model based connected automated. *Available at SSRN 4760730*.

Yao, Yifan, Yang Zhou, Jingxin Xia, Xin Wang, Xiaotian Li, and Bin Ran. 2022a. Rolling-horizon–based strategy of fully cooperative traffic under signalized intersections. *Computer-Aided Civil and Infrastructure Engineering*.

———. 2023. Rolling-horizon–based strategy of fully cooperative traffic under signalized intersections. *Computer-Aided Civil and Infrastructure Engineering* 38(4):454–469.

Yao, Zhihong, Yuting Jin, Haoran Jiang, Lu Hu, and Yangsheng Jiang. 2022b. Ctm-based traffic signal optimization of mixed traffic flow with connected automated vehicles and human-driven vehicles. *Physica A: Statistical Mechanics and its Applications* 603:127708.

Zhang, Lei, and David Levinson. 2010. Ramp metering and freeway bottleneck capacity. *Transportation Research Part A: Policy and Practice* 44(4):218–235.

Zheng, Yuan, Bin Ran, Xu Qu, Jian Zhang, and Yi Lin. 2019. Cooperative lane changing strategies to improve traffic operation and safety nearby freeway off-ramps in a connected and automated vehicles environment. *IEEE Transactions on Intelligent Transportation Systems* 21(11):4605–4614.

Zhou, Bin, Yunpeng Wang, Guizhen Yu, and Xinkai Wu. 2017a. A lane-change trajectory model from drivers' vision view. *Transportation Research Part C: Emerging Technologies* 85:609–627.

Zhou, Fang, Xiaopeng Li, and Jiaqi Ma. 2017b. Parsimonious shooting heuristic for trajectory design of connected automated traffic part i: Theo-

retical analysis with generalized time geography. *Transportation Research Part B: Methodological* 95:394–420.

Zhou, Yang, Soyoung Ahn, Meng Wang, and Serge Hoogendoorn. 2020. Stabilizing mixed vehicular platoons with connected automated vehicles: An h-infinity approach. *Transportation Research Part B: Methodological* 132: 152–170.

Zhou, Yang, Meng Wang, and Soyoung Ahn. 2019. Distributed model predictive control approach for cooperative car-following with guaranteed local and string stability. *Transportation research part B: methodological* 128:69–86.

Zhu, Jie, Said Easa, and Kun Gao. 2022a. Merging control strategies of connected and autonomous vehicles at freeway on-ramps: a comprehensive review. *Journal of Intelligent and Connected Vehicles* 5(2):99–111.

Zhu, Jie, Ivana Tasic, and Xiaobo Qu. 2022b. Flow-level coordination of connected and autonomous vehicles in multilane freeway ramp merging areas. *Multimodal transportation* 1(1):100005.